PARAMETRIC OSCILLATIONS OF A NOTCHED COLUMN

A THESIS

Presented to

The Faculty of the Division of Graduate

Studies and Research

by

Vijaykumar Navnitlal Parekh

In Partial Fulfillment of the

Requirements for the

Degree of Doctor of Philosophy in the

School of Aerospace Engineering

Georgia Institute of Technology

April, 1975

PARAMETRIC OSCILLATIONS OF A NOTCHED COLUMN

Approved:

Dr. R. L. Carlson, Chairman

Dr. G. A. Pierce

Dr. C. V. Smith, Jr.

Date approved by Chairman: April 10, 1975

ACKNOWLEDGMENTS

My sincere gratitude is expressed to all who have helped in any way to make this study possible. I owe a special word of gratitude to the following:

To Dr. Robert L. Carlson, who served as my advisor and committee chairman, for his encouragement, instruction, advice and personal guidance during my graduate study;

To Dr. W. W. King, Dr. G. A. Pierce, Dr. C. V. Smith and Dr. C. E. Ueng, who extended their constructive criticism and valuable suggestions for improvements;

To the Lockheed-Georgia Company Management, in particular the General Structural Analysis Management and the School of Aerospace Engineering of the Georgia Institute of Technology for the financial support during my graduate study;

To Mr. S. Virk for assisting me in conducting experiments;

To Mrs. P. Weldon for her typing and final preparation of the manuscript.

TABLE OF CONTENTS

TABLE OF CONTENTS (Continued)

LIST OF TABLES

LIST OF ILLUSTRATIONS

LIST OF ILLUSTRATIONS (Continued)

LIST OF ILLUSTRATIONS (Continued)

LIST OF SYMBOLS

$v(x,t), W(x,t)$	transverse displacement of the column
$v_{xx}(x,t)$	second partial derivative with respect to x of $v(x,t)$
t	time
(a,b)	region of discontinuity
C	location of discontinuity
$2R$	region of discontinuity (a,b)
h, b'	cross-sectional dimensions of the column
$P(t)$	time dependent periodic load = $P_o + P_1 \cos \theta t$
ℓ	length of the column
θ	applied frequency
K	effective stiffness parameter
T	kinetic energy of the system
U	strain energy of the system
Q_i	generalized force
$f_1(t)$	generalized co-ordinates
m	mass per unit length of the column
e_{ni}	integrals defined by Equations (5) in Chapter II
α, β	load parameter
$\underline{A}, \underline{B}, \underline{C}$ $\underline{O}, \underline{E}, \underline{f}$	matrices defined by equation (6) or (21) or (29) or (56) in Chapter II
$\underline{\phi}, \underline{\psi}, \underline{A}, \underline{R}, \underline{S}, \underline{D}, \underline{X}_i, \underline{P}_i, \mu_i, \rho_i$	Notations defined in Appendix A
ω	uniform column natural frequency
γ	eigenvalue of Equation (14) for $k = 2$ in Chapter II

Ω	natural frequency with initial load, P_o
$\underset{\sim}{a}_k, \underset{\sim}{b}_k$	non-null constant vectors
θ_*	frequency at parametric oscillation occur
Ω_*	free vibration frequency
P_*	buckling load
$\bar{e}_{11}$	defined by Equation (21) in Chapter II
d_1, d_2, d_3	defined by Equation (30) in Chapter II
$\theta_i; i=1,2,3,4$	defined by Equation (32) in Chapter II
c_1, c_2	defined by Equation (35) and (36) or (63) in Chapter II
$\bar{c}_1, \bar{c}_2$	defined by Equations (40) and (41) or (51) and (52) or (64) or (68) and (69) in Chapter II
$\|D_1\|$, $\|D_2\|$, $\|D_3\|$	defined by Equation (45) or (65) in Chapter II
$\|\bar{D}_1\|$, $\|\bar{D}_2\|$, $\|\bar{D}_3\|$	defined by Equation (46) in Chapter II
$\underset{\sim}{\tilde{E}}$	defined by Equation (57) or (58) in Chapter II
$\underset{\sim}{\hat{E}}$	defined by Equation (59) in Chapter II
$\hat{e}_{ij}$	defined by Equation (59) in Chapter II
θ_U^S, θ_L^S	parametric frequency, defined by Equation (1) in Chapter III
θ_U^P, θ_L^P	
μ	excitation parameter
D_1, D_2, D_3	dial gages readings 0.0001 of inches
$\left.\frac{\Delta P}{\Delta y}\right\|_{\ell'/2}$	the slope
a, M_o, M_L, R, L	defined by Figure 16
a_n	defined by Equation (3) in Chapter III
$h_i; i=1,\ldots,4$	defined by Equation (7) in Chapter III
A	defined by Equation (7) in Chapter III

$\|\|D\|\|$, $\|\|D_1\|\|$, $\|\|D_2\|\|$	defined by Equation (8) in Chapter III
$\frac{dP}{dv}$	analytical slopes = c_s, experimentally obtained slopes
$\bar{h}_1, \bar{h}_2, \bar{h}_3$	defined by equation (9) in Chapter III
[ ]	reference indicator
( )	equation indicator
ND	subscript indicating non-dimensional quantities
D	subscript indicating dimensional quantities
UN	subscript indicating dimensional uniform column quantities
$\triangleq$	definition symbol
$\equiv$	identically equal to
"."	time derivative

SUMMARY

Using Lagrange's equations, the equations of motions for column simply supported at both ends under axial load $P(t) = P_0 + P_1 \cos \theta t$ were derived. The approximate formulae for the parametric stability, the free vibration frequency and the buckling load were obtained using the method of successive approximations (note that these formulae apply to a column with a region of discontinuity, e.g. distribution of extensive cracks). The effects of a region of discontinuities on the column were evaluated in terms of three parameters, the size of the discontinuity, the effective stiffness and the location of the discontinuity; i.e., R, K and C. These effects are reported in a non-dimensional form.

A two part experimental program was conducted to evaluate the effective stiffness parameter and the parametric stability results. These experimental results were correlated with the analytically deduced results. The experimental and the analytical stability results were in good agreement.

CHAPTER I

INTRODUCTION

The dynamic stability of mechanical systems constitutes a class of problems in mechanics which is in the border line between static stability and vibration problems. Beilin [1] defines the class of dynamic stability problems as follows: "The essence of the general problems of dynamic instability consists of the study of the motion of elastic systems which are excited by time-dependent external loads, if the latter are so applied that the loads in direction and point of application but not varying in time may cause static loss of stability."

To indicate the basic features of this type of problem, consider a uniform simply supported column of length ℓ, and subjected to a periodic axial load $P\cos(\theta t)$, shown in Figure 1. If the column has flexural rigidity EI and mass per unit length m, then its equation of motion in the lateral direction is

$$EI \frac{\partial^4 W}{\partial x^4} + P \cos(\theta t) \frac{\partial^2 W}{\partial x^2} + m \frac{\partial^2 W}{\partial t^2} = 0 . \qquad (1)$$

It can be seen that the loading enters as a periodic parameter in Equation (1) and hence dynamic instability is called parametric instability of the column.

The displacement $W(x,t)$ can be expanded as a series in the normal modes of the unloaded column, i.e.

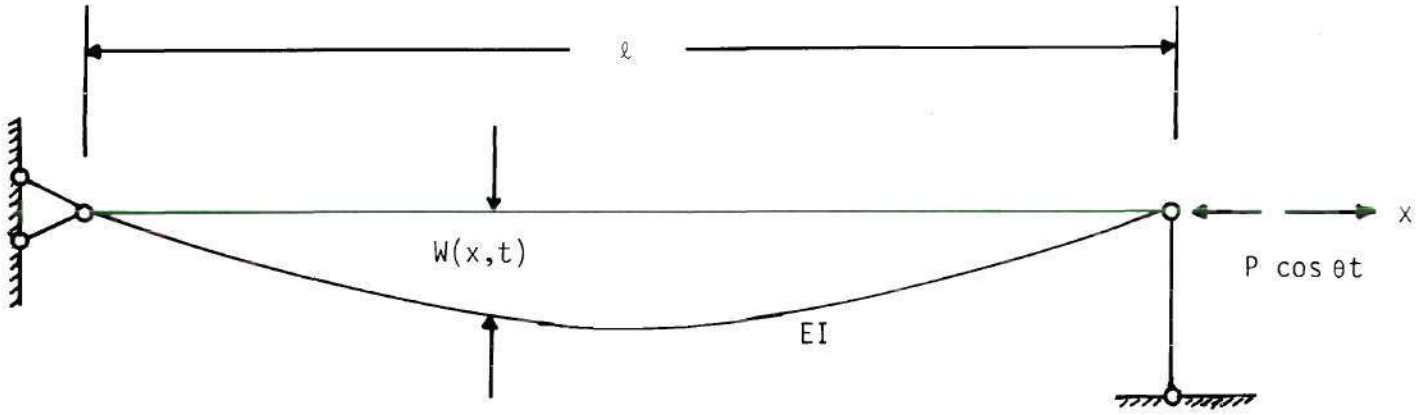

Figure 1. Schematic Representation of a Uniform Column.

$$W(x,t) = \sum_{i=1}^{\infty} q_i(t)\sin(\frac{\pi x i}{\ell}) .$$

A set of equations for the generalized co-ordinate $q_i(t)$ is obtained as follows:

$$\ddot{q}_i + \omega_i^2 (1 - \frac{P}{p_i}) \cos(\theta t)\, q_i = 0 , \qquad (2)$$

in which dots denotes differentiation with respect to time t,

$\omega_i = (\frac{\pi i}{\ell})^2 \sqrt{\frac{EI}{m}}$ is the i^{th} natural frequency and

$p_i = (\frac{\pi i}{\ell})^2 EI$ is the i^{th} buckling load of the column.

The equations (2) are uncoupled and each has the form of a Mathieu equation. In particular the solution for any mode q_i is classified as unstable within certain regions because it can be shown that q_i grows exponentially in those regions [2]. The most significant and largest of these regions exists for $\frac{P}{p_i}$ near an excitation frequency θ given by $\frac{\theta}{2\omega_i} = 1$. A physical reasoning leads directly to the relationship $\theta = 2\omega_i$: for each cycle of the transverse vibration of the column, the right end in Figure 1 completes two cycles. Thus if a frequency of the applied load θ is nearly twice the natural frequency ω_i, then the resonance occurs. Often this type of resonance is called a parametric resonance, and the behavior of the column is termed a sub-harmonic response of order 1/2.

Moreover, the theory indicates that higher order instability zones can be found in the vicinity of

$$\frac{\theta}{2\omega_i} = \frac{1}{n} \ , \ n = 1,2,3,\ldots \ .$$

Thus there exist for each mode countless instability regions being more densely spaced as θ is reduced. The instability regions become thinner with increasing order [3]. It can be also noted that for the zones associated with n = 1,2,3 are called i^{th} principal (primary), secondary and third instability zones (regions) respectively. It can be realized that there exist an infinite number of instability zones corresponding to a mode and there are infinite number of modes which govern the stability of the column. Therefore, in the θ,p-plane, the number of instability zones increase as number of modes are increased for the stability analysis. However these instability zones are not accessible experimentally due to damping.

Therefore, the following conclusions can be drawn for the column in Figure 1.

o If a point exists in $\frac{P}{p_i}, \frac{\theta}{2\omega_i}$- plane in a blank region of Figure 2, then the initial straight form of the column is dynamically stable. However if this point is found in a shaded region, then any initial deviation from the straight form of column will increase unboundedly with time, i.e. the straight form of the column is dynamically unstable.

o The conditions under which the differential equation (2) has periodic solutions are represented by the boundaries of the instability regions in Figure 2. These boundaries describe the relation between the frequencies of the external loading, the natural

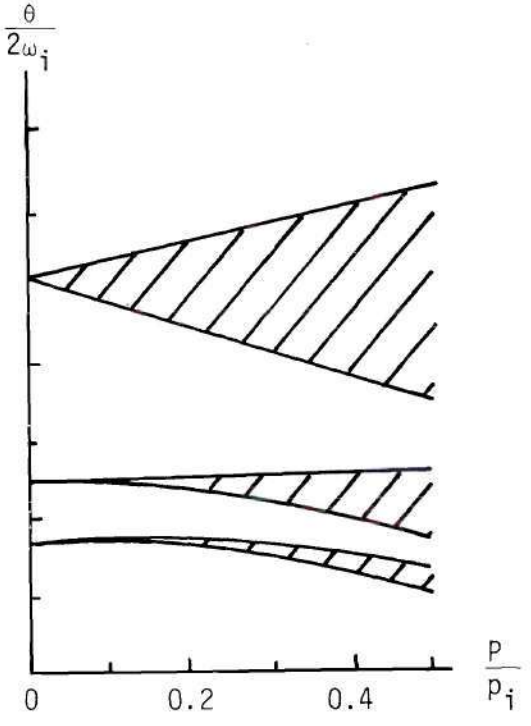

Shaded Areas Represent Unstable Zones

Blank Areas Represent Stable Zones

Figure 2. Regions of Dynamic Instability.

frequency of the column and the magnitude of external force.

o When the displacement W and the external load are independent of time in the equation of motion (1), then this equation represents the corresponding static stability problem. But, if the displacement is time-dependent and the load is time-independent the problem reduces to the usual vibration problem with axial external loading.

During the last decade a considerable amount of theoretical and experimental research has been done in the field of parametric excitation [3,8-12,15-19]. An elegant and systematic presentation of the theory of dynamic stability of elastic systems can be found in the classical textbook on the subject by Bolotin [2].

Historically, the first report of parametric instability was made by Faraday in 1833, when he observed that the liquid in a cylindrical glass was parametrically excited by movement of moist fingers around the glass edge [4]. Melde in 1859 gave a demonstration of the parametric resonance phenomenon using a system involving a string and a tuning fork [5]. A mathematical analysis of this phenomenon was provided by Lord Rayleigh in 1885 [1].

Thus, the study of the parametric resonance commenced early in the 19^{th} century. About 100 years elapsed, however, before Beliaev in 1924 described the first engineering problem in which parametric instability was studied analytically (Figure 1). Later, experimental work by Bolotin and others confirmed the analytical results for this problem [2,6]. An interesting review on the development of the field up to 1965 has been given by Evan-Iwanowski [4].

Since 1965 the literature on parametric excitation has taken a

direction of accounting for nonlinear, inertial, damping and viscoelastic effects [1,4-12]. Recently, Haight and King [9] reported a theoretical and experimental investigation of the loss due to parametric coupling of stability of steady-state plane transverse response of a slender elastic rod subjected to a harmonic longitudinal excitation. Their analysis shows that, provided an arbitrarily small viscous damping term is present, plane motion is stable for all values of the parameters when the natural frequency ratio for motions in the two principal planes is unity. Only when the natural frequencies are detuned (difference between oscillation and excitation frequencies) does the original planar response lose its stability. They found that when the frequency ratio is near unity there is a critical excitation frequency which causes the original planar response to exhibit an amplitude jump and a simultaneous plane shift to stable motions in the other principal plane. It can be noted that these results were obtained by use of a set of nonlinear equations for the stability of the uniform column with one end fixed and other end free. In present investigation linearized equations of motion are obtained for a simply supported column with a region of discontinuities. Naturally, it can be extended to study steady-state amplitude-frequency response by a nonlinear formulation of the problem. There has also been an increased effort to identify examples of dynamic instability in the various areas of mechanics, transportation, and industrial construction. The possibility of parametric excitation in aircraft structures has been discussed by Barr and Done [3]. They pointed out that as structures are progressively refined an associated refinement of the dynamic analysis

becomes necessary and that a parametric stability analysis may often be desirable. For example a close observation indicates that fatigue failure develops in the following pattern:

o repeated cyclic stressing causes incremental slip and cold-working locally

o gradual reduction of ductility in strain-hardened area results in the formation of submicroscopic cracks

o and the notched effect of the submicroscopic cracks concentrates stresses until complete fracture occurs.

Fatigue failure is thus related to localized nonuniform plastic deformation, rather than to ideal reversible elastic behavior. Therefore, it is possible that the existence of parametric excitation in a structure may provide the cyclic loading which will bring out both an initiation of cracks and an accelerated propagation of existing cracks.

A general observation of the trend of the research in the field can be summarized as follows [13-19]:

o Some structural failures may be traced to parametric oscillations [3].

o Sustained parametric excitation may accelerate or initiate fatigue failures in a complex structure; therefore a thorough understanding of parametric response is of basic significance [3].

o There is an urgent need on a broad experimental basis for theoretical work in this field [3,7].

For the past 20 years considerable attention has been focused

on the strength behavior of cracked structural elements. A wide variety of elements has been considered, including plates, shells, beams, etc. [20-26]. Recently, Liebowitz and Vanderveldt [27] described several types of behaviors of notched columns. Among these, one of particular interest in this thesis is the reduction of column strength due to notches. Berkovits and Golad [28] conducted an experimental program on slender columns with centrally located cracks. They found that relatively little effect on the column strength was observed when the crack closes during buckling. In the majority of cases, however, the crack tends to open and the strength was reduced significantly. Thus the common assumption that fatigue damage is not harmful in compression-design problems was shown to be unconservative.

In the static problems the loss in strength can be associated with the amplification of stress accompanying increasing lateral deflection. The development of deflection is not only connected with static behavior, but it may also occur in dynamic behavior during oscillatory motion. In particular, any resonant type behavior would be expected to introduce much more severe conditions than those encountered in a static test. These conditions are even more severe when a region of discontinuities is present in the column.

To date very little has been done on the dynamic stability of elastic systems with cut-outs, notches or cracks. Such systems are a step closer to the corresponding realistic systems.

In the present investigation such a general problem involving

the dynamic stability of a simply supported slender column with a region of discontinuities under parametric excitation is examined. The problem of interest is illustrated in Figure 3. It may be noted that the shaded region depicted in Figure 3 represents a region in which discontinuities are present; e.g. multiple cracks, or notches which may be either internal or external. Note that the region 2R: $a < x < b$ is slightly larger than the actual region of discontinuities, so that $\frac{d^2(EI)}{dx^2}$ at $x = a$ and $x = b$ will be continuous for the analytical development of the stability model.

The presence of such regions has, in recent years, become increasingly possible as strength requirements have increased and as new types of materials have been introduced. These include the ultra-high strength steels and heat resisting alloys. Concrete has, of course, always involved a brittle response which is susceptible to cracking. More recently, the use of fiber reinforced composites has created concern about the effect of cracks. For example, it has been found that the graphite composites are embrittled by surface impact which can introduce cracks.

The objectives of the research described here are:

- to develop an analytical model for determining the boundaries of instability regions for a bar within which a region of discontinuities is present,
- to determine the instability boundaries for a notched column by conducting an experimental investigation, and
- to correlate the analytical and experimental results on buckling strength and vibration characteristics.

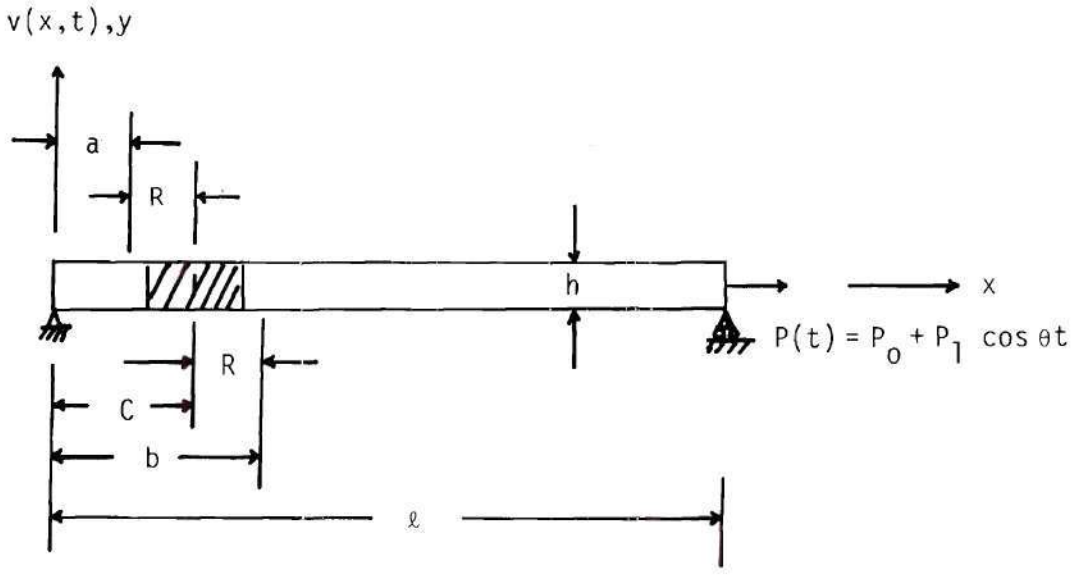

Figure 3. Objective Column Schematic.

Chapter II contains the development of the stability model for the column and the analysis using the variational method. In Chapter III experimental procedures to establish the instability boundaries for the column and the needed instrumentation are described. The analytical and experimental results, including the effects of notches on the buckling strength and the vibration characteristics, are presented in Chapter IV. Finally, conclusions and recommendations regarding the investigation are reported in Chapter V.

CHAPTER II

THEORETICAL ANALYSIS

The developments in this chapter include a statement of the basic assumptions made for the idealization of the subject problem, a derivation of the governing differential equations of motion for the column, and a determination of the equations for the boundaries between the stable and unstable regions. Finally, approximate relations for the parametric, buckling and vibration characteristics of the column are presented. Applications of these relations and numerical results are presented in Chapter IV.

Basic Assumption

To develop the analytical stability model for the column described in Figure 3, the following assumptions apply:

- Except for the region within which the discontinuities occur, the column is a uniform solid homogeneous prismatic bar and the maximum cross-sectional dimension is small compared with length ℓ.
- Shear stress and rotatory inertia effects are negligible.
- The maximum stress is within the proportional limit of the material.
- The lateral displacement $v(x,t)$ due to $P(t)$ is small relative to ℓ.
- The forces $P(t)$ applied at the ends of the column result in forces throughout the column which are uniform to a sufficiently close

approximation. Lubkin and Stoker [29] showed that this assumption is justified if the bending frequency is well below the first longitudinal vibration frequency of the column.

o The column axis is assumed to be incompressible, which means $\varepsilon_x = 0$ everywhere along the axis. Since $\varepsilon_x = \frac{u}{x} + \frac{1}{2}(\frac{v}{x})^2$, it follows that

$$\frac{\partial u}{\partial x} = -\frac{1}{2}(\frac{\partial v}{\partial x})^2 .$$

Therefore the work done by the external force P(t) can be written as

$$P(t)u\Big|_{x=\ell} = P(t)\int_0^{\ell} \frac{\partial u}{\partial x}\,dx = -\frac{P(t)}{2}\int_0^{\ell} (\frac{\partial v}{\partial x})^2 dx .$$

o The mass per unit length of the beam is assumed to be constant, i.e., the absence of mass at the void is neglected.

o The bending strain energy of the element from x = a to x = b shown in Figure 3 is proportional to $\frac{E}{2}\int_a^b v_{xx}^2(x,t)dx$; i.e. the strain energy is equal to $\frac{EK}{2}\int_a^b v_{xx}^2(x,t)dx$ for the element containing the notch, and K is a constant of proportionality. The constant K is a function of the characteristic variables of the sub-element; i.e., the type of material, the nature and distribution of the discontinuities. Thus, its value reflects the effect of the discontinuities on the capacity of the sub-element to store strain energy.

This approximation is very similar to that used by Tsalik [20] in the free vibration analysis of bars with cracks. He assumed that

the relation between the bending moment and the stiffness could be represented by a weighted linear relationship. It can be noted that bending strain energy estimation of the beam element a-b provides an integrated representation of the characteristics of the section. The details of the local properties are not specified; e.g., the stress distribution in the vicinity of the notch is not described in this representation.

In this connection reference to results obtained by Stahl and Keer [30], and by Lynn and Kumbasar [31] for vibration and stability of cracked rectangular plates is of special interest. Stahl and Keer developed a cracked plate analysis in which the local effect of the crack-tip singularity was incorporated in the determination of global properties such as natural frequency of vibration and buckling load. The development of Lynn and Kumbasar, on the other hand, did not incorporate the local crack-tip stress singularity in their analysis. In effect, their representation was global in character. A comparison of these results [30] revealed good agreement between the two analyses with regard to the global properties; i.e., frequencies. However, the moment distributions and bending stress in the vicinity of the crack tip, a local effect, were significantly different. This indicates that in some instances, global properties can be correctly deduced from analyses which do not include a detailed representation of localized effects.

It should be noted that since the details of the bar within the region denoted by 2R are expressed only in terms of the constant K,

different possibilities may be envisioned. For example, in addition to a single slot, a series of cracks indicated in Figure 4(b) may exist. Naturally the values of R and K must appropriately reflect the effective stiffness in the strain energy estimation of the beam element a-b. Methods for determining the R and the K are discussed in Chapter IV.

Equations of Motion

In this section an infinite set of differential equations of motion in terms of the generalized coordinates, $\{f_i(t)\}_1^\infty$ are derived using Lagrange's equations. The Lagrangian equations for an elastic system are [2]:

$$\frac{d}{dt}\left(\frac{\partial T}{\partial \dot{f}_i}\right) - \frac{\partial}{\partial f_i}(T - U) = Q_i \; ; \qquad (1)$$

$$i = 1,2,3,\ldots \; .$$

In these equations T is the kinetic and U the strain energy of the system, and Q_i is the generalized force corresponding the generalized coordinate, $f_i(t)$. A sequence of admissible functions* for deflection can be selected as $\{\sin \frac{n\pi x}{\ell}\}_1^\infty$ for the subject problem. Therefore, time-dependent deflection of the column shown in Figure 3 may be represented as

---

*Admissible functions are defined as those functions which satisfy both geometric and natural boundary conditions of the problem.

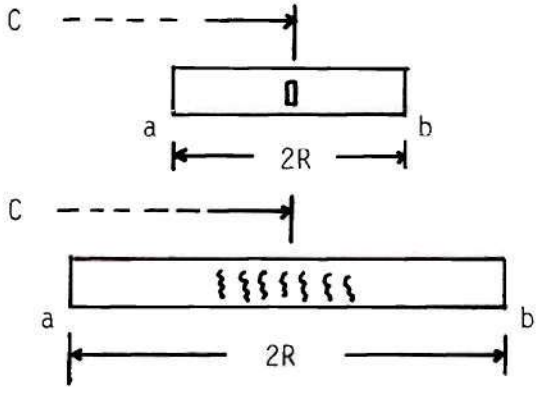

(a) Single Slot Geometry in Element a-b.

(b) Series of Cracks Geometry in Element a-b.

Figure 4. Possible Discontinuities.

$$v(x,t) = \sum_{n=1}^{\infty} f_n(t) \sin \frac{n\pi x}{\ell} . \qquad (2)$$

The potential and the kinetic energy, and the generalized forces of the column shown in Figure 3 with the idealization described in the previous section are:

$$U = \frac{EI}{2} \int_o^{\ell} \left(\frac{\partial^2 v}{\partial x^2}\right)^2 dx + \frac{E(K-I)}{2} \int_a^b \left(\frac{\partial^2 v}{\partial x^2}\right)^2 dx$$

$$T = \frac{m}{2} \int_o^{\ell} \left(\frac{\partial v}{\partial t}\right)^2 dx \qquad (3)$$

$$Q_i = - \frac{\partial}{\partial f_i} \left(\frac{1}{2} P(t) \int_o^{\ell} \left(\frac{\partial v}{\partial x}\right)^2 dx\right) .$$

In Equations (3), EI and EK are the uniform and the effective bending stiffness of the column. The mass per unit length is m and $P(t) = P_o + P_1 \cos \theta t$ is the external oscillating tension with circular frequency, θ for the column. Substituting Equations (2) and (3) into (1), the equations of motion for the column in terms of the generalized coordinates are obtained as

$$\frac{m\ell}{2} f_n + \frac{n^4 \pi^4 EI}{2\ell^3} f_n + \frac{n^2 \pi^4 E(K-I)}{2\ell^4} \sum_{i=1}^{\infty} i^2 f_i e_{ni} + \frac{n^2 P_o \pi^2}{2\ell} f_n + \frac{n^2 P_1 \pi^2}{2\ell} \cos\theta t \, f_n = 0$$

where, $n = 1,2,3,\ldots,\infty$; and (4)

$$e_{in} = e_{ni} = \int_{a=C-R}^{b=C+R} \sin \frac{i\pi x}{\ell} \sin \frac{n\pi x}{\ell} dx = \begin{cases} R - \frac{\ell}{2\pi i} \cos \frac{2\pi iC}{\ell} \sin \frac{2\pi iR}{\ell}, & i=n \\ \frac{\ell}{(i-n)\pi} \cos \frac{(i-n)\pi C}{\ell} \sin \frac{(i-n)\pi R}{\ell} & \\ - \frac{\ell}{(i+n)\pi} \cos \frac{(n+i)\pi C}{\ell} \sin \frac{(n+i)\pi R}{\ell}, & i \neq n. \end{cases} \quad (5)$$

Equations (4) are a system of ordinary second order linear homogeneous coupled differential equations. The coefficient of the last term is a periodic function of the independent variable t. It is convenient to rewrite Equations (4) in matrix form:

$$\underline{C} \frac{d^2 \underset{\sim}{f}}{dt^2} + (\underline{E} - \alpha \underline{A} - \beta \underline{B} \cos \theta t) \underset{\sim}{f} = 0 \quad (6)$$

where,

$$\alpha \triangleq - \frac{P_o \pi^2}{m\ell^2},$$

$$\beta \triangleq - \frac{P_1 \pi^2}{m\ell^2},$$

$$\underset{\sim}{f}(t) \triangleq \begin{bmatrix} f_1(t) \\ f_2(t) \\ \cdot \\ \cdot \\ \cdot \\ f_\infty(t) \end{bmatrix}_{(\infty \text{ by } 1)},$$

$$\underset{\sim}{0} \triangleq \begin{bmatrix} 0 \\ 0 \\ 0 \\ \\ \\ 0 \end{bmatrix}_{(\infty \text{ by } 1)},$$

$$\underline{C} \triangleq \begin{bmatrix} 1 & 0 & 0 & 0 & 0 & 0 & \cdot & \cdot \\ 0 & 1 & 0 & 0 & 0 & 0 & \cdot & \cdot \\ 0 & 0 & 1 & 0 & 0 & 0 & \cdot & \cdot \\ 0 & 0 & 0 & 1 & 0 & 0 & \cdot & \cdot \\ 0 & 0 & 0 & 0 & 1 & 0 & \cdot & \cdot \\ 0 & 0 & 0 & 0 & 0 & 1 & \cdot & \cdot \\ \cdot & \cdot & \cdot & \cdot & \cdot & \cdot & \cdot & \cdot \\ \cdot & \cdot & \cdot & \cdot & \cdot & \cdot & \cdot & \cdot \end{bmatrix}_{(\infty \text{ by } \infty)},$$

$$\underline{A} \triangleq \begin{bmatrix} 1 & & 0 & 0 & 0 & 0 & \cdot & \cdot \\ 0 & 2^2 & & 0 & 0 & 0 & \cdot & \cdot \\ 0 & 0 & 3^2 & & 0 & 0 & \cdot & \cdot \\ 0 & 0 & 0 & 4^2 & & 0 & \cdot & \cdot \\ 0 & 0 & 0 & 0 & 5^2 & 0 & \cdot & \cdot \\ 0 & 0 & 0 & 0 & 0 & 6^2 & \cdot & \cdot \\ \cdot & \cdot & \cdot & \cdot & \cdot & \cdot & \cdot & \cdot \\ \cdot & \cdot & \cdot & \cdot & \cdot & \cdot & \cdot & \cdot \end{bmatrix}_{(\infty \text{ by } \infty)},$$

$$\underline{B} \triangleq \begin{bmatrix} 1 & 0 & 0 & 0 & 0 & \cdot & \cdot \\ 0 & 2^2 & 0 & 0 & 0 & \cdot & \cdot \\ 0 & 0 & 3^2 & 0 & 0 & \cdot & \cdot \\ 0 & 0 & 0 & 4^2 & 0 & \cdot & \cdot \\ 0 & 0 & 0 & 0 & 5^2 & \cdot & \cdot \\ \cdot & \cdot & \cdot & \cdot & \cdot & \cdot & \cdot \\ \cdot & \cdot & \cdot & \cdot & \cdot & \cdot & \cdot \end{bmatrix}_{(\infty \text{ by } \infty)} ,$$

and,

$$\underline{E} \triangleq \frac{\pi^4 EI}{m\ell^4} \begin{bmatrix} 1 + \frac{\bar{e}_{11}}{\ell} & 2^2 \frac{\bar{e}_{12}}{\ell} & 3^2 \frac{\bar{e}_{13}}{\ell} & 4^2 \frac{\bar{e}_{14}}{\ell} & \cdot & \cdot \\ 2^2 \frac{\bar{e}_{21}}{\ell} & 2^4 + 2^4 \frac{\bar{e}_{22}}{\ell} & 2^2 \cdot 3^2 \frac{\bar{e}_{23}}{\ell} & 2^2 \cdot 4^2 \frac{\bar{e}_{24}}{\ell} & \cdot & \cdot \\ 3^2 \frac{\bar{e}_{31}}{\ell} & 3^2 \cdot 2^2 \frac{\bar{e}_{32}}{\ell} & 3^4 + 3^4 \frac{\bar{e}_{33}}{\ell} & 3^2 \cdot 4^2 \frac{\bar{e}_{34}}{\ell} & \cdot & \cdot \\ 4^2 \frac{\bar{e}_{41}}{\ell} & 4^2 \cdot 2^2 \frac{\bar{e}_{42}}{\ell} & 4^2 \cdot 3^2 \frac{\bar{e}_{43}}{\ell} & 4^4 + 4^4 \frac{\bar{e}_{44}}{\ell} & \cdot & \cdot \\ \cdot & \cdot & \cdot & \cdot & \cdot & \cdot \\ \cdot & \cdot & \cdot & \cdot & \cdot & \cdot \end{bmatrix}_{(\infty \text{ by } \infty)}$$

with, $\bar{e}_{ni} \triangleq (\frac{K}{I} - 1)e_{ni}$ $\quad i = 1,2,3,\ldots ,$

$n = 1,2,3,\ldots .$

Equations for the Boundary Frequencies

The finding of the regions of instability reduces to the determination of conditions under which the differential equation system (6) has periodic solutions with period T or 2T (Appendix A). The solution with period $2T = \frac{4\pi}{\theta}$ of Equation (6) in the form of the following series is desired.

$$\underset{\sim}{f}(t) = \sum_{k=1,3,5}^{\infty} (\underset{\sim}{a}_k \sin \frac{k\theta t}{2} + \underset{\sim}{b}_k \cos \frac{k\theta t}{2}) , \qquad (7)$$

where $\underset{\sim}{a}_k$ and $\underset{\sim}{b}_k$ are vectors which are independent of time and they have an infinite number of components. The series (7) is equivalent to the infinite Fourier series for the components of vector $\underset{\sim}{f}(t)$. These series converge, since the periodic solutions (7) of the differential equation system in all cases satisfy the Dirichlet conditions (Appendix A).

Substituting Equations (7) into (6) and comparing coefficients of $\sin \frac{k\theta t}{2}$ and $\cos \frac{k\theta t}{2}$ gives the following system of matrix equations:

$$(\underline{E} - \alpha\underline{A} + \tfrac{1}{2}\beta\underline{B} - \tfrac{1}{4}\theta^2\underline{C})\underset{\sim}{a}_1 - \tfrac{1}{2}\beta\underline{B}\,\underset{\sim}{a}_3 = \underset{\sim}{0} ,$$

$$(\underline{E} - \alpha\underline{A} - \tfrac{1}{4}k^2\theta^2\underline{C})\underset{\sim}{a}_k - \tfrac{1}{2}\beta\underline{B}(\underset{\sim}{a}_{k-2} + \underset{\sim}{a}_{k+2}) = \underset{\sim}{0},$$

$$(k = 3,5,\ldots) ; \qquad (7a)$$

$$(\underline{E} - \alpha\underline{A} - \tfrac{1}{2}\beta\underline{B} - \tfrac{1}{4}\theta^2\underline{C})\underset{\sim}{b}_1 - \tfrac{1}{2}\beta\underline{B}\,\underset{\sim}{b}_3 = \underset{\sim}{0} ,$$

$$(\underline{E} - \alpha\underline{A} - \tfrac{1}{4}k^2\theta^2\underline{C})\underset{\sim}{b}_k - \tfrac{1}{2}\beta\underline{B}(\underset{\sim}{b}_{k-2} + \underset{\sim}{b}_{k+2}) = \underset{\sim}{0},$$

$$(k = 3,5,\ldots) .$$

Note that the above equations are uncoupled with respect to the a's and b's. Also it should be noted that in deriving the above equations the following trigonometric identities were found useful:

$$\cos\theta t \sin\frac{k\theta t}{2} = \frac{1}{2}\{\sin\frac{(k-2)\theta t}{2} + \sin\frac{(k+2)\theta t}{2}\}, \text{ and}$$

$$\cos\theta t \cos\frac{k\theta t}{2} = \frac{1}{2}\{\cos\frac{(k-2)\theta t}{2} + \cos\frac{(k+2)\theta t}{2}\}.$$

For non-trivial values of $\underset{\sim}{a}_k$ and $\underset{\sim}{b}_k$ the determinants of the coefficients of $\underset{\sim}{a}_k$ and $\underset{\sim}{b}_k$ must be zero. Thus the conditions for the existence of periodic solutions with period $2T = \frac{4\pi}{\theta}$ have the form*

$$\begin{vmatrix} E-\alpha\underline{A}\pm\frac{1}{2}\beta\underline{B}-\frac{1}{4}{}^{2}\underline{C} & -\frac{1}{2}\beta\underline{B} & \underline{0} & \cdot \\ -\frac{1}{2}\beta\underline{B} & \underline{E}-\alpha\underline{A}-\frac{9}{4}\theta^2\underline{C} & -\frac{1}{2}\beta\underline{B} & \cdot \\ \underline{0} & -\frac{1}{2}\beta\underline{B} & \underline{E}-\alpha\underline{A}-\frac{25}{4}\theta^2\underline{C} & \cdot \\ \cdot & \cdot & \cdot & \cdot \end{vmatrix} = 0 \qquad (8)$$

Similarly, substitution of the series

$$\underset{\sim}{f}(t) = \frac{1}{2}\underset{\sim}{b}_0 + \sum_{k=2,4,6}^{\infty}(\underset{\sim}{a}_k \sin\frac{k\theta t}{2} + \underset{\sim}{b}_k \cos\frac{k\theta t}{2}), \qquad (8a)$$

into the differential Equation (6), the following conditions for the existence of solutions with a period $\frac{2\pi}{\theta} = T$ are obtained:

---

*Here two conditions corresponding to a's and b's are combined under the ± sign.

$$\begin{vmatrix} \underline{E} - \alpha\underline{A} - \theta^2\underline{C} & -\frac{1}{2}\beta\underline{B} & \underline{0} & \cdot \\ -\frac{1}{2}\beta\underline{B} & \underline{E} - \alpha\underline{A} - 4\theta^2\underline{C} & -\frac{1}{2}\beta\underline{B} & \cdot \\ \underline{0} & -\frac{1}{2}\beta\underline{B} & \underline{E} - \alpha A - 9\theta^2\underline{C} & \cdot \\ \cdot & \cdot & \cdot & \cdot \end{vmatrix} = 0 \quad \text{and} \quad (9)$$

$$\begin{vmatrix} \underline{E} - \alpha\underline{A} & -\beta\underline{B} & \underline{0} & \underline{0} & \cdot \\ -\frac{1}{2}\beta\underline{B} & \underline{E} - \alpha\underline{A} - \theta^2\underline{C} & -\frac{1}{2}\beta\underline{B} & \underline{0} & \cdot \\ \underline{0} & -\frac{1}{2}\beta\underline{B} & \underline{E} - \alpha\underline{A} - 4\theta^2\underline{C} & -\frac{1}{2}\beta\underline{B} & \cdot \\ \underline{0} & \underline{0} & -\frac{1}{2}\beta\underline{B} & \underline{E} - \alpha\underline{A} - 9\theta^2\underline{C} & \cdot \\ \cdot & \cdot & \cdot & \cdot & \cdot \end{vmatrix} = 0 . \quad (10)$$

The infinite determinants obtained belong to the class of normal determinants [2]. It may be noted here that the matrix elements in these determinants are infinite.

In the following an observation of Equation (7a) is presented.

An Observation of Equations (7a)

It is interesting to note that the terms involving $\beta = -\frac{P_1\pi^2}{m\ell^2}$ (P_1, m and ℓ are defined in Equation (6)) in Equation (7a) can be neglected when β is made vanishingly small. Then, Equation (7a) degenerates into the following form

$$\left[\underline{E} - \alpha\underline{A} - \frac{k^2\theta^2}{4}\underline{C}\right] \underset{\sim}{a}_k = \underset{\sim}{0} \quad \text{and}$$

$$\left[\underline{E} - \alpha\underline{A} - \frac{k^2\theta}{4}\underline{C}\right] \underset{\sim}{b}_k = \underset{\sim}{0}, \text{ where}$$

$$k = 1,3,5 \ldots .$$

For non-trivial values of $\underset{\sim}{a}_k$ and $\underset{\sim}{b}_k$ the determinants of the coefficients $\underset{\sim}{a}_k$ and $\underset{\sim}{b}_n$ must be zero. Thus the condition for the existence of periodic solution given by Equation (7) with period $2T = \frac{4\pi}{\theta}$ have the form

$$\left|\underline{E} - \alpha\underline{A} - \frac{k^2\theta^2}{4}\underline{C}\right| = 0, \text{ where} \qquad (12)$$

$$k = 1,3,5 \ldots .$$

Similarly, the following condition for the existence of periodic solution given by Equation (8a) can be derived as

$$\left|\underline{E} - \alpha\underline{A} - \frac{k^2\theta^2}{4}\underline{C}\right| = 0, \quad \text{where} \qquad (13)$$

$$k = 0,2,3, \ldots .$$

An examination of Equations (12) and (13) reveals that these equations can both be represented as

$$\left|\underline{E} - \alpha\underline{A} - \frac{k^2\theta^2}{4}\underline{C}\right| = 0, \quad \text{where} \qquad (14)$$

$$k = 0,1,2,3,\ldots .$$

It should be noted that this observation is physically realized when there is no damping in the system. An interpretation of the limiting process implied in Equation (14) will be discussed in the next section.

Consider that the column is loaded with $P_0 + P_1 \cos \theta t$. Then the frequency boundaries can be schematically represented as shown in Figure 5(a) (numerical results are presented in Chapter IV). Note that γ is the eigenvalue of Equation (14) for $k = 2$. If the amplitude of the oscillating load, $P_1 \cos \theta t$ is reduced slowly when the system is just on the 2T or T type frequency boundary as shown in Figure 5(a), then the system will be vibrating with initial load at a frequency defined by the curves shown in Figure 5(b). Thus the equations which express the conditions for existence of solutions with the same period coincide in pairs when $\beta \to 0$ i.e. $P_1 \to 0$. This means that the regions of instability, bounded by solutions with same period, degenerate into curves.* These regions are determined from Equation (14).

In the following sections special cases of physical interest are considered (free vibration and buckling) and discussed in connection with Equation (14).

Free Vibration

It was pointed out in Chapter I that if the load is independent of time, then the parametric excitation problem reduces to a free

---

*Each of these degenerate curves may be physically visualized as a limiting process in which a resonance response is initiated for a very small value of P_1. This response may then be used as an initial condition to develop the indicated oscillations for $P_1 = 0$.

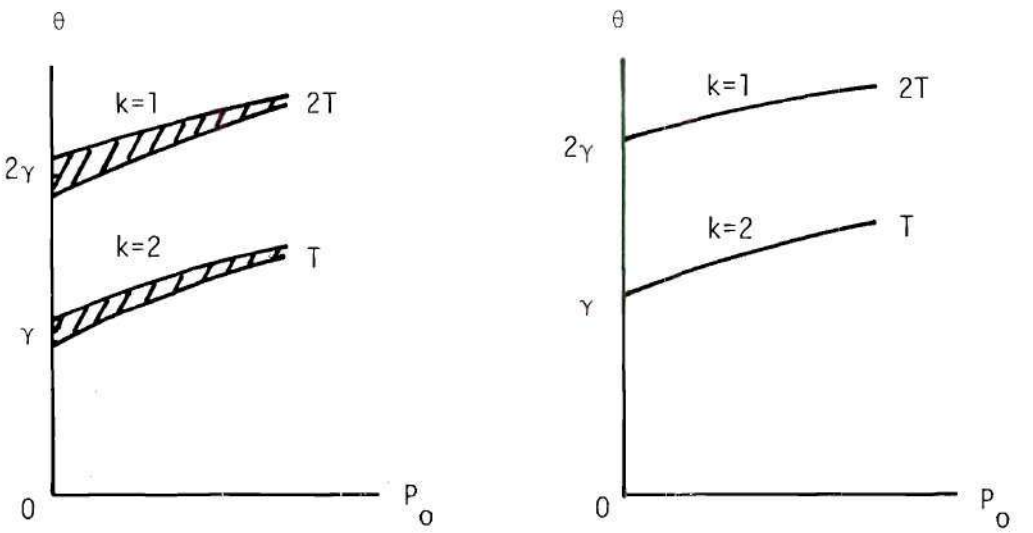

(a) P_1 = Constant > 0 (b) P_1 = Zero

Figure 5. Schematic Representation of Dynamic Instability, P_1 = Constant > 0 and P_1 = Zero.

vibration with initial load. When $\beta = 0$ in Equation (6), the equation of the free vibration can be identified as

$$\underline{C}\frac{d^2\underset{\sim}{f}(t)}{dt^2} + [\underline{E} - \alpha\underline{A}]\underset{\sim}{f}(t) = \underset{\sim}{0} \qquad (15a)$$

Using $\underset{\sim}{f}(t) = \underset{\sim}{a}e^{i\Omega t}$ as a solution for simple harmonic motion in the above equation gives the following characteristic equation of the eigenvalue problem associated with free vibration:

$$|\underline{E} - \alpha\underline{A} - \Omega^2\underline{C}| = 0\,, \qquad (15)$$

where Ω is the eigenvalue parameter. That is, the roots for Ω in the characteristic equation are the natural frequencies of free vibration with initial load.

Comparison of Equations (14) and (15)

A comparison of Equations (14) and (15) reveals that

$$\frac{k^2\theta^2}{4} = \Omega \text{ for } k = 1,2,3,\ldots\ ;$$

or

$$\theta = \frac{2\Omega}{k} \quad \text{for } k = 1,2,3\ldots\ . \qquad (16)$$

If definition of the lowest natural frequency of free vibration is ω, then $\Omega = \omega$ for $P_o = 0$. Therefore Equation (17) may be written as

$$\theta = \frac{2\omega}{k} \quad \text{for } P_o = 0\ .$$

Examination of Figures 5(a) and 5(b) now reveals that

$$\gamma = \omega.$$

That is, the value of γ indicated in Figures 5(a) and 5(b) can be related to a value of natural frequency associated with free vibration. Equation (16) is valid, of course, for $P_1 \neq 0$.

The preceding correlation can be useful in preliminary considerations of dynamic stability behavior. This follows from the fact that for vanishingly small values of P_1, the frequencies of the excitation force near which unboundedly increasing vibrations are possible can be determined from the above equation. However, if the excitation frequency of the force near which unbounded vibrations occur is known then frequency of free vibrations can be calculated from Equation (16) for each value of k.

Buckling

Note that if the displacement and the load are independent of time, then the eigenvalue problem associated with buckling is obtained. The characteristic equation of this problem can be obtained from Equation (6) by setting $\frac{d^2\tilde{f}}{dt^2} = 0$ and $\beta = 0$. Thus,

$$|\underline{E} - \alpha \underline{A}| = 0, \quad \text{where} \tag{17}$$

$\alpha = -\frac{P_o \pi^2}{m\ell^2}$ is the eigenvalue parameter which represents the buckling load. It should also be noted that in Equation (14) this corresponds to the case k = 0.

The characteristic equation for buckling can therefore be extracted either prior to or after substitution for $\underset{\sim}{f}$ in Equation (15a).

In the next section approximate equations for the boundary frequencies are presented.

Approximate Equation for Frequency Boundary

An approximate expression for the boundaries of the principal regions of instability is obtained by equating to zero the determinant of the first matrix element in the principal diagonal of Equation (8).

$$|\underline{E} - \alpha \underline{A} \pm \frac{1}{2}\beta \underline{B} - \frac{1}{4}\theta^2 \underline{C}| = 0 . \tag{18}$$

This approximation is equivalent to the assumption that the periodic solutions on the boundaries of principal regions of instability are harmonic functions [2],

$$\underset{\sim}{f}(t) = \underset{\sim}{a}_1 \sin \frac{\theta t}{2} + \underset{\sim}{b}_1 \cos \frac{\theta t}{2} . \tag{18a}$$

Similarly, the conditions (9) and (10) may be approximated for the calculation of secondary regions of instability as [2],

$$|\underline{E} - \alpha \underline{A} - \theta^2 \underline{C}| = 0 \tag{19}$$

$$\begin{vmatrix} \underline{E} - \alpha \underline{A} & -\beta \underline{B} \\ -\frac{1}{2}\beta \underline{B} & \underline{E} - \alpha \underline{A} - \theta^2 \underline{C} \end{vmatrix} = 0 \tag{20}$$

which correspond to a harmonic approximation

$$\underset{\sim}{f}(t) = \frac{1}{2}\,\underset{\sim}{b}_0 + \underset{\sim}{a}_2 \sin\theta t + \underset{\sim}{b}_2 \cos\theta t \qquad (20a)$$

It can be noted that if Equation (20a) is substituted into Equation (6) and the coefficients of $\sin\theta t$ and $\cos\theta t$ are compared

$$(\underline{E} - \alpha\underline{A})\underset{\sim}{b}_0 - \beta\underline{B}\,\underset{\sim}{b}_2 = 0$$

$$-\frac{1}{2}\beta\underline{B}\,\underset{\sim}{b}_0 + (\underline{E} - \alpha\underline{A} - \theta^2\underline{C})\underset{\sim}{b}_2 = 0$$

where $\sin\theta t\cos\theta t$ and $\cos^2\theta t$ terms are neglected. Since $\underset{\sim}{b}_0$ and $\underset{\sim}{b}_2$ are non-null vectors, Equation (20) is obtained as the condition for existence of the periodic solution with period T. Similarly Equations (18) and (19) can be verified.

It should also be noted that equations (18) correspond to the truncation of the series solution (7) at k = 1. However equations (19) and (20) correspond to the truncation of the series solution (8a) at k = 2. Thus, k = 1 and k = 2 yield the boundaries of instability for the principal and secondary regions respectively. Naturally, for more accuracy in the calculation of the boundary frequencies of the principal zone, an approximation involving a truncation of the series solutions (7) at larger values of k may be required. With approximations k > 2 not only more accurate results for the principal zones are obtained, but also additional zones of instability are obtained. These zones are defined as the third, fourth,... instability zones.

Theoretically, it is possible to obtain instability zones for any odd integral value of k. However, literature survey and the experimental results reported in this thesis indicate that zones corresponding to k = 3,5,7... could not be observed experimentally. These observations

may be expected due to the smaller size of these zones and the effect of presence of structural damping in the system [2]. Similarly, instability zones corresponding to k = 4,6,8... can be obtained, but again experimental results did not verify their presence. However, an investigation of improved results for the first principal and secondary zones due to k = 3 and k = 4 was considered. It was found that the boundary frequency values were improved by less than one percent. Typical numerical results and the analysis for k = 3 and k = 4 are presented in Appendix B. Also it should be noted that the equations for determining free vibration frequencies of a loaded system and the corresponding boundaries of static stability are Equations (15) and (17). An examination of these equations reveals that the harmonic solutions corresponding to $k \geq 3$ do not have any influence on the calculations of the first or second free vibration frequency and buckling load.

The matrix elements, $\underline{E}$, $\underline{A}$, $\underline{B}$ and $\underline{C}$ are of ∞ by ∞ order. The order of these elements is determined by the number of deflection functions used among $\{\sin \frac{n\pi x}{\ell}\}_{n=1}^{\infty}$ in Lagrange's formulation of the problem. To make the stability analysis tractable, it is necessary to approximate the actual deflection shape by a finite number of functions. This means that finite number of deflection shapes must be cautiously selected to represent the dynamic behavior of the column with sufficient accuracy. Three example cases are considered to illustrate this approximation in conjunction with the stability determinants of Equations (18) through (20) and (15) and (17). These analyses are presented in the next three sub-sections.

Case I

Let the deflection shape of the subject column be represented by $\sin \frac{\pi x}{\ell}$. Then the matrices involved in Equation (6) become ,

$$\underline{A} = \underline{B} = \underline{C} = 1$$

$$\underline{E} = \frac{EI}{m} \left(\frac{\pi}{\ell}\right)^4 \left(1 + \frac{\bar{e}_{11}}{\ell}\right)$$

$$\alpha = - \frac{P_o}{m} \left(\frac{\pi}{\ell}\right)^2 \tag{21}$$

$$\beta = - \frac{P_1}{m} \left(\frac{\pi}{\ell}\right)^2$$

where, $\bar{e}_{11} = \left(\frac{K}{I} - 1\right) e_{11} = \left(\frac{K}{I} - 1\right)\left(R - \frac{\ell}{2\pi} \cos \frac{2\pi C}{\ell} \sin \frac{2\pi R}{\ell}\right)$.

Substituting Equation (21) into (18) and solving for θ, yields the approximate formula for the boundaries of the principal region,

$$\theta_* = 2\left[\frac{EI}{m} \left(\frac{\pi}{\ell}\right)^4 \left(1 + \frac{\bar{e}_{11}}{\ell}\right) + \frac{1}{m}\left(\frac{\pi}{\ell}\right)^2 \left(P_o \pm \frac{P_1}{2}\right)\right]^{1/2} . \tag{22}$$

Similarly, substituting Equation (21) into (19) and (20) and solving for θ, the formulae for the boundaries of the secondary region are obtained as

$$\theta_* = \left[\frac{EI}{m} \left(\frac{\pi}{\ell}\right)^4 \left(1 + \frac{\bar{e}_{11}}{\ell}\right) + \frac{P_o}{m} \left(\frac{\pi}{\ell}\right)^2\right]^{1/2} , \tag{23}$$

and

$$\theta_* = \left[\frac{EI}{m} \left(\frac{\pi}{\ell}\right)^4 \left(1 + \frac{\bar{e}_{11}}{\ell}\right) + \frac{P_o}{m} \left(\frac{\pi}{\ell}\right)^2 - \frac{\left(\frac{P_1}{m}\right)^2 \left(\frac{\pi}{\ell}\right)^4}{2\left[\frac{EI}{m} \left(\frac{\pi}{\ell}\right)^4 \left(1 + \frac{\bar{e}_{11}}{\ell}\right) + \frac{P_o}{m}\left(\frac{\pi}{\ell}\right)^2\right]}\right]^{1/2} \tag{24}$$

Using Equation (21) in (15) yields the free vibration frequency of the loaded column:

$$\Omega_{\star} = \left[\frac{EI}{m} \left(\frac{\pi}{\ell}\right)^4 \left(1 + \frac{\bar{e}_{11}}{\ell}\right) + \frac{P_o}{m} \left(\frac{\pi}{\ell}\right)^2 \right]^{1/2} \tag{25}$$

Thus, the results for the dynamic stability of Case I can be schematically represented as shown in Figure 6. A three dimensional schematic representation of the primary and the secondary regions is given in Appendix B. To obtain the boundaries of static stability, Equations (21) and (17) are used to solve for P_o.

$$P_{\star} = - \frac{EI\pi^2}{\ell^2} \left(1 + \frac{\bar{e}_{11}}{\ell}\right) . \tag{26}$$

It may be noted here that the negative sign in Equation (26) means that the buckling load is in the opposite direction of the external P_o as shown in Figure 3. Also, the effect of the region of discontinuities, namely the region from x = a to x = b with cracks or notches, on $\theta_{\star}$, $\Omega_{\star}$ and $P_{\star}$ is included in the term $\bar{e}_{11}$. That is, as noted earlier $\bar{e}_{ni} \triangleq \left(\frac{K}{I} - 1\right) e_{ni}$, where K is implicitly defined in Equation (3).

An examination of the matrix, $\underline{E}$, in the equation of motion reveals that in general it must be a non-diagonal matrix. This implies that the representation of the deflection shape of the subject column by only $\sin \frac{\pi x}{\ell}$ may not be sufficient. Nevertheless, the above development yields formulae for the preliminary design of a column with discontinuities and a periodic external load. A more refined stability analysis is presented in the next sub-section.

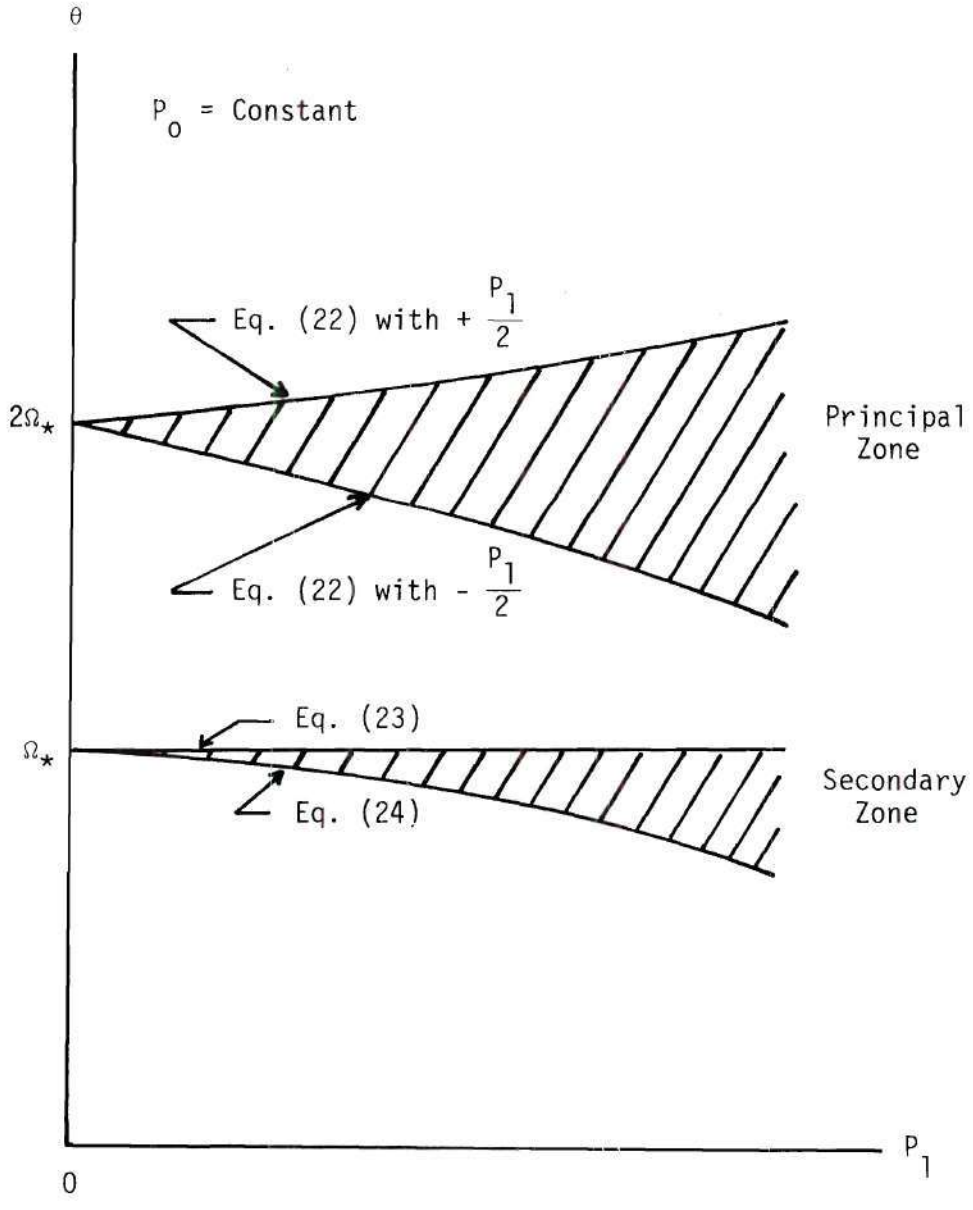

Figure 6. Schematic Presentation of Instability Zones for Case I.

Case II

The deflection shape of the column was represented by $\sin \frac{\pi x}{\ell}$ to derive the stability criteria of Equations (23) through (26) in the last sub-section. It was noted that these results are perhaps over simplified for the stability behavior of the column. In this section a more refined analysis is presented and additional characteristic features of the stability behavior are deduced.

Representing the deflection shape of the column by $\sin \frac{\pi x}{\ell}$ and $\sin \frac{2\pi x}{\ell}$ (the first two functions among the $\{\sin \frac{n\pi x}{\ell}\}_1^\infty$ are used in Equation (27)), the matrices involved in the equation of motion become,

$$\underline{A} = \underline{B} = \begin{bmatrix} 1 & 0 \\ 0 & 2^2 \end{bmatrix},$$

$$\underline{C} = \begin{bmatrix} 1 & 0 \\ 0 & 1 \end{bmatrix},$$

$$\underline{E} = \omega^2 \begin{bmatrix} 1 + \frac{\bar{e}_{11}}{\ell} & 2^2 \frac{\bar{e}_{12}}{\ell} \\ 2^2 \frac{\bar{e}_{21}}{\ell} & 2^4 + 2^4 \frac{\bar{e}_{22}}{\ell} \end{bmatrix}, \text{ where} \qquad (27)$$

$$\begin{bmatrix} \bar{e}_{11} & \bar{e}_{12} \\ \bar{e}_{21} & \bar{e}_{22} \end{bmatrix} \triangleq \left(\frac{K}{I} - 1\right) \begin{bmatrix} R - \frac{\ell}{2\pi} \cos \frac{2\pi C}{\ell} \sin \frac{2\pi R}{\ell} & \frac{1}{\pi} \cos \frac{\pi C}{\ell} \sin \frac{\pi R}{\ell} - \frac{\ell}{3\pi} \cos \frac{3\pi C}{\ell} \sin \frac{3\pi R}{\ell} \\ \frac{\ell}{\pi} \cos \frac{\pi C}{\ell} \sin \frac{\pi R}{\ell} - \frac{\ell}{3\pi} \cos \frac{3\pi C}{\ell} \sin \frac{3\pi R}{\ell} & R - \frac{\ell}{4\pi} \cos \frac{4\pi C}{\ell} \sin \frac{4\pi R}{\ell} \end{bmatrix}$$

and $$\alpha = -\frac{P_o}{m}\left(\frac{\pi}{\ell}\right)^2,\ \beta = -\frac{R}{m}\left(\frac{\pi}{\ell}\right)^2 \text{ and } \omega^2 = \frac{EI}{m}\left(\frac{\pi}{\ell}\right)^4 .$$

Substituting Equation (27) into (18) yields the equations for the boundaries of principal regions as

$$\begin{vmatrix} \omega^2\left(1 + \frac{\bar{e}_{11}}{\ell}\right) - \alpha \pm \frac{1}{2}\beta - \frac{1}{4}\theta^2 & 4\frac{\bar{e}_{12}}{\ell}\omega^2 \\ 4\frac{\bar{e}_{21}}{\ell}\omega^2 & \omega^2\left(2^4 + 2^4\frac{\bar{e}_{22}}{\ell}\right) - 4\alpha \pm 2\beta - \frac{1}{4}\theta^2 \end{vmatrix} = 0. \quad (28)$$

Equation (28) represents two quartic equations in θ. These two equations (equations corresponding to $\pm$ sign in the determinant of Equation (28)) are the conditions under which the equation of motion has periodic solutions,

$$\underset{\sim}{f}(t) = \underset{\sim}{a}_1 \sin\frac{\theta t}{2} + \underset{\sim}{b}_1 \cos\frac{\theta t}{2} \quad (29)$$

with period $2T = \frac{4\pi}{\theta}$. Formally, denote

$$\begin{aligned} d_1 &= \omega^2\left(1 + \frac{\bar{e}_{11}}{\ell}\right) - \alpha \pm \frac{1}{2}\beta \\ d_2 &= \omega^2\left(16 + 16\frac{\bar{e}_{22}}{\ell}\right) - 4\alpha \pm 2\beta \quad (30) \\ d_3 &= 4\frac{\bar{e}_{12}}{\ell}\omega^2 \end{aligned}$$

in the determinantal Equation (28). Then expanding the determinant yields

$$\theta^4 - 4(d_1 + d_2)\theta^2 - 16(d_3^2 - d_1 d_2) = 0 . \quad (31)$$

The solutions to this equation can be written as

$$\theta_1 = \sqrt{2}\,[(d_1 + d_2) + \sqrt{(d_1 - d_2)^2 + 4d_3^2}\,]^{1/2},$$

$$\theta_2 = -\sqrt{2}\,[(d_1 + d_2) + \sqrt{(d_1 - d_2)^2 + 4d_3^2}\,]^{1/2},$$

$$\theta_3 = \sqrt{2}\,[(d_1 + d_2) - \sqrt{(d_1 - d_2)^2 + 4d_3^2}\,]^{1/2}, \text{ and} \tag{32}$$

$$\theta_4 = -\sqrt{2}\,[(d_1 + d_2) - \sqrt{(d_1 - d_2)^2 + 4d_3^2}\,]^{1/2}.$$

Since d_1 and d_2 each represent two definitions, there are eight roots of Equation (31). These roots may in general be complex, imaginary or real. To examine the above possibilities, consider the quantity

$$(d_1 - d_2)^2 + 4d_3^2$$

in Equations (32). Clearly, this quantity is positive since d_1, d_2 and d_3 are real functions of the physical parameters, P_o, P_1, EI, K, ℓ etc. This means that none of the roots in Equations (32) can be complex.

To examine the remaining possibilities, consider the quadratic formula

$$\theta^2 = 2\,[(d_1 + d_2) \pm \sqrt{(d_1 + d_2)^2 + 4(d_3^2 - d_1 d_2)}\,] \tag{33}$$

which is equivalent to Equation (32). If $\theta^2 < 0$, imaginary roots will be obtained. If $\theta^2 > 0$, real roots will be obtained.

For the positive sign, $\theta^2 > 0$ if $d_1 > 0$ (an examination of Equations (30) reveals for small values of $\frac{\bar{e}_{11}}{\ell}$ and $\frac{\bar{e}_{22}}{\ell}$. $d_2 > d_1$ and $(d_1 + d_2) > 0$ if $d_1 > 0$.). This corresponds to a condition on the applied load $-P_o - P_1$; i.e., it must be greater than the lowest buckling load (compressive loads are negative in this development).

Examination of Equation (33) with the negative sign reveals that $\theta^2 < 0$, if $(d_3^2 - d_1 d_2) > 0$. Thus, if $d_3^2 > d_1 d_2$, imaginary roots may be obtained from negative sign of Equation (33). Conversely, if $d_3^2 < d_1 d_2$, real roots are obtained.

Further examination of the inequality $d_3^2 < d_1 d_2$ reveals that this also corresponds to a condition on the applied load. That is, compressive loads exceeding the lowest buckling load cannot be permitted.

To illustrate this, recall that the buckling loads are evaluated using Equation (17).

$$|\underline{E} - \alpha \underline{A}| = 0, \quad \text{where } \alpha = -\frac{P_o}{m}\left(\frac{\pi}{\ell}\right)^2 .$$

Suppose that the column is loaded with the first buckling load, P_{*1}, as shown in Figure 7. Note that $P_1 > 0$, $P_1 > 0$, $P_o > 0$, and negative sign indicates compression. Substituting Equation (27) into (17) and expanding the determinant yields

$$[\omega^2(1 + \frac{\bar{e}_{11}}{\ell}) - \alpha^*][16\omega^2(1 + \frac{\bar{e}_{22}}{\ell}) - 4\alpha^*] = d_3^2 , \qquad (33a)$$

where $$\alpha^* = -\frac{P_{*1}}{m}\left(\frac{\pi}{\ell}\right)^2 = -\frac{P_o + P_1}{m}\left(\frac{\pi}{\ell}\right)^2 .$$

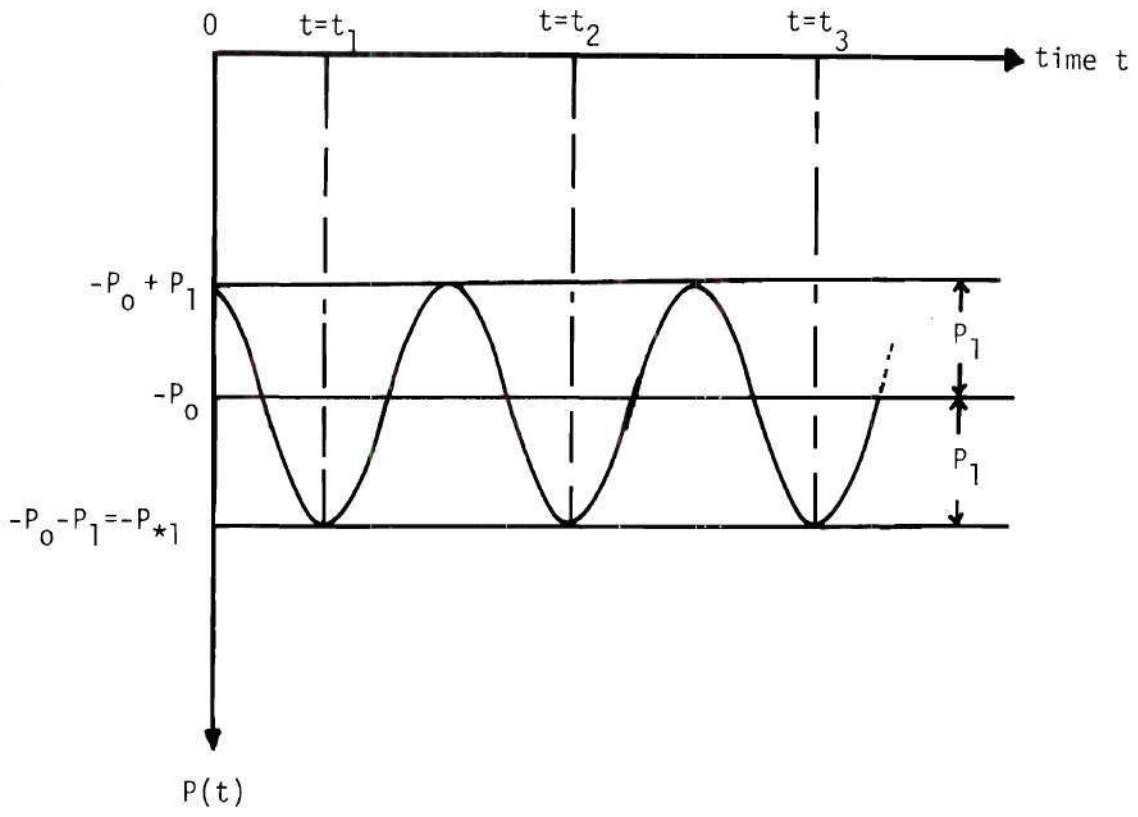

Figure 7. Schematic for the Column Load-Time History.

An examination of the above equation reveals that $d_3^2 \geq 0$. If $d_3^2 > 0$, then left hand side of (33a) must be positive. It follows from Equations (30) that

$$d_1 d_2 = \left[\omega^2\left(1 + \frac{\bar{e}_{11}}{\ell}\right) - \alpha \pm \frac{\beta}{2}\right]\left[16\omega^2\left(1 + \frac{\bar{e}_{22}}{\ell}\right) - 4\alpha \pm 2\beta\right],$$

where $\beta = -\frac{P_1}{m}\left(\frac{\pi}{\ell}\right)^2$. At the buckling load (points $t = t_1$ and $t = t_2$) the above equation assumes the form,

$$d_1 d_2 = \left[\omega^2\left(1 + \frac{\bar{e}_{11}}{\ell}\right) - \alpha^*\right]\left[16\omega^2\left(1 + \frac{\bar{e}_{22}}{\ell}\right) - 4\alpha^*\right]$$

$$= \text{left hand side of Equation (33a)} .$$

Therefore if $|-P_0 - P_1| > |P_{*1}|$ then $d_1 d_2 < d_3^2$ and the column is loaded beyond the first buckling load. Similarly it can be shown that the column is loaded beyond the first buckling load when $d_3^2 = 0$ and $d_1 d_2 < d_3^2$.

It follows then that if the above inequalities are satisfied, Equations (31) yields eight real roots, four pairs of plus and minus real roots for θ. The negative root may be dropped, since it is merely equivalent to a phase shift in the solution given by Equation (29). Thus θ_1 and θ_3 roots are two positive roots of Equation (31) which describe the boundaries of the instability regions. θ_3 corresponds to the boundaries for the lowest region and θ_1 the next higher region.

Similarly, the condition for an imaginary root for Case I can be obtained. For columns in the post buckling range an analysis developed by Lubkin and Stoker [29] should be consulted. It may be noted that

their analysis involved uncoupled Mathieu equations for uniform columns (no region of discontinuity). For a post buckling analysis a new system of equations of motion must be formulated for the column with discontinuities. The present investigation is limited to columns loaded below the buckling load.

The boundaries of the principal regions of instability can be found from Equation (28) using the method of successive approximations (Appendix B) as described below.

Setting the first element of the diagonal of equation (28) to zero and solving for θ gives

$$\theta = 2\left[\omega^2\left(1 + \frac{\bar{e}_{11}}{\ell}\right) - \alpha \pm \frac{1}{2}\beta\right]^{1/2} \tag{34}$$

Substituting Equation (34) into the second element on the principal diagonal of the determinant in Equation (28), setting the determinant equal to zero, and solving for θ yields,

$$\theta_\star = 2\left[\omega^2\left(1 + \frac{\bar{e}_{11}}{\ell}\right) - \alpha \pm \frac{1}{2}\beta - c_1\omega^2\right]^{1/2},$$

where

$$c_1 = \frac{\dfrac{16\bar{e}_{12}\bar{e}_{21}}{\ell^2}}{15 + 16\,\dfrac{\bar{e}_{22}}{\ell} - \dfrac{\bar{e}_{11}}{\ell} - \dfrac{3\alpha}{\omega^2} \pm \dfrac{3}{2}\,\dfrac{\beta}{\omega^2}}. \tag{35}$$

Equation (35) is called the first successive approximation to θ and the term c_1 may be considered as a first correction to the initial approxi-

mation given by Equation (34). Substitution of Equation (35) into the second element on the principal diagonal of the determinant in the Equation (28) and solving for θ yields

$$\theta_* = 2[\omega^2(1 + \frac{\bar{e}_{11}}{\ell}) - \alpha \pm \frac{1}{2}\beta - c_2\omega^2]^{1/2},$$

$$c_2 \triangleq \frac{(\frac{16\bar{e}_{12}\bar{e}_{21}}{\ell^2})}{(15 + 16\frac{\bar{e}_{22}}{\ell} - \frac{\bar{e}_{11}}{\ell} - 3\frac{\alpha}{\omega^2} \pm \frac{3}{2}\frac{\beta}{\omega^2} + c_1)}. \tag{36}$$

Equation (36) represents the second successive approximation to θ and c_2 is the corresponding second correction. This process of successive approximations may be continued until the corresponding numerical values of corrections do not change significantly.

Similarly, setting the second element on the diagonal of Equation (28) equal to zero and solving for θ gives

$$\theta_* = 2[\omega^2(16 + 16\frac{\bar{e}_{22}}{\ell}) - 4\alpha \pm 2\beta]^{1/2}. \tag{37}$$

Substituting Equation (37) into the first element on the principal diagonal of determinant in Equation (28), setting the determinant equal to zero, and solving for θ gives

$$\theta_* = 2[\omega^2(16 + 16\frac{\bar{e}_{22}}{\ell}) - 4\alpha \pm 2\beta + c_1\omega^2]^{1/2}, \tag{38}$$

where c_1 is defined by Equation (35). Equation (38) is the first successive approximation with the initial approximation given by Equa-

tion (37) and the corresponding second successive approximation is

$$\theta_* = 2[\omega^2(16 + 16\frac{\bar{e}_{22}}{\ell}) - 4\alpha \pm 2\beta + c_2\omega^2]^{1/2}, \qquad (39)$$

where c_2 is given by Equation (36).

Thus, the analysis of Case II provides the location of the boundaries of the first two principal regions as depicted qualitatively in Figure 8. It is clear that the instability zone A is of interest from a practical viewpoint because it occurs at lower frequency range.

Corresponding to each principal instability zone, i.e. A and B, there exists a secondary instability zone, a free vibration frequency boundary and a buckling load. Using Equations (27) in (19) and applying the above successive approximation technique, the first two successive approximations formulae for the lower boundary frequencies of the first secondary zone of instability are obtained as

$$\theta_* = [\omega^2(1 + \frac{\bar{e}_{11}}{\ell}) - \alpha - \bar{c}_1\omega^2]^{1/2}, \text{ where} \qquad (40)$$

$$\bar{c}_1 = \frac{\frac{16\bar{e}_{12}\bar{e}_{21}}{\ell^2}}{15 + 16\frac{\bar{e}_{22}}{\ell} - \frac{\bar{e}_{11}}{\ell} - \frac{3\alpha}{\omega^2}}; \text{ and}$$

$$\theta_* = [\omega^2(1 + \frac{\bar{e}_{11}}{\ell} - \alpha - \bar{c}_2\omega^2]^{1/2}, \text{ where} \qquad (41)$$

(cont.)

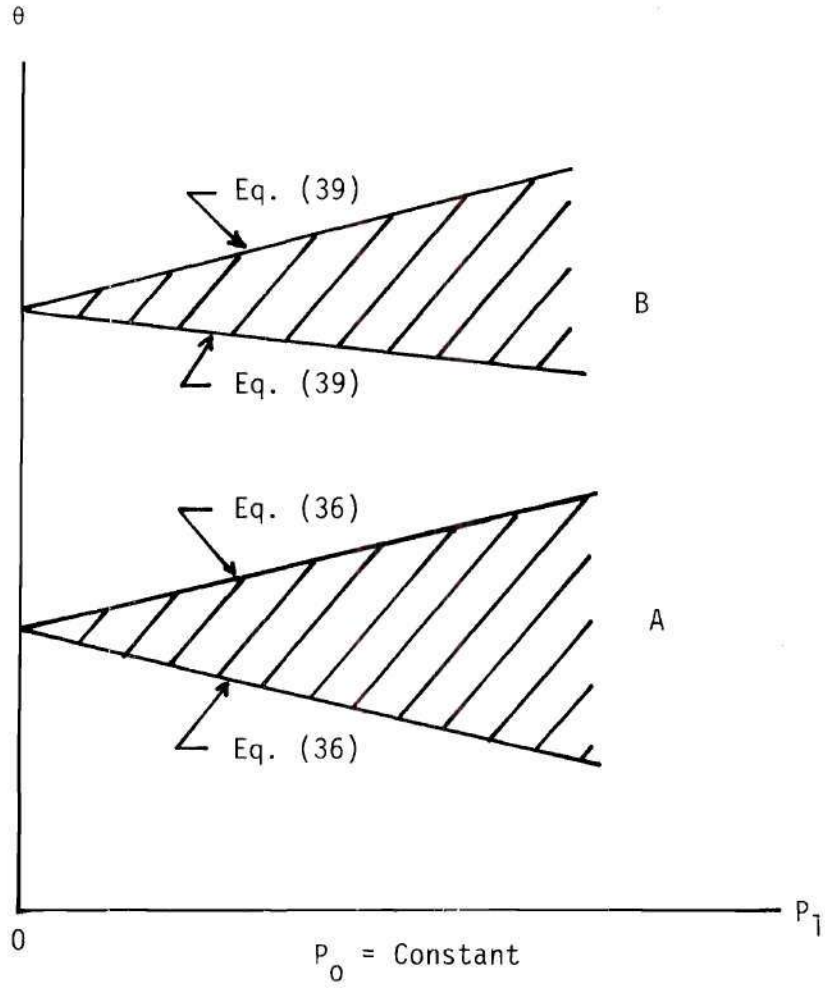

Figure 8. Schematic Presentation of Principal Zones for Case II.

$$\bar{c}_2 = \frac{\dfrac{16\bar{e}_{12}\bar{e}_{21}}{\ell^2}}{15 + 16\,\dfrac{\bar{e}_{22}}{\ell} - 3\,\dfrac{\alpha}{\omega^2} + \bar{c}_1} \quad .$$

Similarly, for the secondary zone the first two successive approximations formulae for the lower boundary frequency are

$$\theta_* = \left[\omega^2\left(16 + 16\,\frac{\bar{e}_{22}}{\ell}\right) - 4\alpha + \bar{c}_1\omega^2\right]^{1/2} \quad \text{and} \tag{42}$$

$$\theta_* = \left[\omega^2\left(16 + 16\,\frac{\bar{e}_{22}}{\ell}\right) - 4\alpha + \bar{c}_2\omega^2\right]^{1/2} , \tag{43}$$

where $\bar{c}_1$ and $\bar{c}_2$ are defined in Equations (40) and (41) respectively. Note that $\bar{c}_1 = c_1\big|_{\beta=0}$ and $\bar{c}_2 = c_2\big|_{\beta=0,c_1=\bar{c}_1}$.

Use of Equations (27) in (20) gives a formula for the upper boundary frequencies of the secondary zone. If Equations (27) are substituted into (20), then the upper boundary frequency corresponding to the first secondary zone is obtained from the determinantal equation:

$$\begin{vmatrix} \omega^2\left(1+\dfrac{\bar{e}_{11}}{\ell}\right) - \alpha & 4\,\dfrac{\bar{e}_{12}}{\ell}\,\omega^2 & -\beta & 0 \\ 4\,\dfrac{\bar{e}_{21}}{\ell}\,\omega^2 & \omega^2\left(16+16\,\dfrac{\bar{e}_{22}}{\ell}\right) - 4\alpha & 0 & -4\beta \\ -\dfrac{1}{2}\,\beta & 0 & \omega^2\left(1+\dfrac{\bar{e}_{11}}{\ell}\right)-\alpha-\theta^2 & 4\,\dfrac{\bar{e}_{12}}{\ell}\,\omega^2 \\ 0 & -2\beta & 4\,\dfrac{\bar{e}_{21}}{\ell}\,\omega^2 & \omega^2\left(16+16\,\dfrac{\bar{e}_{22}}{\ell}\right)-4\alpha-\theta^2 \end{vmatrix} = 0 \tag{44}$$

Setting the third element on the principal diagonal in the determinant of Equation (44) equal to zero and solving for θ gives

$$\theta = [\omega^2(1 + \frac{\bar{e}_{11}}{\ell}) - \alpha]^{1/2}.$$

Clearly, this initial approximation to obtain the results for the first secondary zone of instability is natural since the zone is located near the first fundamental frequency of vibration (Figure 5(a)T type solution).

Using the above equation in the last element on the principal diagonal of the determinant in Equation (44), and expanding it by the third column yields:

$$-\beta \begin{vmatrix} 4\frac{\bar{e}_{21}\omega^2}{\ell} & \omega^2(16 + 16\frac{\bar{e}_{22}}{\ell}) - 4\alpha & -4\beta \\ -\frac{1}{2}\beta & 0 & 4\frac{\bar{e}_{12}\omega^2}{\ell} \\ 0 & -2\beta & \omega^2(15 + 16\frac{\bar{e}_{22}}{\ell} - \frac{\bar{e}_{11}}{\ell}) - 3\alpha \end{vmatrix}$$

$$+[\omega^2(1 + \frac{\bar{e}_{11}}{\ell}) - \alpha - \theta^2] \begin{vmatrix} \omega^2(1 + \frac{\bar{e}_{11}}{\ell}) - \alpha & 4\frac{\bar{e}_{12}\omega^2}{\ell} & 0 \\ 4\frac{e_{21}\omega^2}{\ell} & \omega^2(16 + 16\frac{\bar{e}_{22}}{\ell}) - 4\alpha & -4\beta \\ 0 & -2\beta & \omega^2(15 + 16\frac{\bar{e}_{22}}{\ell} - \frac{\bar{e}_{11}}{\ell}) - 3\alpha \end{vmatrix}$$

$$-4\,\frac{\bar{e}_{21}\omega^2}{\ell}\begin{vmatrix} \omega^2\left(1+\frac{\bar{e}_{11}}{\ell}\right)-\alpha & 4\,\frac{\bar{e}_{12}\omega^2}{\ell} & 0 \\ 4\,\frac{\bar{e}_{21}\omega^2}{\ell} & \omega^2\left(16+16\,\frac{\bar{e}_{22}}{\ell}\right)-4\alpha & -4\beta \\ -\frac{1}{2}\,\beta & 0 & 4\,\frac{\bar{e}_{12}\omega^2}{\ell} \end{vmatrix} = 0\,.$$

Denoting $\|D_1\|$, $\|D_2\|$ and $\|D_3\|$ as the minors of the non-zero elements of the third column in the determinant of Equation (44) and solving for θ gives

$$\theta_\star = \left[\omega^2\left(1+\frac{\bar{e}_{11}}{\ell}\right) - \alpha - \beta\,\frac{\|D_1\|}{\|D_2\|} - 4\,\frac{\bar{e}_{21}\omega^2}{\ell}\,\frac{\|D_3\|}{\|D_2\|}\right]^{1/2}, \qquad (45)$$

where

$$\|D_1\| = \frac{1}{2}\,\beta\left[[16\omega^2\left(1+\frac{\bar{e}_{22}}{\ell}\right)-4\alpha]\left[\left(15+16\,\frac{\bar{e}_{22}}{\ell}-\frac{\bar{e}_{11}}{\ell}\right)\omega^2-3\alpha\right]-16\beta^2+\left(4\,\frac{\bar{e}_{12}\omega^2}{\ell}\right)^2\right],$$

$$\|D_2\| = \left[\omega^2\left(1+\frac{\bar{e}_{11}}{\ell}\right)-\alpha\right]\left[[16\omega^2\left(1+\frac{\bar{e}_{22}}{\ell}\right)-4\alpha]\left[15+16\,\frac{\bar{e}_{22}}{\ell}-\frac{\bar{e}_{11}}{\ell}-3\alpha\right]\omega^2-8\beta^2\right]$$

$$-\left(4\,\frac{\bar{e}_{12}\omega^2}{\ell}\right)^2\left[\left(15+16\,\frac{\bar{e}_{22}}{\ell}-\frac{\bar{e}_{11}}{\ell}\right)\omega^2-3\alpha\right]$$

$$\|D_3\| = 4\,\frac{\bar{e}_{12}\omega^2}{\ell}\left[\left[\omega^2\left(1+\frac{\bar{e}_{11}}{\ell}\right)-\alpha\right]\left[16\omega^2\left(1+\frac{\bar{e}_{22}}{\ell}\right)-4\alpha\right]-\left[4\,\frac{\bar{e}_{12}\omega^2}{\ell}\right]^2+2\beta^2\right].$$

Thus, Equations (45) and (40) are formulae* for the upper and lower boundary frequencies of the secondary zone of instability corresponding to the principal zone A in Figure 8. Similarly, the results

*Appendix B: Discussion on Equations (45) and (40).

for the second boundary corresponding to Equation (42) is obtained as

$$\theta_{\star} = \left[16\omega^2\left(1+\frac{\bar{e}_{22}}{\ell}\right) - 4\alpha - 4\beta\,\frac{\|\bar{D}_1\|}{\|\bar{D}_2\|} - \frac{4\bar{e}_{12}\omega^2}{\ell}\,\frac{\|\bar{D}_2\|}{\|\bar{D}_2\|}\right]^{1/2}, \qquad (46)$$

where

$$\|\bar{D}_1\| = -\beta\left[2\left[\omega^2\left(1+\frac{\bar{e}_{11}}{\ell}\right)-\alpha\right]\left[\omega^2\left(15+16\,\frac{\bar{e}_{22}}{\ell}-\frac{\bar{e}_{11}}{\ell}\right)-3\alpha\right]-\left(\frac{2\bar{e}_{12}\omega^2}{\ell}\right)^2-\beta^2\right],$$

$$\|\bar{D}_2\| = \left[\omega^2\left(1+\frac{\bar{e}_{11}}{\ell}\right)-\alpha\right]\left[\omega^2\left(16+16\,\frac{\bar{e}_{22}}{\ell}\right)-4\alpha\right]\left[-\frac{1}{2}\,\beta^2-3\alpha+\omega^2\left(15+16\frac{\bar{e}_{22}}{\ell}-\frac{\bar{e}_{11}}{\ell}\right)\right]$$

$$-\left[\omega^2\left(15+16\,\frac{\bar{e}_{22}}{\ell}-\frac{\bar{e}_{11}}{\ell}\right)-3\alpha\right]\left[4\,\frac{\bar{e}_{12}\bar{e}_{21}\omega^2}{\ell}\right]^2, \text{ and}$$

$$\|\bar{D}_3\| = \left[\omega^2\left(1+\frac{\bar{e}_{11}}{\ell}\right)-\alpha\right]\left[\omega^2\left(16+16\,\frac{\bar{e}_{22}}{\ell}\right)-4\alpha\right]\left(\frac{4\bar{e}_{12}\bar{e}_{21}}{\ell}\right)^2-\left(\frac{4\bar{e}_{12}\bar{e}_{21}}{\ell}\right)^3-2\beta^2.$$

Substituting Equation (27) into (15) and solving for Ω by the successive approximation procedure, the first and second approximations for the natural frequency with initial load P_o is obtained as

$$\Omega_{\star} = \left[\omega^2\left(1+\frac{\bar{e}_{11}}{\ell}\right) - \alpha - \bar{c}_1\omega^2\right]^{1/2} \text{ and} \qquad (47)$$

$$\Omega_{\star} = \left[\omega^2\left(1+\frac{\bar{e}_{11}}{\ell}\right) - \alpha - \bar{c}_2\omega^2\right]^{1/2}, \text{ where} \qquad (48)$$

$\bar{c}_1$ and $\bar{c}_2$ are defined by Equations (40) and (41) respectively. Equations (47) and (48) are results corresponding to the instability zone A

shown in Figure 8. The natural frequencies associated with the instability zone B are

$$\Omega_* = \left[\omega^2(16 + 16\,\frac{\bar{e}_{22}}{\ell}) - 4\alpha + \bar{c}_1\omega^2\right]^{1/2} \text{ and} \tag{49}$$

$$\Omega_* = \left[\omega^2(16 + 16\,\frac{\bar{e}_{22}}{\ell}) - 4\alpha + \bar{c}_2\omega^2\right]^{1/2}, \text{ where} \tag{50}$$

Equations (49) and (50) are the first and second successive approximations respectively.

Using Equations (27) in (17) and solving for P_o by the method of successive approximations, the buckling load formulae for the first and second successive approximations are obtained as

$$P_* = -\frac{m\ell^2}{\pi^2}\left[\omega^2(1 + \frac{\bar{e}_{11}}{\ell}) - \bar{c}_1\omega^2\right], \quad \text{where}$$

$$\bar{c}_1 = \frac{\dfrac{4\bar{e}_{12}^2}{\ell^2}}{3 + 4\,\dfrac{\bar{e}_{22}}{\ell} - \dfrac{\bar{e}_{11}}{\ell}}\,; \quad \text{and} \tag{51}$$

$$P_* = -(\frac{m\ell^2}{\pi^2})\left[\omega^2(1 + \frac{\bar{e}_{11}}{\ell}) - \bar{c}_2\omega^2\right], \quad \text{where}$$

$$\bar{c}_2 = \frac{\dfrac{4\bar{e}_{12}^2}{\ell^2}}{3 + 4\,\dfrac{\bar{e}_{22}}{\ell} - \dfrac{\bar{e}_{11}}{\ell} + \bar{c}_1}\,. \tag{52}$$

Formula (51) and (52) represent the first buckling load of the column shown in Figure 3. The two successive approximations corresponding to the second buckling load are

$$P_* = -\left(\frac{m\ell^2}{4\pi^2}\right)\left[\omega^2\left(16 + 16\,\frac{\bar{e}_{22}}{\ell}\right) + \bar{c}_1\omega^2\right], \quad \text{and} \tag{53}$$

$$P_* = -\left(\frac{m\ell^2}{4\pi^2}\right)\left[\omega^2\left(16 + 16\,\frac{\bar{e}_{22}}{\ell}\right) + 4\bar{c}_2\omega^2\right] . \tag{54}$$

The results of stability analyses for the case II are summarized in Figure 9. The principal zones A, B and the secondary zones C,D are qualitatively represented in Figure 9. The corresponding free vibration frequencies are indicated by Ω_1, Ω_2 on the θ axis. Substitution of $C = \ell/2$ in $\underline{E}$ of Equation (27) yields

$$\underline{E} = \omega^2 \begin{bmatrix} R + \frac{\ell}{2\pi}\sin\frac{2\pi R}{\ell} & 0 \\ 0 & R - \frac{\ell}{4\pi}\sin\frac{4\pi R}{\ell} \end{bmatrix} \left(\frac{K}{I} - 1\right) .$$

This means that for the special case in which the cracked or notched region is centrally located, Case II does not give better results than Case I. Indeed, in this case Case II reduces to Case I for the first primary and secondary zones.

However, improved results have been obtained for non-central discontinuous regions, and additional results corresponding to the

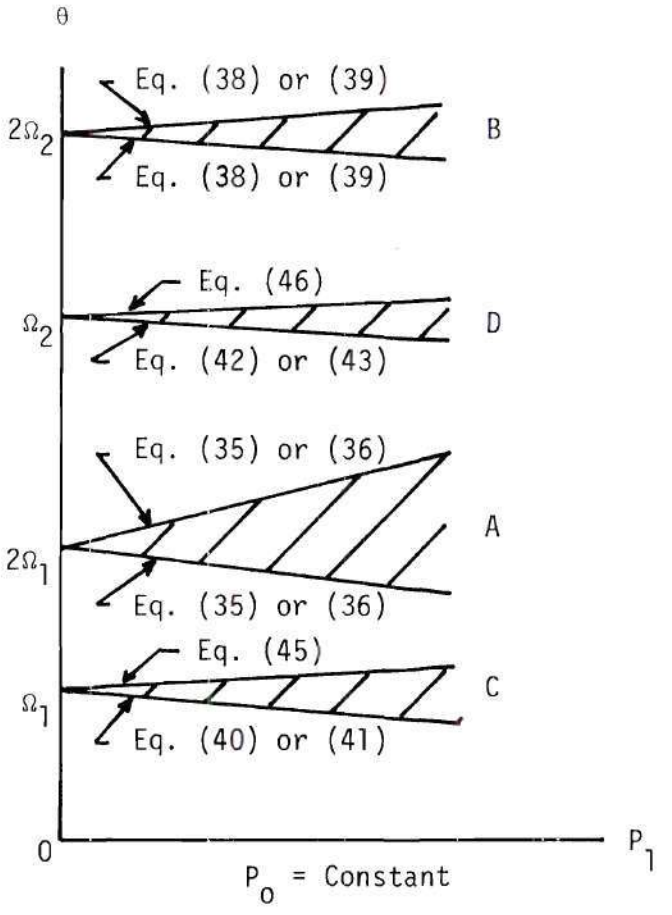

Figure 9. Schematic Presentation of Instability Boundaries for Case II with P_o = Constant.

second principal and secondary zones of instability have also been obtained. In the next subsection improved results are presented for $C = \ell/2$ by use of the method of successive approximations.

Case III

In the last two subsections the stability formulae with the representation of the deflection shape by $\sin \frac{\pi x}{\ell}$ was developed in Case I and with $\sin \frac{\pi x}{\ell}$ and $\sin \frac{2\pi x}{\ell}$ was developed in Case II. Approximations for only the first primary and secondary zones of instability are provided by the stability model of Case I. The first two primary and secondary regions of instability are located in the θ-p characteristic plane by use of the model in Case II. Naturally, a representation of the deflection shape of the column by $\sin \frac{\pi x}{\ell}$, $\sin \frac{2\pi x}{\ell}$ and $\sin \frac{3\pi x}{\ell}$ will provide the first three primary and secondary regions of instability. Physically, among these three zones, the first primary and secondary regions, being in the lower frequency range, are of most interest. Therefore, the following presentation will be restricted to obtaining the first primary and secondary instability regions.

If the deflection shape is represented by $\sin \frac{\pi x}{\ell}$, $\sin \frac{2\pi x}{\ell}$ and $\sin \frac{3\pi x}{\ell}$, then matrices involved in the equations of motion become,

$$\underline{A} = \underline{B} = \begin{bmatrix} 1 & 0 & 0 \\ 0 & 2^2 & 0 \\ 0 & 0 & 3^2 \end{bmatrix}, \tag{55}$$

$$\underline{E} = \omega^2 \begin{bmatrix} 1 + \frac{\bar{e}_{11}}{\ell} & 2^2 \frac{\bar{e}_{12}}{\ell} & 3^2 \frac{\bar{e}_{13}}{\ell} \\ 2^2 \frac{\bar{e}_{21}}{\ell} & 2^4 + 2^4 \frac{\bar{e}_{22}}{\ell} & 2^2 \cdot 3^2 \cdot \frac{\bar{e}_{23}}{\ell} \\ 3^2 \frac{\bar{e}_{31}}{\ell} & 3^2 \cdot 2^2 \frac{\bar{e}_{32}}{\ell} & 3^4 + 3^4 \frac{\bar{e}_{33}}{\ell} \end{bmatrix} \quad \text{where,} \tag{56}$$

$$\begin{bmatrix} \bar{e}_{11} & \bar{e}_{12} & \bar{e}_{13} \\ \bar{e}_{21} & \bar{e}_{22} & \bar{e}_{23} \\ \bar{e}_{31} & \bar{e}_{32} & \bar{e}_{33} \end{bmatrix} \triangleq$$

$$\tilde{\underline{E}} = (\frac{K}{I} - 1) \begin{bmatrix} R - \frac{\ell}{2\pi} \cos\frac{2\pi C}{\ell} \sin\frac{2\pi R}{\ell} & \frac{\ell}{\pi} \cos\frac{\pi C}{\ell} \sin\frac{\pi R}{\ell} - \frac{\ell}{3\pi} \cos\frac{3\pi C}{\ell} \sin\frac{3\pi R}{\ell} & \frac{\ell}{2\pi} \cos\frac{2\pi C}{\ell} \sin\frac{2\pi R}{\ell} - \frac{\ell}{4\pi} \cos\frac{4\pi C}{\ell} \sin\frac{4\pi R}{\ell} \\ \frac{1}{\pi} \cos\frac{\pi C}{\ell} \sin\frac{\pi R}{\ell} - \frac{\ell}{3\pi} \cos\frac{3\pi C}{\ell} \sin\frac{3\pi R}{\ell} & R - \frac{\ell}{4\pi} \cos\frac{4\pi C}{\ell} \sin\frac{4\pi R}{\ell} & \frac{\ell}{\pi} \cos\frac{\pi C}{\ell} \sin\frac{\pi R}{\ell} - \frac{\ell}{5\pi} \cos\frac{5\pi C}{\ell} \sin\frac{5\pi R}{\ell} \\ \frac{\ell}{2\pi} \cos\frac{2\pi C}{\ell} \sin\frac{2\pi R}{\ell} - \frac{\ell}{4\pi} \cos\frac{4\pi C}{\ell} \sin\frac{4\pi R}{\ell} & \frac{\ell}{\pi} \cos\frac{\pi C}{\ell} \sin\frac{\pi R}{\ell} - \frac{\ell}{5\pi} \cos\frac{5\pi C}{\ell} \sin\frac{5\pi R}{\ell} & R - \frac{\ell}{6\pi} \cos\frac{6\pi C}{\ell} \sin\frac{6\pi R}{\ell} \end{bmatrix},$$

and

$$\alpha = -\frac{P_o}{m}(\frac{\pi}{\ell})^2 \ , \quad \beta = -\frac{P_1}{m}(\frac{\pi}{\ell})^2 \quad \text{and} \quad \omega^2 = \frac{EI}{m}(\frac{\pi}{\ell})^4 \ . \tag{57}$$

For the sake of simplicity here the case with $C = \ell/2$ will be considered. Then,

$$\tilde{\underline{E}} = \left(\frac{K}{I} - 1\right) \begin{bmatrix} R + \frac{\ell}{2\pi} \sin \frac{2\pi R}{\ell} & 0 & -\frac{\ell}{2\pi} \sin \frac{2\pi R}{\ell} - \frac{\ell}{4\pi} \sin \frac{4\pi R}{\ell} \\ 0 & R - \frac{\ell}{4\pi} \sin \frac{4\pi R}{\ell} & 0 \\ -\frac{\ell}{2\pi} \sin \frac{2\pi R}{\ell} - \frac{\ell}{4\pi} \sin \frac{4\pi R}{\ell} & 0 & R + \frac{\ell}{6\pi} \sin \frac{6\pi R}{\ell} \end{bmatrix} . \tag{58}$$

It is convenient to rewrite Equation (58) in the following form

$$\tilde{\underline{E}} \triangleq \begin{bmatrix} \hat{e}_{11} & \hat{e}_{12}=0 & \hat{e}_{13} \\ \hat{e}_{21}=0 & \hat{e}_{22} & \hat{e}_{23}=0 \\ \hat{e}_{31} & \hat{e}_{32}=0 & \hat{e}_{33} \end{bmatrix} . \tag{59}$$

Substituting Equation (59) into the $\underline{E}$ matrix of Equation (56) yields

$$\underline{E} = \omega^2 \begin{bmatrix} 1 + \frac{\hat{e}_{11}}{\ell} & 0 & 9\frac{\hat{e}_{13}}{\ell} \\ 0 & 16(1 + \frac{\hat{e}_{22}}{\ell}) & 0 \\ 9\frac{\hat{e}_{31}}{\ell} & 0 & 81(1 + \frac{\hat{e}_{33}}{\ell}) \end{bmatrix} \tag{60}$$

If Equations (55) through (57) and (60) are substituted into Equation (18), the equations for the boundaries of the principal regions are

$$\begin{vmatrix} \omega^2(1+\frac{\hat{e}_{11}}{\ell})-\alpha\pm\frac{1}{2}\beta-\frac{1}{4}\theta^2 & 0 & 9\frac{\hat{e}_{13}}{\ell}\omega^2 \\ 0 & 16\omega^2(1+\frac{\hat{e}_{22}}{\ell})-4\alpha\pm2\beta-\frac{1}{4}\theta^2 & 0 \\ 9\frac{\hat{e}_{31}}{\ell}\omega^2 & 0 & 81\omega^2(1+\frac{\hat{e}_{33}}{\ell})-9\alpha\pm\frac{9}{2}\beta-\frac{\theta^2}{4} \end{vmatrix} = 0$$

The above equation is the condition under which the equation motion has a periodic solution given by Equation (29) with period $2T = \frac{4\pi}{\theta}$ and the deflection shape represented by $v(x,t) = \sum_{i=1}^{3} f_i(t) \sin\frac{i\pi x}{\ell}$. Clearly, this determinantal equation degenerates into the following two independent equations:

$$\begin{vmatrix} \omega^2(1+\frac{\hat{e}_{11}}{\ell}) - \alpha\pm\frac{1}{2}\beta - \frac{1}{4}\theta^2 & 9\frac{\hat{e}_{13}}{\ell}\omega^2 \\ 9\frac{\hat{e}_{31}}{\ell}\omega^2 & 81\omega^2(1+\frac{\hat{e}_{33}}{\ell}) - 9\alpha\pm\frac{9}{2}\beta - \frac{1}{4}\theta^2 \end{vmatrix} = 0, \qquad (61)$$

and

$$16\omega^2(1+\frac{\hat{e}_{22}}{\ell}) - 4\alpha\pm2\beta - \frac{1}{4}\theta^2 = 0 \; . \qquad (62)$$

Equation (61) represents the frequency boundaries of the first and the third principal regions of instability, while the second principal region of instability is given by Equation (62). Applying the method of successive approximation to Equation (61), the boundaries of the first principal regions of instability are obtained as

$$\theta_* = 2\left[\omega^2\left(1 + \frac{\hat{e}_{11}}{\ell}\right) - \alpha \pm \frac{1}{2}\beta - c_1\omega^2\right]^{1/2},$$

$$\theta_* = 2\left[\omega^2\left(1 + \frac{\hat{e}_{11}}{\ell}\right) - \alpha \pm \frac{1}{2}\beta - c_2\omega^2\right]^{1/2}, \text{ where}$$

$$c_1 = \frac{\frac{81\hat{e}_{13}^2}{\ell^2}}{80 + 81\,\frac{\hat{e}_{33}}{\ell} - \frac{\hat{e}_{11}}{\ell} + \frac{8\alpha}{\omega^2} \pm \frac{4\beta}{\omega^2}}, \text{ and} \tag{63}$$

$$c_2 = \frac{\frac{81\hat{e}_{13}^2}{\ell^2}}{80 + 81\,\frac{\hat{e}_{33}}{\ell} - \frac{\hat{e}_{11}}{\ell} - \frac{8\alpha}{\omega^2} \pm \frac{4\beta}{\omega^2} + c_1}.$$

The first and the second relations of Equations (63) are the first and second successive approximate formulae for the first principal region of instability. Clearly, using as a guideline the previous subsection, the formulae for boundaries of the second and third principal regions may be deduced.

Similarly, substitution of Equations (55) through (57) and (60) into (19) followed by the method of successive approximations gives

$$\theta_* = \left[\omega^2\left(1 + \frac{\hat{e}_{11}}{\ell}\right) - \alpha - \bar{c}_1\omega^2\right]^{1/2},$$

$$\theta_* = \left[\omega^2\left(1 + \frac{\hat{e}_{11}}{\ell}\right) - \alpha = \bar{c}_2\omega^2\right]^{1/2}; \text{ and} \tag{64}$$

$$\bar{c}_1 = c_1\Big|_{\beta=0} \quad \text{and} \quad \bar{c}_2 = c_2\Big|_{\beta=0, c_1=\bar{c}_1},$$

c_1 and c_2 are given by Equation (63). The relations in Equation (64) are the first and the second successive approximate formulae of the first secondary region of instability for the lower boundary frequencies. By use of Equations (55) through (57) and (60) in (20), then adopting the method of successive approximation yields the first successive approximate formula for the upper boundary of frequencies for the first secondary region of instability as

$$\theta_\star = \left[\omega^2\left(1+\frac{\hat{e}_{11}}{\ell}\right) - \alpha - \beta\frac{||D_1||}{||D_2||} - \frac{9\hat{e}_{13}}{\ell}\omega^2\frac{||D_3||}{||D_2||}\right]^{1/2}, \text{ where}$$

$$||D_1|| = \beta\left[\frac{9}{2}d_3^2 + \frac{1}{2}d_2^2 - \frac{1}{2}d_1d_2 - \frac{81}{4}\beta^2\right],$$

$$||D_2|| = d_1d_2^2 - d_1^2d_2 - \frac{81}{2}\beta^2d_1 - d_3^2d_2 + d_1d_2, \tag{65}$$

$$||D_3|| = d_1d_2d_3 - d_3^3 - \frac{9}{2}\beta^2d_3 \text{ ; with}$$

$$d_1 \triangleq \omega^2\left(1+\frac{\hat{e}_{11}}{\ell}\right) - \alpha, \quad d_2 \triangleq 81\omega^2\left(1+\frac{\hat{e}_{33}}{\ell}\right) - 9\alpha, \text{ and } d_3 \triangleq \frac{9\hat{e}_{13}\omega^2}{\ell}.$$

Substituting Equations (55) through (57) and (60) into (15) and solving for Ω by the method of successive approximations the first and second approximations are obtained for the first natural frequency with initial load P_o as

$$\Omega_\star = \left[\omega^2\left(1+\frac{\hat{e}_{11}}{\ell}\right) - \alpha - \bar{c}_1\omega^2\right]^{1/2}, \text{ and} \tag{66}$$

$$\Omega_* = \left[\omega^2\left(1 + \frac{\hat{e}_{11}}{\ell}\right) - \alpha - \bar{c}_2\omega^2\right]^{1/2}, \text{ where} \tag{67}$$

$\bar{c}_1$ and $\bar{c}_2$ are defined in Equation (64). Using Equations (55) through (57) and (60) in (17) and solving for P_o by the method of successive approximations, the buckling load formulae for the first and second successive approximations are obtained as

$$P_* = -\left(\frac{m\ell^2}{\pi^2}\right)\left[\ ^2\left(1 + \frac{\hat{e}_{11}}{\ell}\right) - \bar{c}_1\omega^2\right], \text{where}$$

$$\bar{c}_1 = \frac{\dfrac{9\hat{e}_{13}^2}{\ell^2}}{8 + 9\,\dfrac{\hat{e}_{33}}{\ell} - \dfrac{\hat{e}_{11}}{\ell}}\ ; \text{ and} \tag{68}$$

$$P_* = -\left(\frac{m\ell^2}{\pi^2}\right)\left[\omega^2\left(1 + \frac{\hat{e}_{11}}{\ell}\right) - \bar{c}_2\omega^2\right], \text{ where}$$

$$\bar{c}_2 = \frac{\dfrac{9\hat{e}_{13}^2}{\ell^2}}{8 + 9\,\dfrac{\hat{e}_{33}}{\ell} - \dfrac{\hat{e}_{11}}{\ell} + \bar{c}_1}\ . \tag{69}$$

Formulae (68) and (69) are associated with first instability region.

The results of stability analysis for Case III are summarized Figure 10. The first instability zones are qualitatively represented in Figure 10. Since only the first principal and the secondary instability regions are physically of significance, the formulae corresponding to the A and B zones are enumerated in this subsection. The formulae corresponding to the second and the third i.e. zones D through E may be

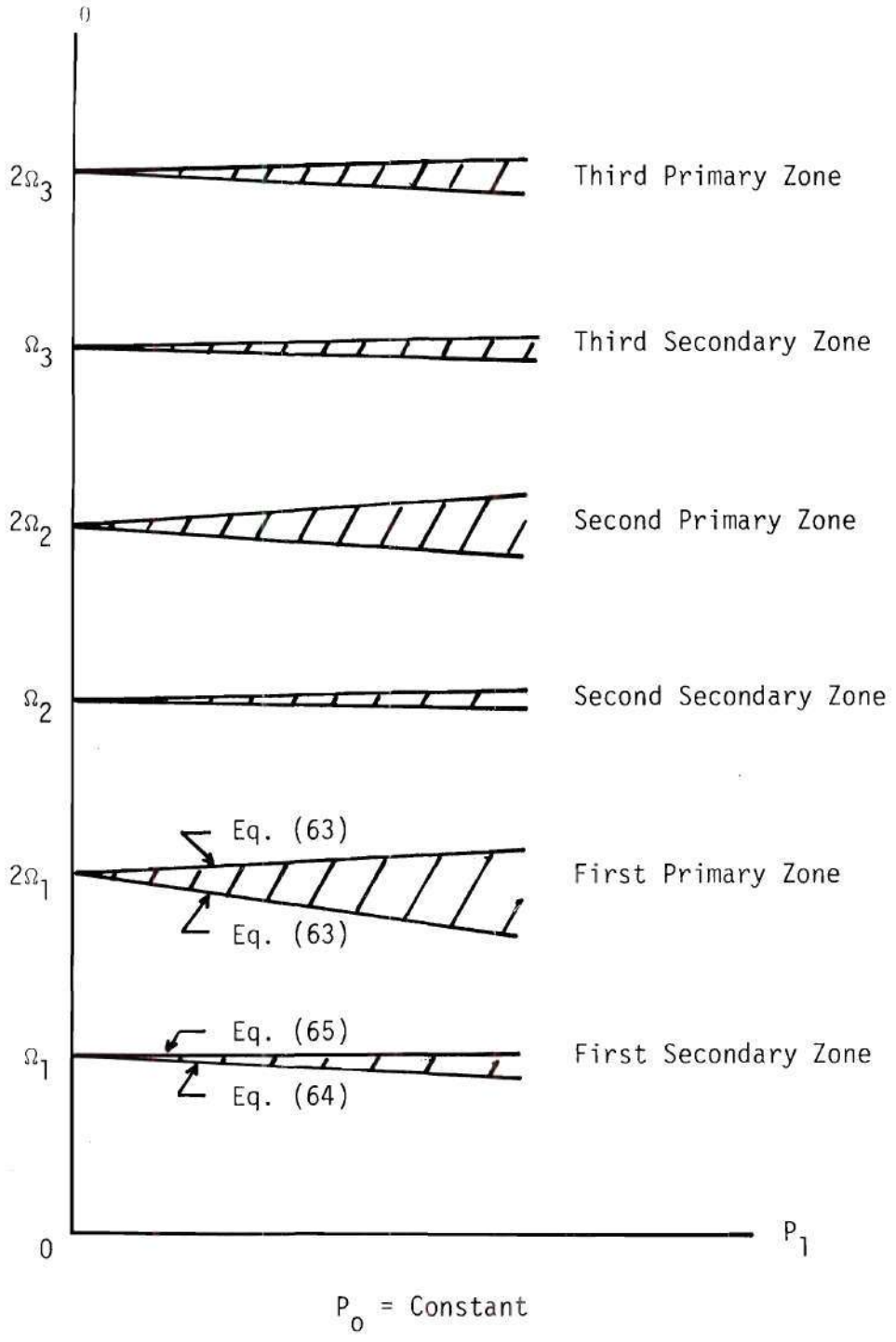

Figure 10. Schematic Presentation of Instability Boundaries, for Case III with C = ℓ/2.

deduced by use of the procedures of the previous subsection. However, they are qualitatively presented in Figure 10. Recall that the formulae derived in this subsection are for the special case $C = \ell/2$. It is also noteworthy that these formulae are representing behavior of the column better than the corresponding formulae for the special case $C = \ell/2$ in the previous two subsections. This conclusion is justified on the basis that in a vibration problem the results will, in general, be improved when the stiffness representation is improved; and Case III stiffness is better than Case II (Equations (56) and (21)) for $C = \ell/2$.

The analyses presented in the last three subsections involve two types of approximations:

- the representation of the deflection shape of the column by a finite number of sine functions of the independent variable, x; and
- the use of a finite number of time dependent harmonic functions in the generalized co-ordinates, $\underset{\sim}{f}(t)$.

Specifically, $\sin \frac{\pi x}{\ell}$ was used in Case I, $\{\sin \frac{n\pi x}{\ell}\}_{n=1}^{n=2}$ in Case II and $\{\sin \frac{n\pi x}{\ell}\}_{n=1}^{n=3}$ in Case III for the deflection shape representation. However, the generalized co-ordinates, $\underset{\sim}{f}(t) = \underset{\sim}{a}_1 \sin \frac{\theta t}{2} + \underset{\sim}{b}_1 \cos \frac{\theta t}{2}$ and $\underset{\sim}{f}(t) = \frac{1}{2} \underset{\sim}{b}_o + \underset{\sim}{a}_2 \sin \theta t + \underset{\sim}{b}_2 \cos \theta t$ were used in obtaining the solution of the equation of motion in all three cases. A greater number of deflection functions to represent the deflection shape and more time dependent harmonics in the generalized co-ordinates may be used to obtain improved results. However, a proper balance of these two should

yield sufficiently accurate results.*

Numerical results of these case studies are presented in Chapter IV. There, some additional features of the problem are discussed in conjunction with the experimental findings described in the next chapter.

---

*Appendix B: An Analysis with k = 3, k = 4 and Typical Numerical Results.

CHAPTER III

EXPERIMENTAL PROGRAM

Introduction

The test facilities and procedures with the test specimen geometries for the dynamic stability and the stiffness measurements are described in this chapter. Also presented are data resulting from these measurements in tabular form. Some data reductions are given in graphical form along with the required calibrations involving these test measurements. The experimental results described here and analytical results presented in the previous chapter are correlated in the next chapter.

Specimens

Four specimens were considered for tests of the dynamic stability analysis. Their geometrical and physical parameters are described in Tables 1 and 2 in conjunction with Figure 11. The test specimens were used to get quantitative data for the dynamic and the stiffness reduction analysis. The test facility, procedure for data recording and the calibration for the parametric stability tests are described in the next sections.

Test Facility

The test facility* used to conduct the dynamic stability

---

*The test facility is described in greater detail in Reference [23].

Table 1. Geometric Properties of Specimens

Specimen No.	Length in	Cross-section in x in	Slot Thickness in	Location of slot in	Length of slot in	No. of slots
1	36	3/8 x 1/2	--	--	--	None
2	36	3/8 x 1/2	1/16	18	0.2	1
3	36	3/8 x 1/2	1/16	18	0.3	1
4	36	3/8 x 1/2	1/16	18	0.4	1

Table 2. Physical Parameters of the Test Specimens*

Property Description	Remarks
Material	AL 7075-T6
Mass Per Unit Length	$.490497\ (10)^{-4}\ \frac{lb\text{-}sec^2}{in^4}$
Estimated Maximum Stress at Slot Tips	15 ksi
Estimated Buckling Load	172.0 lbs
Estimated Lateral Vibration Frequency	26.0 Hz
Estimated Longitudinal Frequency of Vibration	2916.0 Hz
End Conditions	Simply Supported

*These parameters were useful while conducting and designing the tests. Also, note that the values apply to all specimens, i.e., 1,2,3,4.

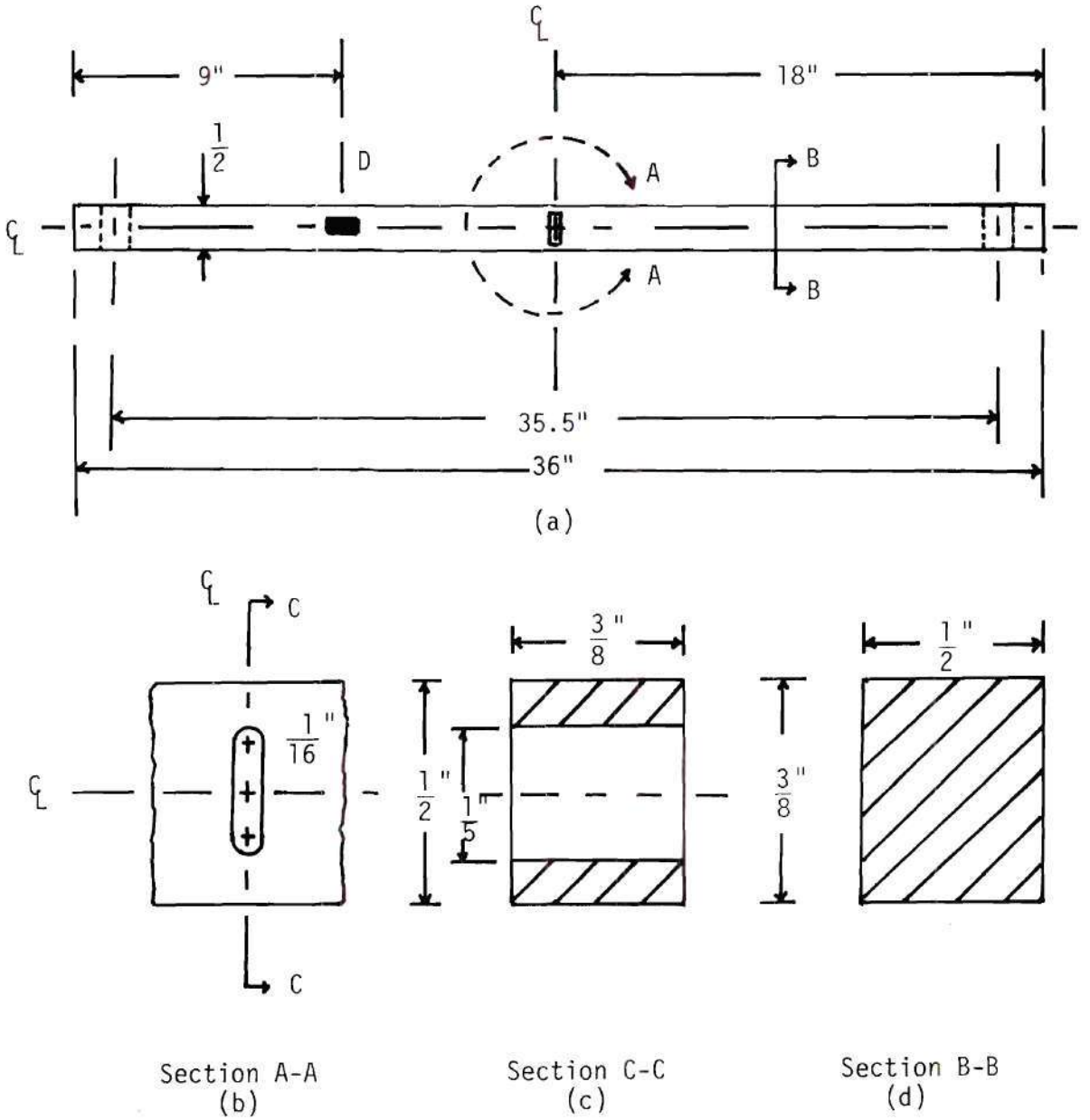

Figure 11. Geometries of the Specimens.

experiments is shown in Figure 12. The frame mounted on the isolation base provides the capability of applying mean axial loads to the specimen through a screw mechanism at the top. The aluminum specimen is attached at the bottom end to a clevis connected to a crossbar fixed to the vertical columns of the frame. A load cell between the top specimen clevis and the loading mechanism is used to determine the applied load.

Four electrical resistance strain gages were bonded to the external surface of the thin walled tube part of the load cell. Two of the gages were aligned in the direction of the longitudinal axis of the tube. These gages were wired into two opposite arms of a Wheatstone bridge. The remaining two arms of the bridge were gages whose sensitive axes were oriented in the circumferential direction of the tube surface.

The alternating component of the applied load was introduced by connecting the lower crossbar to the vibration exciter mounted on the top of the isolation base. The exciter shown in Figure 12 is designated as MB Model C11-D by the manufacturer, MB Electronics. The system has a force range of ±50 pounds. The MB control system, Model T112531, consists of a power supply, a D.C. field supply, an oscillator, and a power amplifier.

The response of the column specimen during most of tests was indicated by measuring the output from two strain gages (M-M: EA-13-125BT-120) bonded back-to-back on the bending surfaces of the specimen at the location indicated by point D in Figure 11. The gages were aligned in the longitudinal direction of the specimen. These two active gages were wired in a circuit designed to measure the bending-strain difference

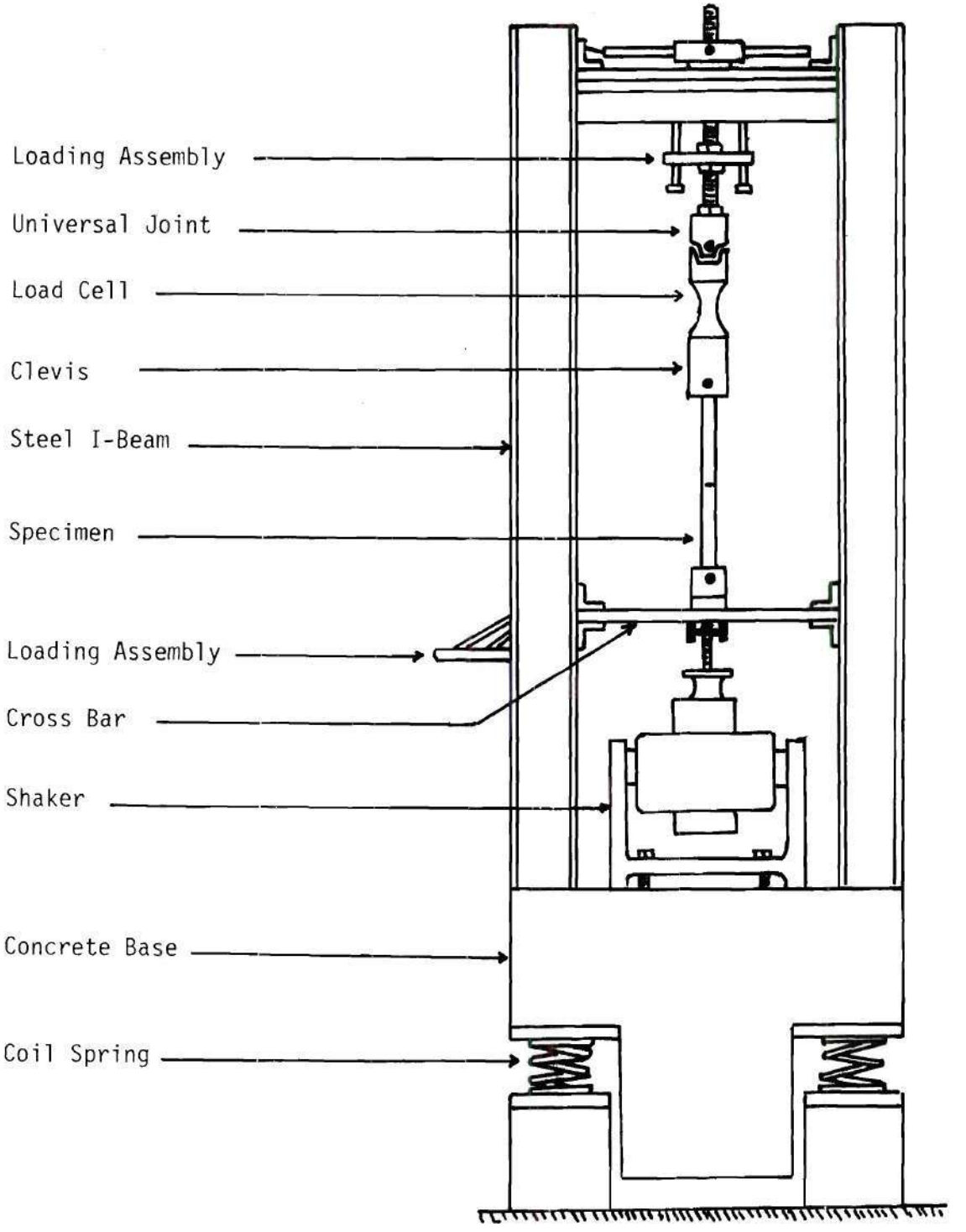

Figure 12. Dynamic Stability Test Facility.

between the two surfaces.

The bridge from the load cell and the bridge for the column response were connected to Hewlett-Packard carrier pre-amplifiers (Model 8805A), and the signals generated were fed to two channels of a Model 7702B Hewlett-Packard recorder.*

Procedure for Data Recording

The objective of the parametric excitation experiments was to determine the location of boundaries which separate the regions of stability and instability. The test conducted did not involve the development of unbounded displacement. However, significantly large amplitude displacements were observed during the resonance.

Three parameters were involved in the experiments: the magnitude of the mean load, P_0; the magnitude of alternating load, P_1; and, the frequency of alternating load, θ. Only tensile mean loads were applied because of particular interest in the effect of tensile loads on structural elements with cracks or crack-producing discontinuities. However, the effect of compressive load is deduced in the next chapter using the analytical stability model developed in Chapter II.

To record the dynamic stability data, the following procedure was adopted.

1. Apply a mean load, P_0, using the screw mechanism.

2. Set the shaker power supply to obtain the desired alternating load, P_1, by observing the load cell response on the Sandborn recorder.

---

*Manufactured by the Sanborn Division of Hewlett-Packard.

3. Set the excitation frequency of the shaker a few Hz below the fundamental transverse natural frequency of the column (approximately calculated natural frequency of the column).

4. With this P_o and P_1 slowly increase the frequency in steps of one half Hz until the bending strain response reaches maximum and then subsides to zero. The frequency corresponding to maximum bending strain is the secondary zone maximum response frequency.* θ^s_{max} from below.

5. Set the excitation frequency of the shaker a few Hz above the fundamental transverse natural frequency of the column for the same P_o and P_1.

6. For this P_o and P_1, slowly decrease the frequency in steps of one half Hz until the bending strain response reaches maximum and then subsides to zero. The frequency corresponding to the maximum bending strain is the secondary zone* maximum response frequency, θ^s_{max} from above. Then the average of the θ^s_{max} from below and from above was obtained.

7. With loads P_o and P_1 in steps (1) through (6), set the excitation frequency of the shaker a few Hz below two times the value of θ^s_{max}.

8. With this P_o and P_1 slowly increase the frequency in steps of one half Hz until the bending strain response reaches significantly large values. The frequency corresponding to this bending strain is the primary zone lower boundary frequency, θ^P_L.

---

*Appendix B: Experimental Instability Zone Response.

9. Set the frequency of excitation of the shaker a few Hz above two times the θ^{s}_{max}, for same P_o and P_1.

10. For this P_o and P_1, slowly decrease the frequency in steps of one half Hz until bending strain response becomes significantly large. The frequency corresponding to this response is the primary zone upper boundary frequency θ^{P}_{U}.

11. Repeat the procedure of steps (1) through (10) with different values of P_o and P_1.

12. Repeat the procedure for different values of slot length in the column.

The dynamic stability information obtained is presented in Table 3.

Calibration for End Conditions

Recall that the experimental data for parametric instability recorded in Table 3 are for the simply supported end conditions. These end conditions were simulated experimentally by pins and over-sized holes in the specimen and clevis. One of these end conditions is depicted in Figure 13. It is apparent that these end conditions are approximately simply supported. Therefore, the uniform column instability data were matched by the analytical uniform column instability formulae for simply supported end conditions using the effective length of the column. The analytical formulae [2] used in the calibration are

Table 3. Dynamic Stability Data Obtained in Experiments

P(t) lb		Frequency in Hz											
		Secondary Zone				Primary Zone							
P_o	P_1	slot length in				slot length in							
		0	0.2	0.3	0.4	0		0.2		0.3		0.4	
		θ^S_{max}	θ^S_{max}	θ^S_{max}	θ^S_{max}	θ^P_L	θ^P_U	θ^P_L	θ^P_U	θ^P_L	θ^P_U	θ^P_L	θ^P_U
30	10	31.0	31.0	30.5	30.5	63.0	63.0	63.0	63.5	63.0	63.0	X	X
	15	N	31.0	30.5	30.0	N	N	62.5	64.0	61.5	63.5	61.0	62.0
	20	31.0	31.0	30.0	29.75	62.25	64.0	63.0	64.0	61.	63.5	59.5	62.5
45	10	N	31.5	32.5	31.0	N	N	64.0	64.5	64.5	66.0	63.0	X
	15	N	31.5	32.5	31.0	N	N	62.5	65.0	64.5	66.0	63.0	63.0
	20	N	32.0	32.0	30.5	N	N	62.5	65.5	64.	66.5	62.0	63.5
50	10	33.0	N	N	N	66.5	67.0	N	N	N	N	N	N
	25	33.0	N	N	N	65.0	68.0	N	N	N	N	N	N
60	10	N	32.5	32.5	32.5	N	N	65.5	66.0	X	X	X	X
	15	N	32.5	32.5	32.5	N	N	65.0	-6.5	66.5	67.0	66.0	66.0
	20	N	32.5	33.0	32.0	N	N	64.5	67.0	66	67.5	64.5	67.0
	30	N	32.5	32.5	32.0	N	N	64.0	67.5	64.5	68.0	64.0	67.5

X - No resonance type response was found*

N - Frequency determination was not attempted.

*Appendix B: Experimental Instability Zone Response.

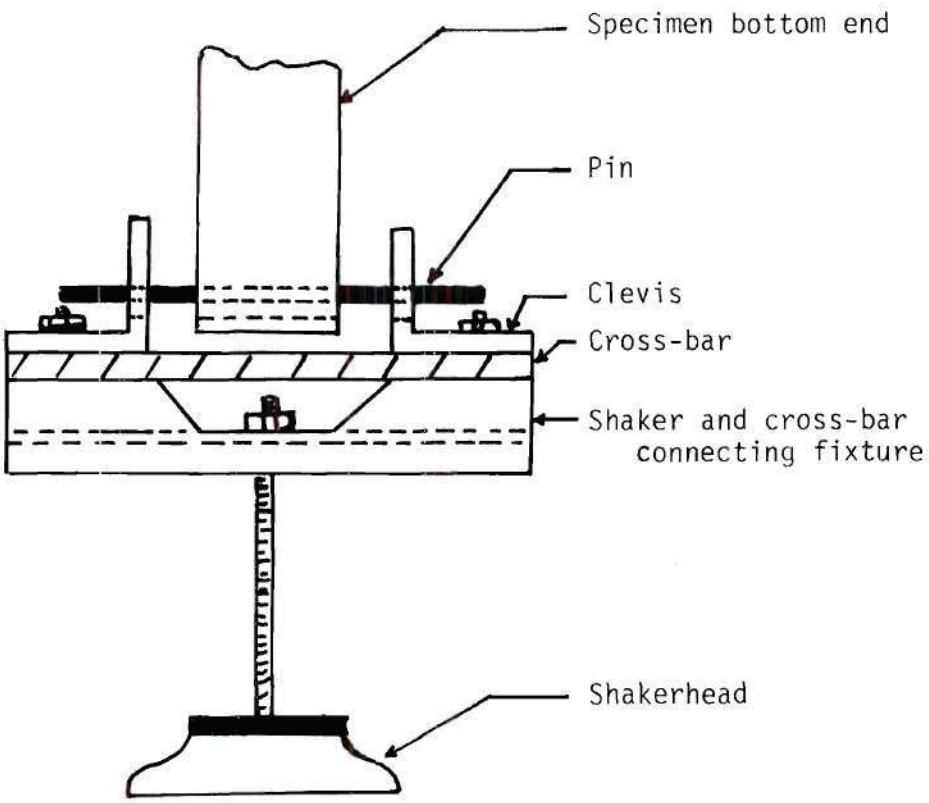

Figure 13. Simply Supported End Condition.

$$\theta_U^P = 2\Omega[1 + \mu]^{1/2} ,$$

$$\theta_L^P = 2\Omega[1 - \mu]^{1/2} ,$$

$$\theta_U^S = \Omega[1 + \frac{1}{3}\mu^2]^{1/2} , \text{ and}$$

$$\theta_L^S = \Omega[1 - 2\mu^2]^{1/2} , \text{ where} \qquad (1)$$

$$\Omega = \frac{\pi^2}{\ell^2}\sqrt{\frac{EI}{m}(1 + \frac{P_o}{P_*})} , \text{ and}$$

$$\mu = \frac{P_1}{2(P_* + P_o)} .$$

In Equations (1) P_o, P_1 and P_* are the mean, oscillating load amplitudes and the buckling load of the uniform column. EI and m are the stiffness and the mass per unit length of the uniform column with length ℓ.

The calibration process is indicated in Figure 14, and the average effective length of the column specimens was found to be 33.85 inches. Thus, the data presented in Table 3 are for specimens of length 33.85 with test simulated simply supported end conditions. Since the actual length between the pin holes was 35.5 inches, this suggests that the ends were not free of moments, i.e., restraints at ends caused the effective length to be smaller than the measured length.

Effective Stiffness Measurements

The details of the experimental program for the dynamic stability of columns with a slot and the resulting instability frequency boundaries have been presented. The effects of notches or discontinuities on

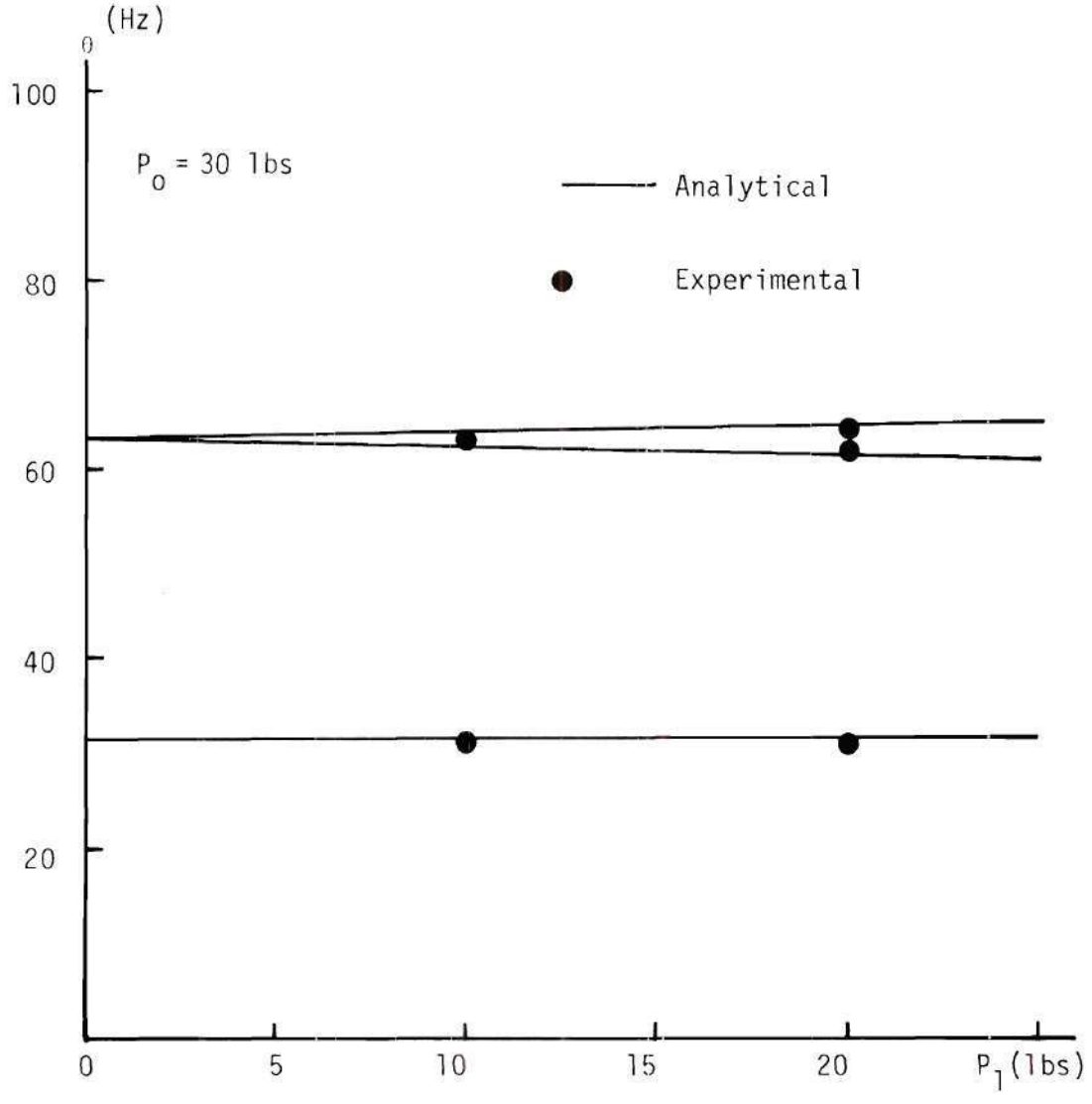

Figure 14. Calibration of End Conditions.

the frequency boundaries are discussed in conjunction with the analytical models in Chapter IV. However, it should be recalled that the analytical models of Chapter II contain the parameters K and R. These parameters represent the effects of regions of discontinuity on the dynamics of the column. Therefore, a unique relationship between K and R for the known values of K or R must be established to obtain the parametric stability results analytically. In this section the test set-up and the method used to determine EK for the four specimens are described.

A four-point-load bending test was used in a universal testing machine (Instron). The test fixture and the set-up shown in Figure 15 were used to record deflection vs. load in pure bending of the element containing the discontinuity. It may be noted that the dial-gages in Figure 15 were placed symmetrically with respect to the slot in the specimen. The data recorded in this test are reported in Table 4.

An examination of Figure 15 shows that the beam element of length L was loaded as shown in Figure 16. It can be noted that L is less than the distance between the rigid pins ⑧ and ⑨, and L is greater than the distance between dial gages G_1 and G_3. The distance between the pins ⑥ to ⑧, a is equal to the distance between the pins ⑦ to ⑨. The load, 2P was applied by the Instron machine as shown in Figure 15.

For a deduction of effective stiffness EK of the beam element of the column with region of discontinuity, the slopes $\frac{\Delta P}{\Delta y}\Big|_{\ell'/2}$ were measured experimentally. The test specimens were tested with a = 1.965" and

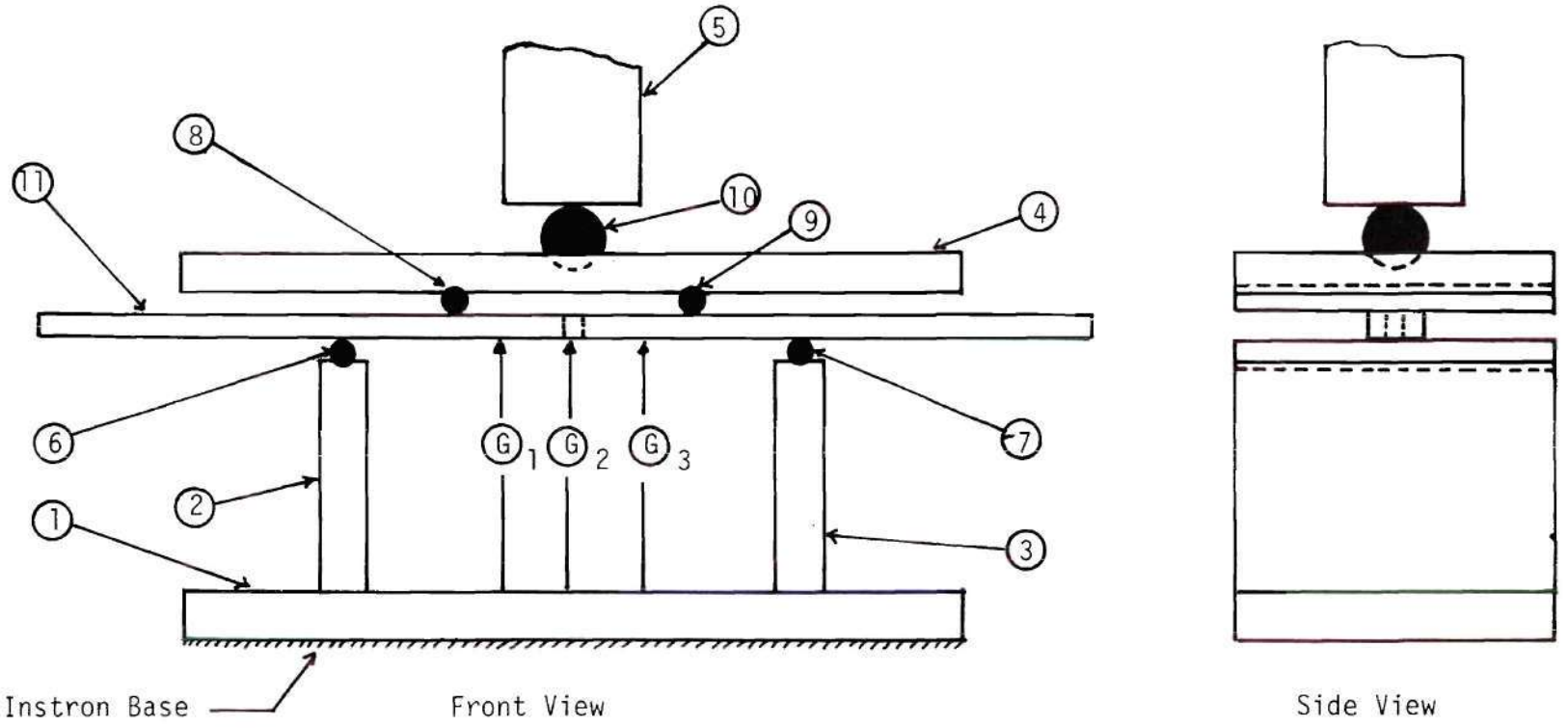

① ② ③ ④ - Rigid Frame for Four Point Loading of Specimen, ⑪ .

⑤ - Instron Moving End for Loading, $G_{1,2,3}$ Three dial-gages.

⑥ ⑦ ⑧ ⑨ - Steel Cylindrical pins, ⑩ - Spherical Steel Ball for Point Loading

Figure 15. Four-Point-Load Bending Test Sep-Up.

Table 4. Four-Point-Load Bending Data

Specimen No.	Slot length inches	Gage Reading in 0.0001 inches			P lbs	$y_{\ell'/2}$ in 0.0001 inches
		Gage 1	Gage 2	Gage 3		
1	0	00.0	00.0	00.0	12.5	00.00
		12.0	17.0	12.0	25.0	05.00
		23.5	35.5	24.0	37.5	11.75
		35.0	53.0	36.0	50.0	17.50
		48.0	72.0	49.0	62.5	23.50
		60.0	90.05	61.0	75.0	30.05
2	0.2	00.0	00.0	00.0	12.5	0.0
		12.0	19.0	12.0	25.0	7.0
		26.0	38.0	25.0	37.5	12.5
		38.0	56.0	37.0	50.0	18.5
		50.0	70.0	50.0	62.5	25.0
		62.0	93.0	62.0	75.0	31.0
3	0.3	52.5	73.0	76.0	12.5	8.75
		64.0	92.0	89.0	25.0	15.50
		76.0	110.0	101.0	37.5	21.50
		88.0	130.0	112.0	50.0	30.00
		101.0	149.0	125.0	62.5	36.50
		113.0	168.0	138.0	75.0	42.50
4	0.4	56.0	75.0	72.0	12.5	11.0
		69.0	95.0	84.0	25.0	18.5
		83.0	117.0	97.0	37.5	27.0
		96.0	138.0	110.0	50.0	35.0
		110.0	160.0	124.0	62.5	43.0
		124.0	182.0	137.0	75.0	51.0

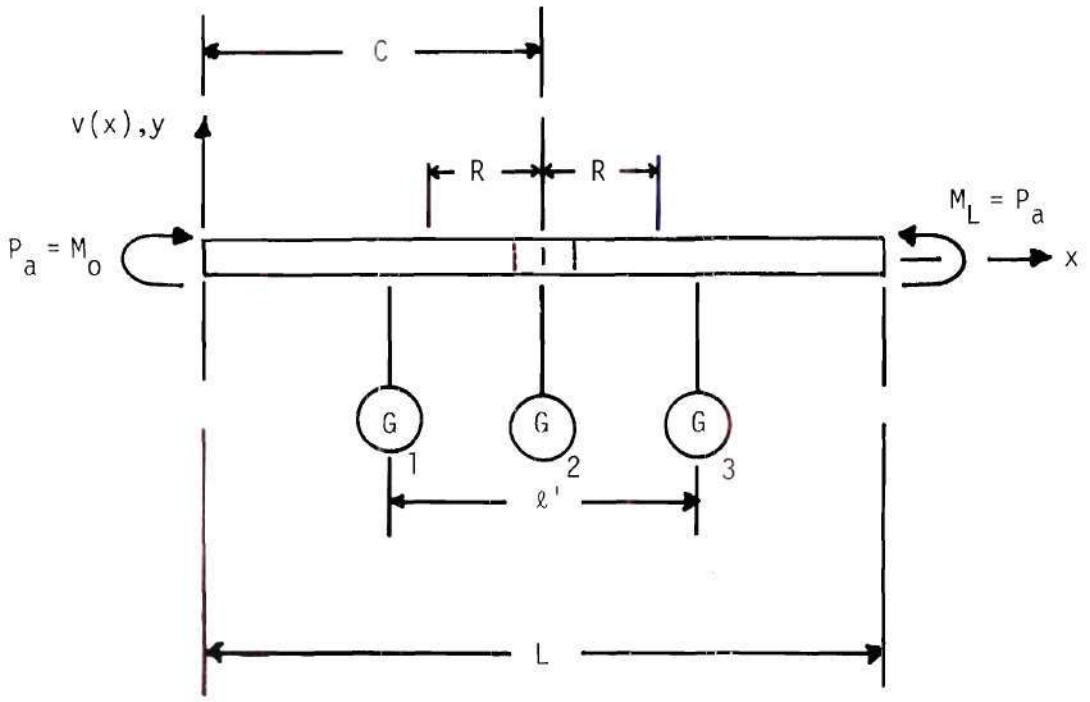

Figure 16. Loading on the Beam Element.

$\ell' = 6.8"$. The values of $y|_{\ell'/2}$ were calculated by use of the formula,

$$y|_{\ell'/2} = D_2 - \frac{D_1 + D_3}{2}, \text{ where}$$

D_1, D_2 and D_3 are the dial gages readings in inches. The slopes, $\frac{\Delta P}{\Delta y}\Big|_{\ell'/2}$ were determined by plotting the measured $y|_{\ell'/2}$ v.s. P values (Table 4) as illustrated by Figure 17.

The slopes, $\frac{\Delta P}{\Delta y}\Big|_{\ell'/2}$ for specimens 1 through 4 are presented in Table 5. Graphically the behavior of slot length vs. slope is given in Figure 18.

Table 5. Slopes $(\frac{\Delta P}{\Delta y})\Big|_{\ell'/2}$

Specimen	$\frac{\Delta P}{\Delta y}\Big\|_{\ell'/2}$ lb/in	Slot length in inches
1	2140.0	0
2	2000.0	0.2
3	1800.0	0.3
4	1545.0	0.4

To compute the effective stiffness EK, a relation between EK and the measured $\frac{\Delta P}{\Delta y}\Big|_{\ell'/2} = c_s$, must be obtained. Using an energy approach with $\{\sin \frac{n\pi x}{L}\}_{n=1}^{N}$ as the deflection functions for the beam element

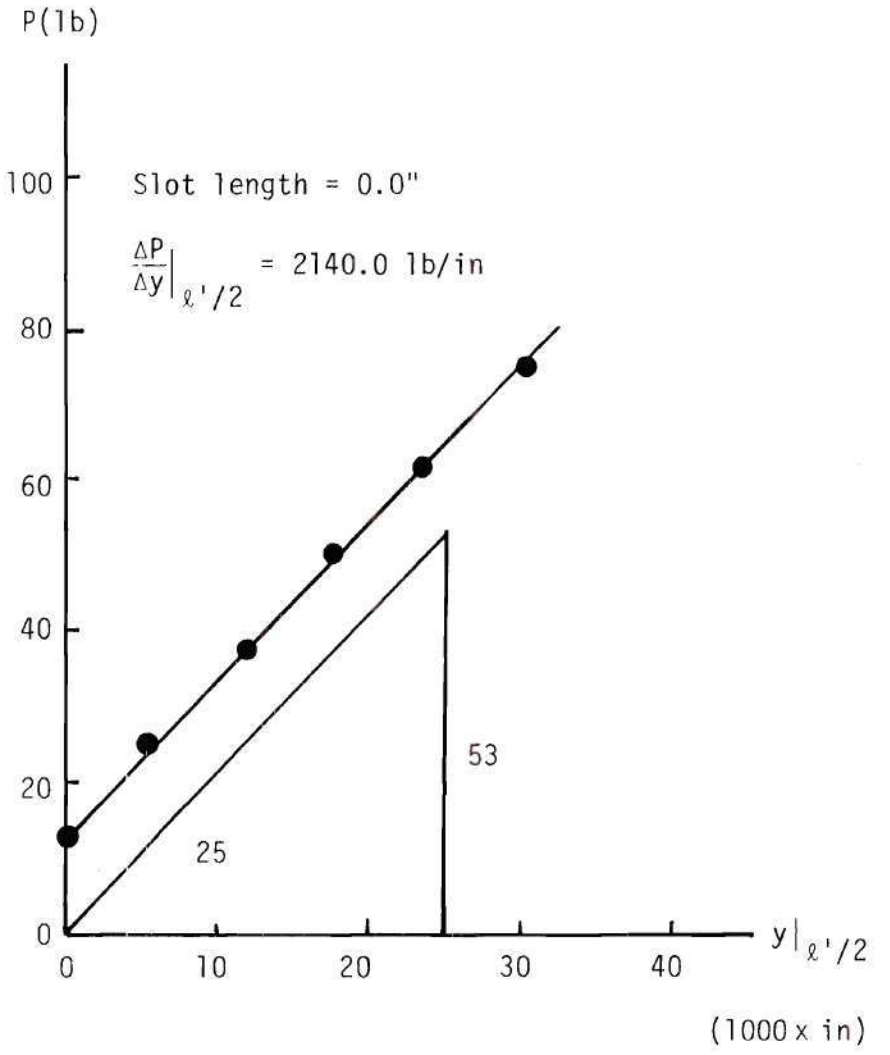

Figure 17. Deflection vs. Load.

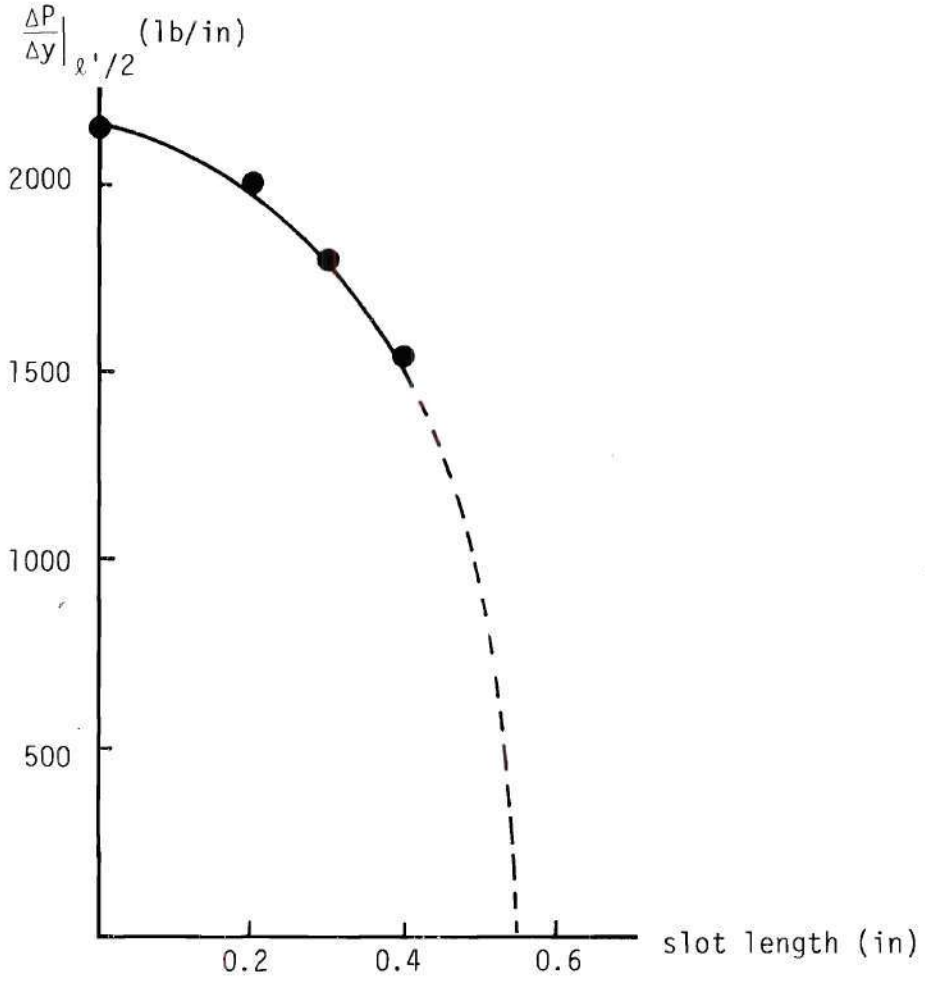

Figure 18. Slot Length vs. $(\Delta P/\Delta y)\big|_{\ell'/2}$.

depicted in Figure 11, the required relationship is deduced. It can be noted that the energy procedure was selected for estimating effective stiffness EK because this approach is consistent with the analyses presented in the previous chapter.

The strain energy and the work done by the end moments for the beam element shown in Figure 11, respectively are

$$U = \frac{EI}{2} \int_{o}^{L} \left(\frac{d^2v}{dx^2}\right)^2 dx + \frac{E(K-I)}{2} \int_{C-R}^{C+R} \left(\frac{d^2v}{dx^2}\right)^2 dx \quad \text{and}$$

$$W = \left[M \frac{dv}{dx}\right]_{x=0}^{x=L} .$$

Thus, the total potential, Π of the beam element can be written as

$$\Pi = \frac{EI}{2} \int_{o}^{L} \left(\frac{d^2v}{dx^2}\right)^2 dx + \frac{E(K-I)}{2} \int_{C-R}^{C+R} \left(\frac{d^2v}{dx^2}\right)^2 dx - \left[M \frac{dv}{dx}\right]_{x=0}^{x=L} . \qquad (2)$$

The deflection shape is approximated as

$$v(x) = \sum_{n=1}^{3} a_n \sin \frac{n\pi x}{L} \qquad (3)$$

which is consistent with the deflection functions used in the previous chapter. Substituting Equation (3) into (2) and minimizing Π with respect to a_n, n = 1,2,3 yields,

$$\frac{n^4 \pi^4 EI}{2L^3} a_n + \frac{n^2 \pi^4 E(K-I)}{L^4} \sum_{i=1}^{3} i^2 a_i e_{ni} - \frac{n\pi aP}{L}[(-1)^n - 1] = 0, \qquad (4)$$

with n = 1,2,3;

and

$$e_{ni} = \int_{C-R}^{C+R} \sin \frac{n\pi x}{L} \sin \frac{i\pi x}{L}\, dx$$

$$= \begin{cases} R - \frac{L}{2\pi i} \cos \frac{2\pi iC}{L} \sin \frac{2\pi iR}{L} & \text{for } i = n \\ \\ \frac{L}{(i-n)\pi} \cos \frac{(i-n)\pi C}{L} \sin \frac{(i-n)\pi R}{L} - \frac{L}{(i+n)\pi} \cos \frac{(n+i)\pi C}{L} \sin \frac{(n+i)\pi R}{L} & \text{for } n \neq i . \end{cases} \tag{5}$$

Substituting C = L/2 (since the experiments were performed with C = L/2) and rewriting Equations (4) in matrix form as

$$\begin{bmatrix} [\frac{1}{2} + (\frac{R}{L} + \frac{1}{2\pi} \sin \frac{2\pi R}{L})(\frac{K}{I} - 1)] & -9[\frac{K}{I} - 1][\frac{1}{2\pi} \sin \frac{2\pi R}{L} + \frac{1}{4\pi} \sin \frac{4\pi R}{L}] \\ -9[\frac{K}{I} - 1][\frac{1}{2} \sin \frac{2\pi R}{L} + \frac{1}{4\pi} \sin \frac{4\pi R}{L}] & 81[\frac{1}{2} + (\frac{R}{L} + \frac{1}{6\pi} \sin \frac{6\pi R}{L})(\frac{K}{I} - 1)] \end{bmatrix} \begin{bmatrix} a_1 \\ a_3 \end{bmatrix} = -AP \begin{bmatrix} 1 \\ 3 \end{bmatrix}, \tag{6}$$

where $A \triangleq 2 \frac{a}{EI} \frac{\ell^2}{\pi^3}$; and

$$\{\frac{1}{2} + [\frac{R}{L} - \frac{1}{4\pi} \sin \frac{4\pi R}{L}][\frac{K}{I} - 1]\}\, a_2 = 0 .$$

It is convenient to rewrite Equation (6) in the following form

$$\begin{bmatrix} \frac{1}{2} + h_1(\frac{K}{I} - 1) & h_3(\frac{K}{I} - 1) \\ h_3(\frac{K}{I} - 1) & \frac{81}{2} + h_2(\frac{K}{I} - 1) \end{bmatrix} \begin{bmatrix} a_1 \\ a_3 \end{bmatrix} = -AP \begin{bmatrix} 1 \\ 3 \end{bmatrix}, \tag{7}$$

and $h_4 a_2 = 0$, where

$$h_1 \triangleq \frac{R}{L} + \frac{1}{2\pi} \sin \frac{2\pi R}{L} ,$$

$$h_2 \triangleq 81\left(\frac{R}{L} + \frac{1}{6\pi} \sin \frac{6\pi R}{L}\right) ,$$

$$h_3 \triangleq -9\left(\frac{1}{2\pi} \sin \frac{2\pi R}{L} + \frac{1}{4\pi} \sin \frac{4\pi R}{L}\right) ,$$

$$h_4 \triangleq \frac{1}{2} + \left(\frac{R}{L} - \frac{1}{4\pi} \sin \frac{4\pi R}{L}\right)\left(\frac{K}{I} - 1\right); \text{ and}$$

$$A \triangleq 2 \frac{a}{EI} \frac{L^2}{\pi^3} .$$

Solving Equations (7) for a_1, a_2 and a_3 yields

$$a_1 = -AP \frac{||D_1||}{||D||} ,$$

$$a_2 = 0 ,$$

$$a_3 = -AP \frac{||D_2||}{||D||} , \text{ where} \qquad (8)$$

$$||D|| = \begin{vmatrix} \frac{1}{2} + h_1\left(\frac{K}{I} - 1\right) & h_3\left(\frac{K}{I} - 1\right) \\ h_3\left(\frac{K}{I} - 1\right) & \frac{81}{2} + h_2\left(\frac{K}{I} - 1\right) \end{vmatrix} ,$$

$$||D_1|| = \begin{vmatrix} 1 & h_3\left(\frac{K}{I} - 1\right) \\ 3 & \frac{81}{2} + h_2\left(\frac{K}{I} - 1\right) \end{vmatrix} , \text{ and}$$

$$||D_2|| = \begin{vmatrix} \frac{1}{2} + h_1(\frac{K}{I} - 1) & 1 \\ h_3(\frac{K}{I} - 1) & 3 \end{vmatrix} .$$

It can be noted that the beam element shown in Figure 11 is loaded symmetrically and the geometry of the beam element is symmetric. Therefore, the coefficient a_2 is zero; i.e. since $h_4 \neq 0$, it follows that $a_2=0$.

Substitution of Equation (6) into Equation (2) yields

$$v(x) = - \frac{AP}{||D||} \{ ||D_1|| \sin \frac{\pi x}{L} + ||D_2|| \sin \frac{3\pi x}{L} \} .$$

Differentiation of the above equation yields

$$\left.\frac{dP}{dv}\right|_{x=\frac{L}{2}} = \frac{||D||}{A\{||D_2|| - ||D_1||\}} = c_s, \text{ where}$$

c_s is the experimentally measured slope $\left.\frac{\Delta P}{\Delta y}\right|_{x=\ell'/2}$. Expanding the determinants in the above equation and solving for $\frac{K}{I}$,

$$\frac{K}{I} = 1 + \frac{-\bar{h}_2 \pm \sqrt{\bar{h}_2^2 - 4\bar{h}_1\bar{h}_3}}{2\bar{h}_1} , \text{ where}$$

$$h_3 = 39Ac_s + \frac{81}{4} ,$$

$$h_2 = \frac{81}{2} h_1 + \frac{h_2}{2} - c_sA(3h_1 - h_2 + 2h_3), \qquad (9)$$

$$\bar{h}_1 = h_1h_2 - h_3^2, \text{ and definitions of}$$

h_1, h_2, h_3 and A are given in Equation (7).

In applying the analysis, the value 2R will represent the length of the region in which the stresses differ from those of elementary beam theory. Thus, 2R will be of the order of the discontinuous region length plus twice the cross-sectional dimension. Then, Equation (9) provides a basis for computation of the K of the beam element in terms of known parameters.

In the next chapter numerical results for Equation (9), and the relationship between the parameters K and R using the slope $(\Delta P/\Delta y)|_{\ell'/2}$ vs. slot length curve are presented in conjunction with the analytical models developed in the previous chapter. Also, the experimental and analytical results for the stability of the columns are correlated.

CHAPTER IV

ANALYTICAL AND EXPERIMENTAL RESULTS

In Chapter II the developments of the analytical stability models and the formulae for the instability analysis were presented. Experimental procedures and results for the columns with and without a region of discontinuity were reported in Chapter III. The present chapter includes the numerical evaluation of the effects of the discontinuities using both analytical and experimental results. It may be noted that these effects are examined by comparisons with corresponding uniform column results. The analytical and experimental results are correlated in graphical form using a non-dimensional notation. Finally, an application of the analytical stability models is illustrated.

Non-dimensionalization

Use of non-dimensional notation not only reveals obvious errors in an analysis, but also brings out universal characteristics of the analysis. Another advantage gained from non-dimensional notation is computational expediency. Therefore, the numerical results of the stability models are presented in non-dimensional form. The length parameters, R and C are non-dimensionalized with respect to the column length, ℓ. The load parameters P_1, P_0 and $P_\star$ are non-dimensionalized with respect to the buckling load of the corresponding uniform column. The frequencies $\theta_\star$'s are non-dimensionalized with respect to twice the free vibration frequency

of the corresponding uniform column. However, the free vibration frequency Ω_* is non-dimensionalized with the free vibration frequency of the corresponding uniform column. The effective stiffness parameter K is non-dimensionalized with I of the corresponding uniform column. Thus,

$$\begin{bmatrix} R \\ C \\ \theta_* \\ \Omega_* \\ P_1 \\ P_0 \\ P_* \\ K \end{bmatrix}_{ND} = \begin{bmatrix} \frac{1}{\ell} & 0 & 0 & 0 & 0 & 0 & 0 & 0 \\ 0 & \frac{1}{\ell} & 0 & 0 & 0 & 0 & 0 & 0 \\ 0 & 0 & \frac{1}{2\Omega_*} & 0 & 0 & 0 & 0 & 0 \\ 0 & 0 & 0 & \frac{1}{\Omega_*} & 0 & 0 & 0 & 0 \\ 0 & 0 & 0 & 0 & \frac{1}{P_*} & 0 & 0 & 0 \\ 0 & 0 & 0 & 0 & 0 & \frac{1}{P_*} & 0 & 0 \\ 0 & 0 & 0 & 0 & 0 & 0 & \frac{1}{P_*} & 0 \\ 0 & 0 & 0 & 0 & 0 & 0 & 0 & \frac{1}{EI} \end{bmatrix}_{UN} \begin{bmatrix} R \\ C \\ \theta_* \\ \Omega_* \\ P_1 \\ P_0 \\ P_* \\ EK \end{bmatrix}_D , \qquad (1)$$

where ND - subscript indicates non-dimensional quantities,

D - subscript indicates dimensional quantities,

and UN - subscript indicates the corresponding uniform column dimensional quantities.

It is convenient to drop the subscript ND in the following presentation and refer all the parameters hereafter in the non-dimensional form unless explicitly stated otherwise. The excitation parameter, $\mu \triangleq \frac{P_1}{2(1 + P_0)}$, ($P_1$ and P_0 are non-dimensional loads as defined in Equation (1)), is also used. Note that for tensile loads, $P_0 > 0$.

Using this non-dimensional notation in the next two sections, the effect of a discontinuity region on the column stability behavior is presented in graphical form. In the last section an application of the analytical model is illustrated.

Examination of Discontinuity Effects by Analytical Models

There are three parameters, R, K and C, which characterize the effects of the discontinuity on the stability behavior of the column. Recall that R is the non-dimensional size of the region of discontinuity, K is the non-dimensional reduced stiffness due to the presence of the discontinuity in the column, and C is the non-dimensional location of the discontinuity region. Further, R, K and C are involved in Cases I and II, while only R and K are involved in Case III. In Case III, the value of C is selected to be 0.5 because of special interest at that location. It can be noted that the second successive approximation stability formulae are used to present results for each case.

The total effect of a discontinuity is the sum of three effects. To examine these effects, however it is convenient to vary only one of the parameters and hold the others constant. For Case I as an example, the effects of a discontinuity may be identified and evaluated as follows:

- Size of Discontinuity: Vary the parameter R and hold K and C constant in the stability formulae.
- Effective Stiffness: Vary the parameter K and hold R and C constant in the stability formulae.

- Location of Discontinuity: Vary the parameter C and hold R and K constant in the stability formulae.

Clearly, these effects of a discontinuity influence the response in terms of parametric stability, free-vibration, and static stability through the stability formulae.

Parametric Stability

The basic parametric stability formulae of Equation (1) in Chapter III, for the uniform column are presented in Figure 19. It can be noted that the zones of instability in the figure represent both the compressive and tensile mean loads. An examination of Equation (1) in Chapter III reveals that the column will be loaded with the buckling load when $\mu = 1/2$. Since the stability results for the column loaded below the buckling load are of interest, the values of μ are chosen to be $0 \leq \mu \leq 1/2$ in the graphical presentation. The boundaries of the zones of instability for the uniform column are shown along with corresponding stability boundaries for the columns with a region of discontinuity in presentations which follow. This facilitates an evaluation of the effects of the discontinuities.

Size of Discontinuity. Figures 20 and 21 show the influence of the size of discontinuity using the stability models, for Case I and Case III. The solid lines represent the corresponding uniform column stability boundaries. The following observations can be made for the stability behavior:

- For non-zero values of C, K, P_o and R, the instability zones

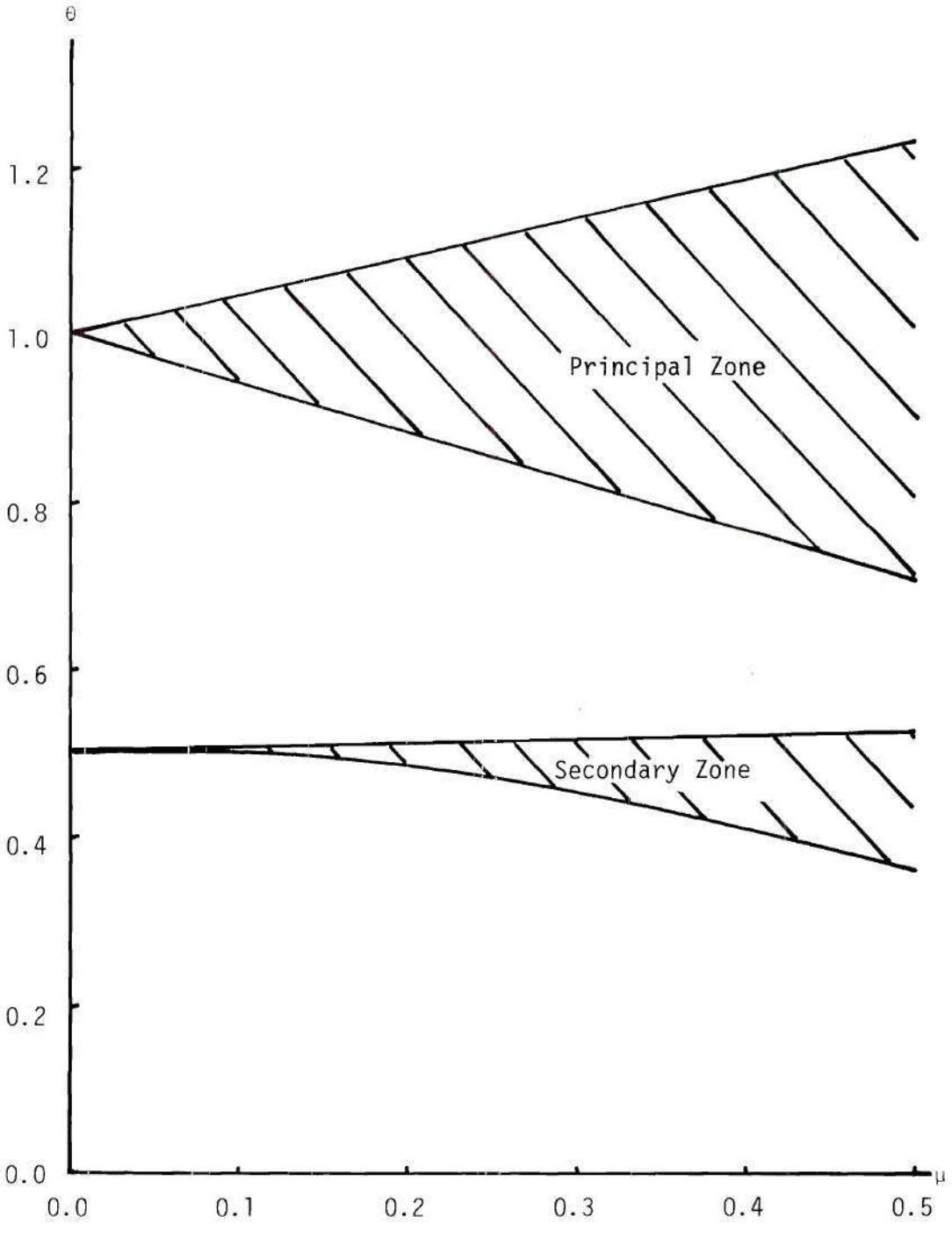

Figure 19. Dynamic Stability of Uniform Column.

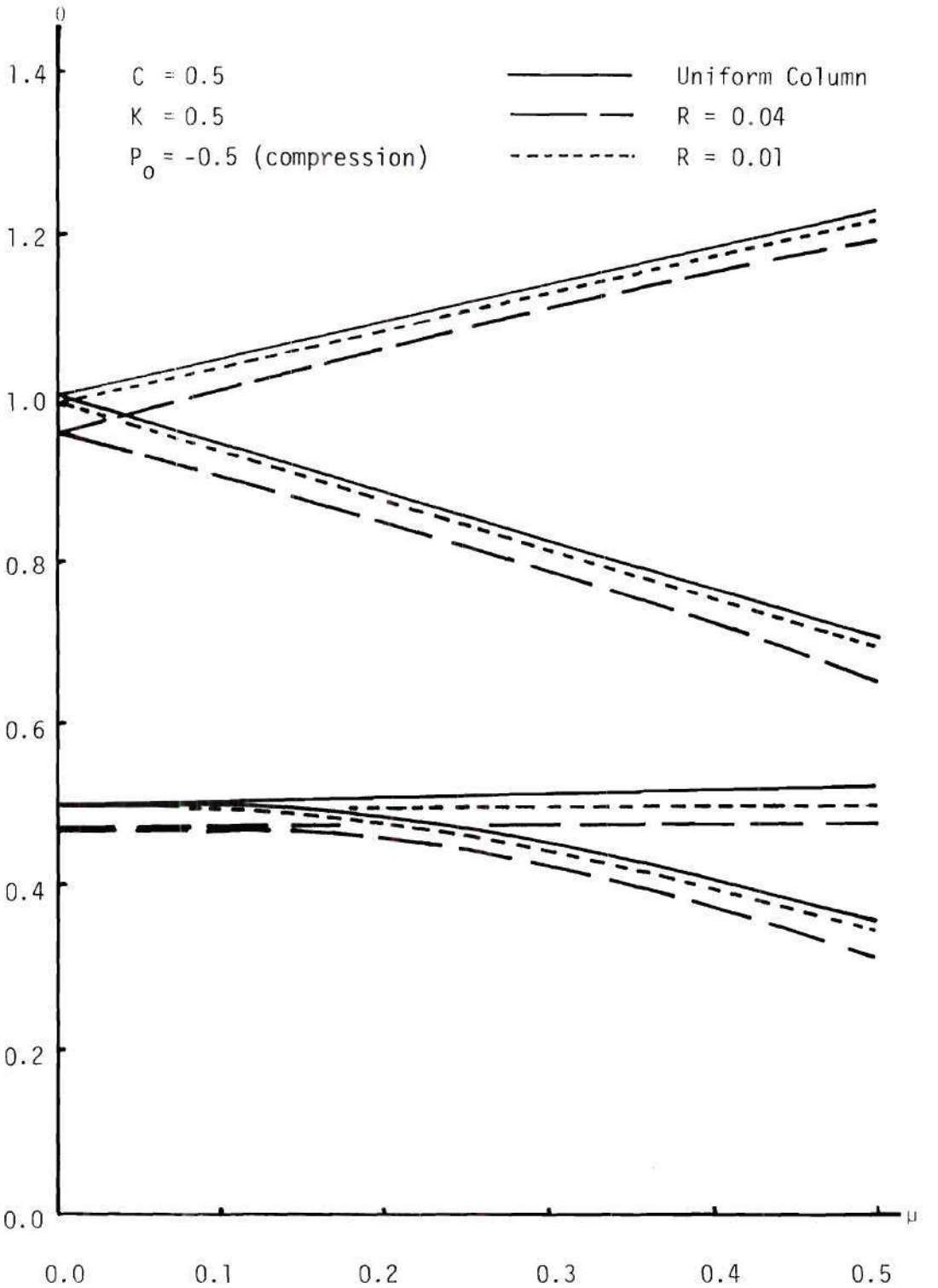

Figure 20. Effect of R on the Dynamic Stability with C = 0.5, K = 0.5 and P_o = -0.5, Case I.

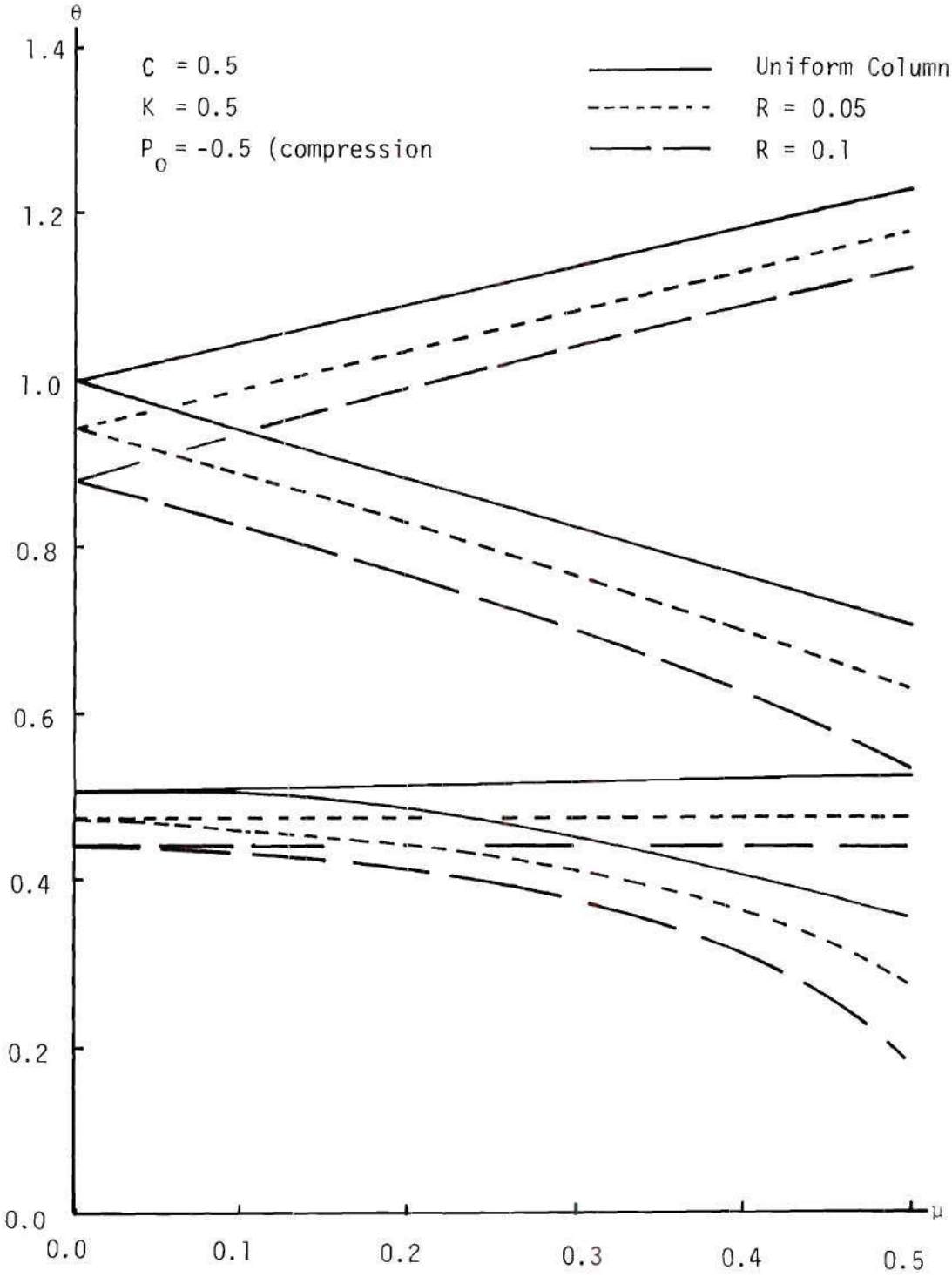

Figure 21. Effect of R on the Dynamic Stability with C = 0.5, K = 0.5 and P_o = -0.5, Case III.

occur at a lower frequency range and are larger* than the corresponding uniform column instability zones.

o For given values of C, K and P_o with the decreasing values of R i.e. size of discontinuity region, the instability zones approach the corresponding uniform column instability zones.

Physically, the size of the discontinuity cannot be greater than the length of the column, which means the possible range of R is $0 \leq R \leq 1/2$ when $C = 1/2$.

From Equation (24) of Chapter II in non-dimensional form as

$$\theta_* = \frac{1}{2}\left[1 + \frac{\bar{e}_{11}}{\ell} + P_o - \frac{P_1^2}{2\left[1 + \frac{\bar{e}_{11}}{\ell} + P_o\right]}\right]^{1/2}$$

it is observed that

$$0 < 1 + \frac{\bar{e}_{11}}{\ell} + P_o - \frac{P_1^2}{2\left[1 + \frac{\bar{e}_{11}}{\ell} + P_o\right]} \quad \text{if } \theta_* > 0 .$$

Substitution of $C = 0.5$, $P_o = -0.5$, $P_1 = 0.5$ and using Equation (21) of Chapter II in non-dimensional form with $K = 0.5$ in above inequality yields

$$0 \leq R \leq \frac{1}{4} \quad \text{if } \theta_* > 0 \text{ and } \left(\frac{1}{2} + \frac{\bar{e}_{11}}{\ell}\right) > 0 .$$

Thus, the stability analysis using Case I with the values of C, P_o, P_1

---

*Appendix B: A Comparison of the Widths of the Instability Zones.

and K illustrated above is valid for $0 \leq R \leq \frac{1}{4}$. It can be noted that $R = \frac{1}{4}$ implies that the size of the discontinuity region is equal to one half the column length. Similarly, the ranges of R for Case I and Case II can be established for given values of P_1 and P_0. Recall that the Case II analysis reduces to Case I when C = 0.5. Therefore, results presented in Figure 20 also apply to Case II.

Effective Stiffness. The influence of the effective stiffness, K on the dynamic stability behavior using Case I and Case III are exemplified in Figures 22 and 23 respectively. It can again be noted that Case I reduces to Case II when C = 0.5. An examination of the results presented in these figures show that as the effective stiffness approaches the uniform column stiffness, the instability zone with effective stiffness approaches the corresponding uniform column instability zone. Also, the instability zones enlarge as the effective stiffness decreases. Clearly, K can assume any value in the interval $0 \leq K \leq 1$. When k = 1, the results for the uniform column are obtained. However, if K = 0 and $R \neq 0$ then the idealized column degenerates into the configuration shown in Figure 24. The shaded region in the figure represents a distributed mass of length 2R with zero bending stiffness. Physically, zero bending stiffness elements can be interpreted as cable or string elements. Clearly, such a system is unstable for oscillating compression but for oscillating tension a meaningful dynamic stability result is possible. It may, in fact, be a condition which may be approached in a composite material in which extensive cracking has occurred in surface layers.

It can be noted that the uniform column results can be recovered if both K and R approach zero.

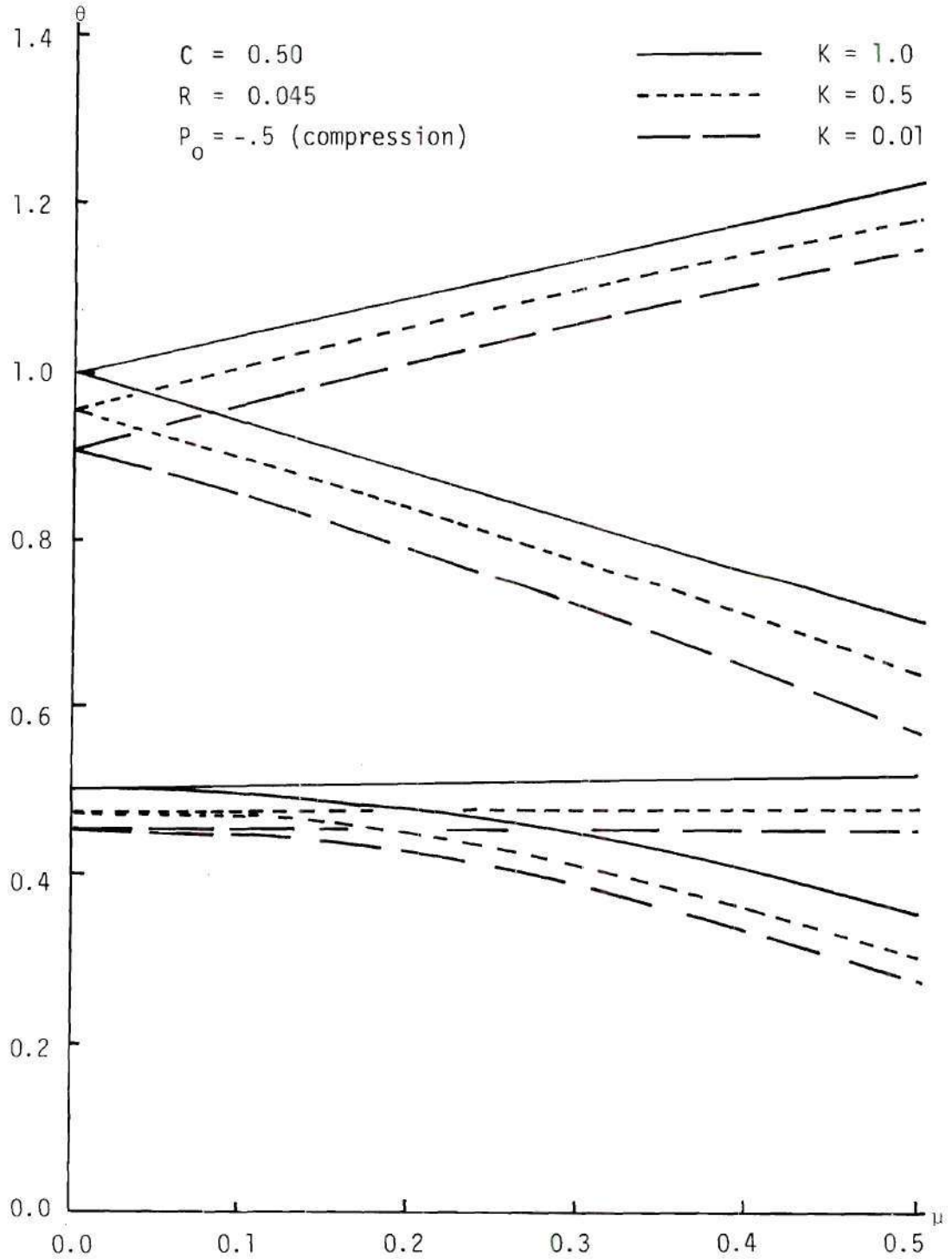

Figure 22. Effect of K on the Dynamic Stability with C = 0.50, R = 0.045 and P_o = -0.5, Case I.

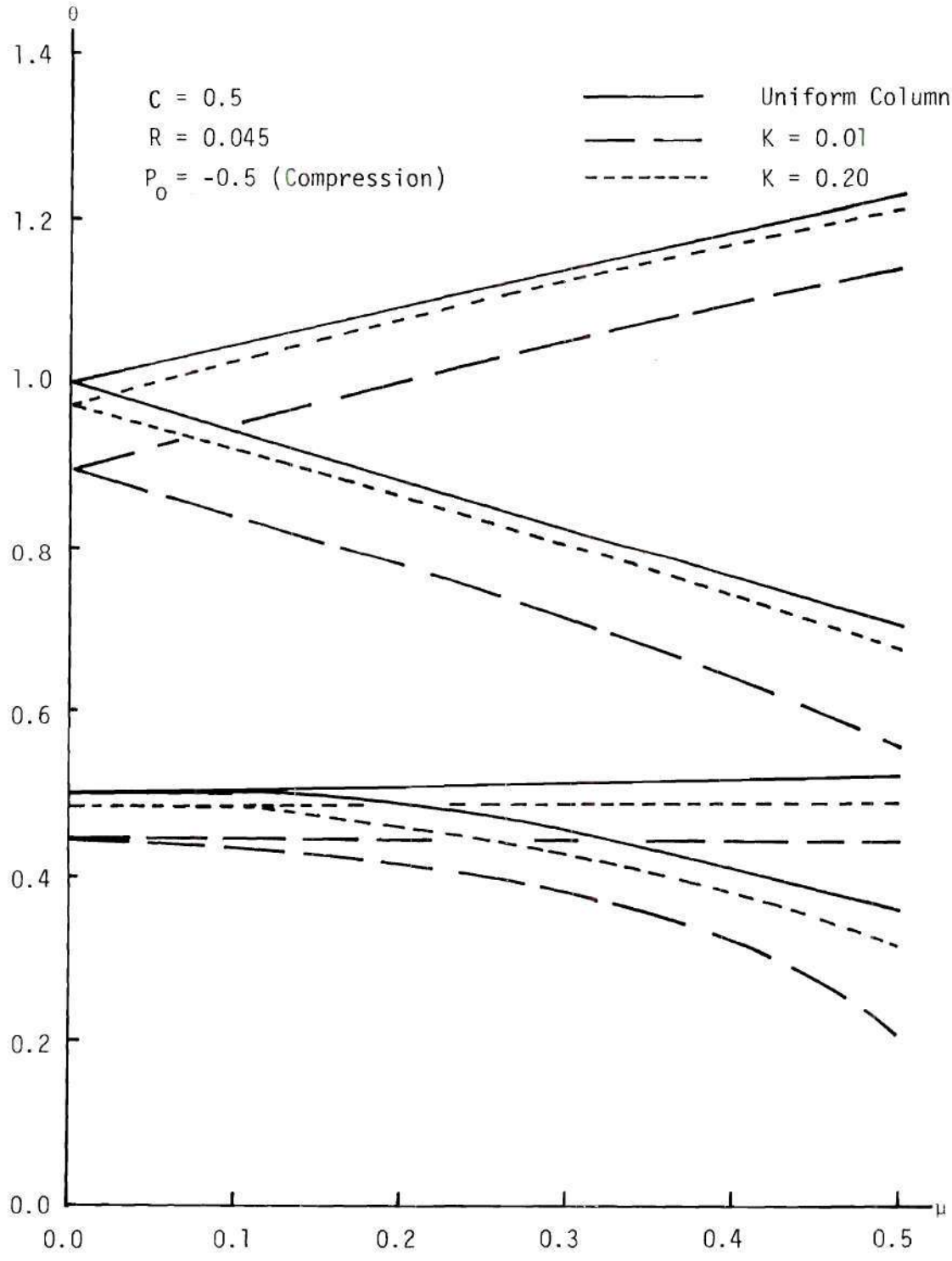

Figure 23. Effect of K on the Dynamic Stability with C = 0.5, R = 0.045 and P_o = -0.5, Case III.

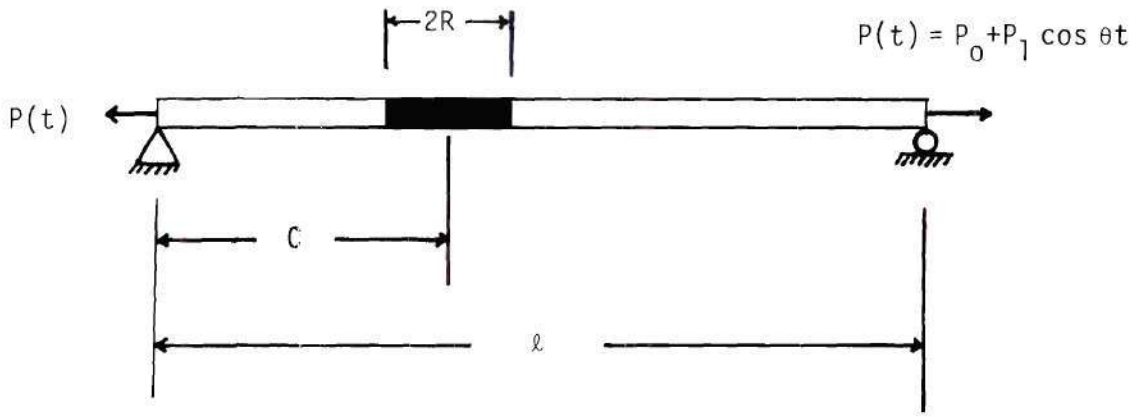

Figure 24. A Degenerate Result.

Location of Discontinuity. The influence of the location of the discontinuity region, C, on the dynamic stability is depicted in Figure 25 for Case I. For R = .02, K = 0.01 and P_0 = -0.5 the instability zone occurs at a lower frequency range and becomes larger as the region of discontinuity moves towards the center of the column. However, when the region of discontinuity moves toward either end of the column, the dynamic stability behavior of the column approaches that of the uniform column. Similar results can be obtained using Case II. It can be recalled, however, that Case III is applicable only for C = .5.

In the above discussion the effects of parameters R, K and C on the stability behavior of the column are considered. The parameters R and C represent the geometric characteristics of the column and K represents geometric-material properties of the column. However, the parameter P_0 and P_1 represent the loading characteristics of the column. The influence of P_0 on the instability is illustrated in Figures 26 and 27 for Case I and Case III respectively. It may be noted that, for C = 0.5, R = 0.045 and K = 0.01 the instability zones occur at a lower frequency range and are enlarged as P_0 decreases from zero to compression. Recall that the corresponding Case II result is the same as for Case I since C = 0.5.

Free-Vibration

In previous paragraphs we considered the influence of a region of discontinuity on the parametric stability behavior of the column. The influence of a region of discontinuity on the free-vibration behavior of the column is depicted in Figures 28 through 32. It can be noted

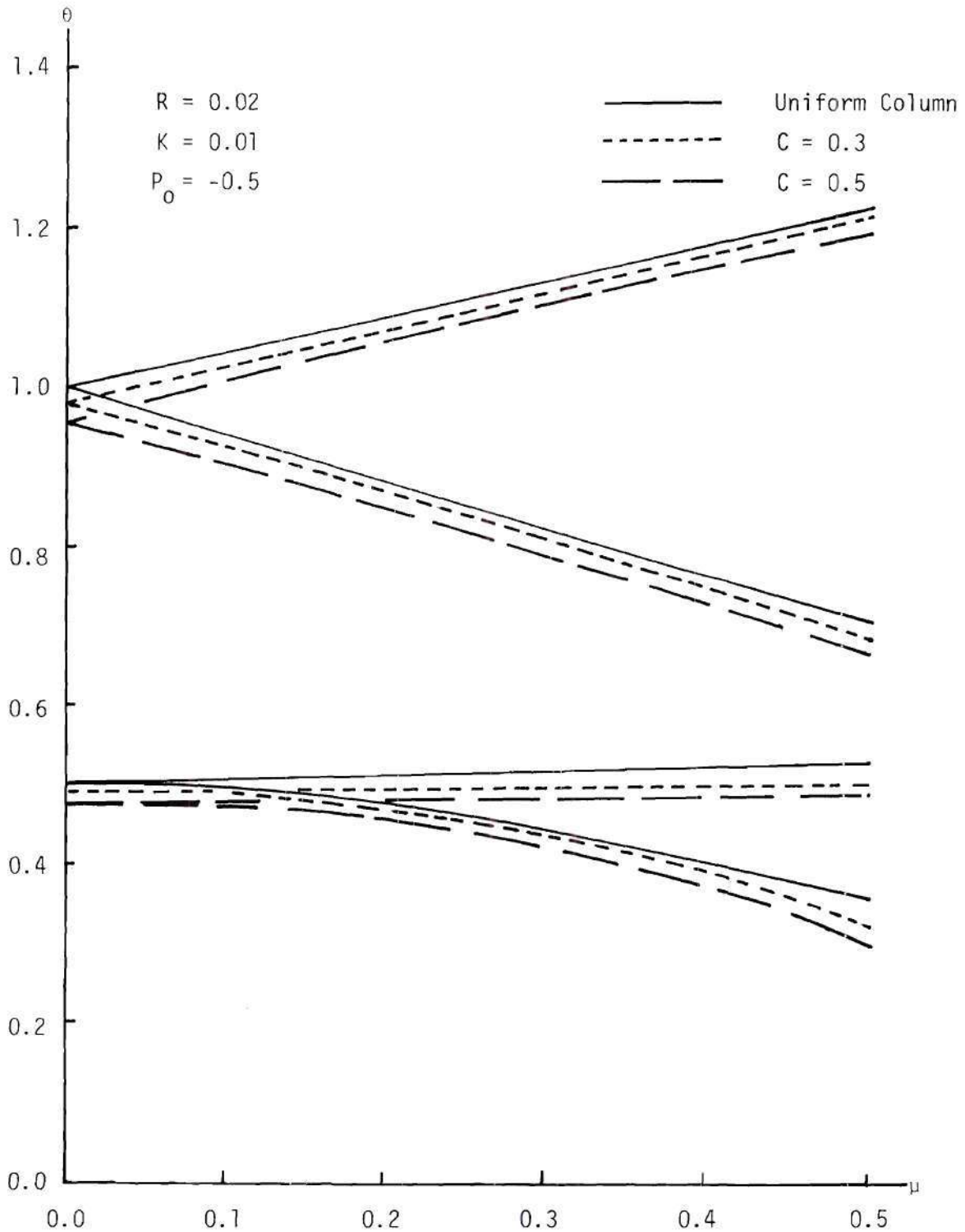

Figure 25. Effect of C on the Dynamic Stability with R = 0.02, K = 0.01 and P_o = -0.5, Case I.

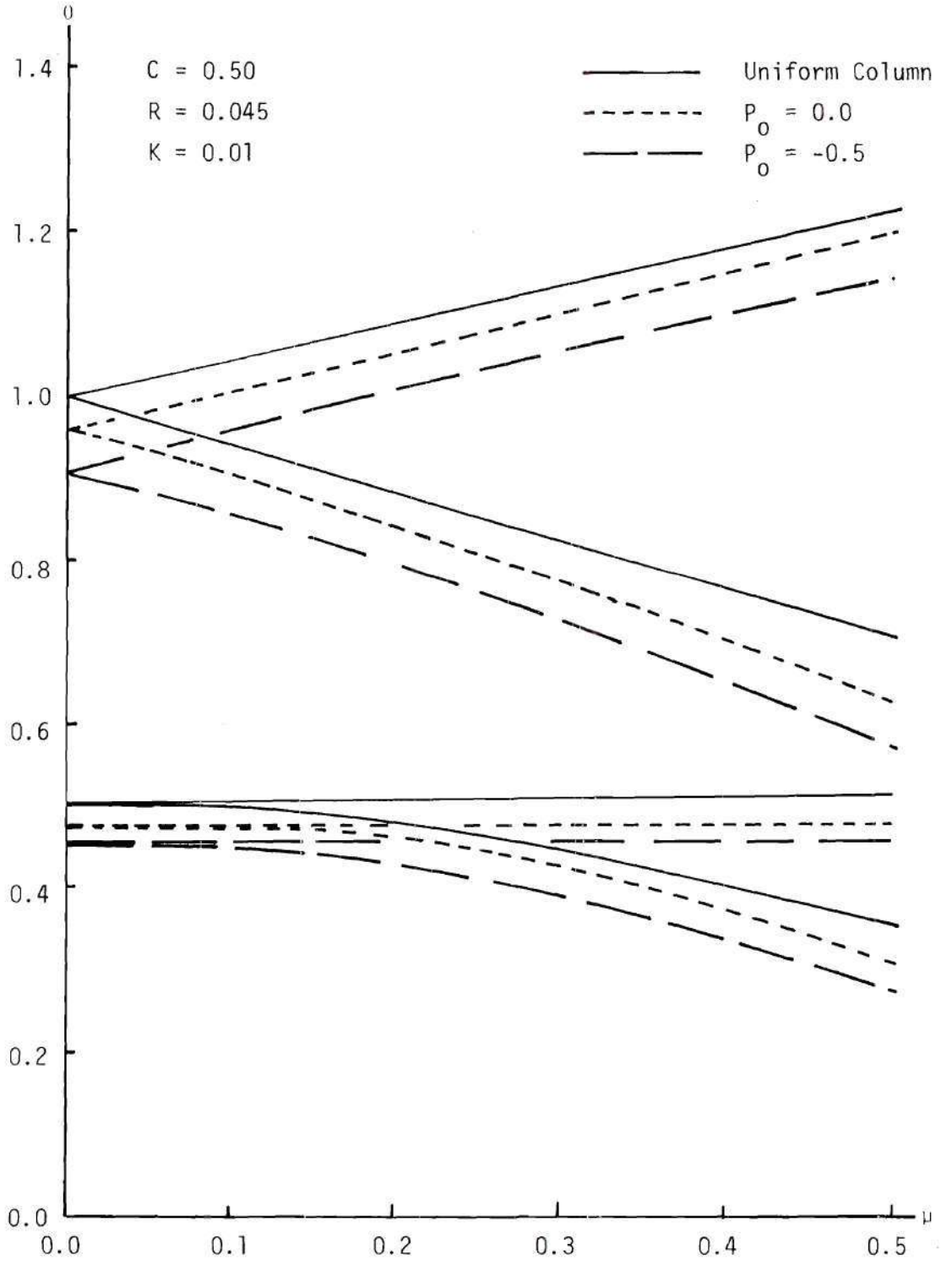

Figure 26. Effect of P_o on the Dynamic Stability with C = 0.5, R = 0.045 and K = 0.01, Case I.

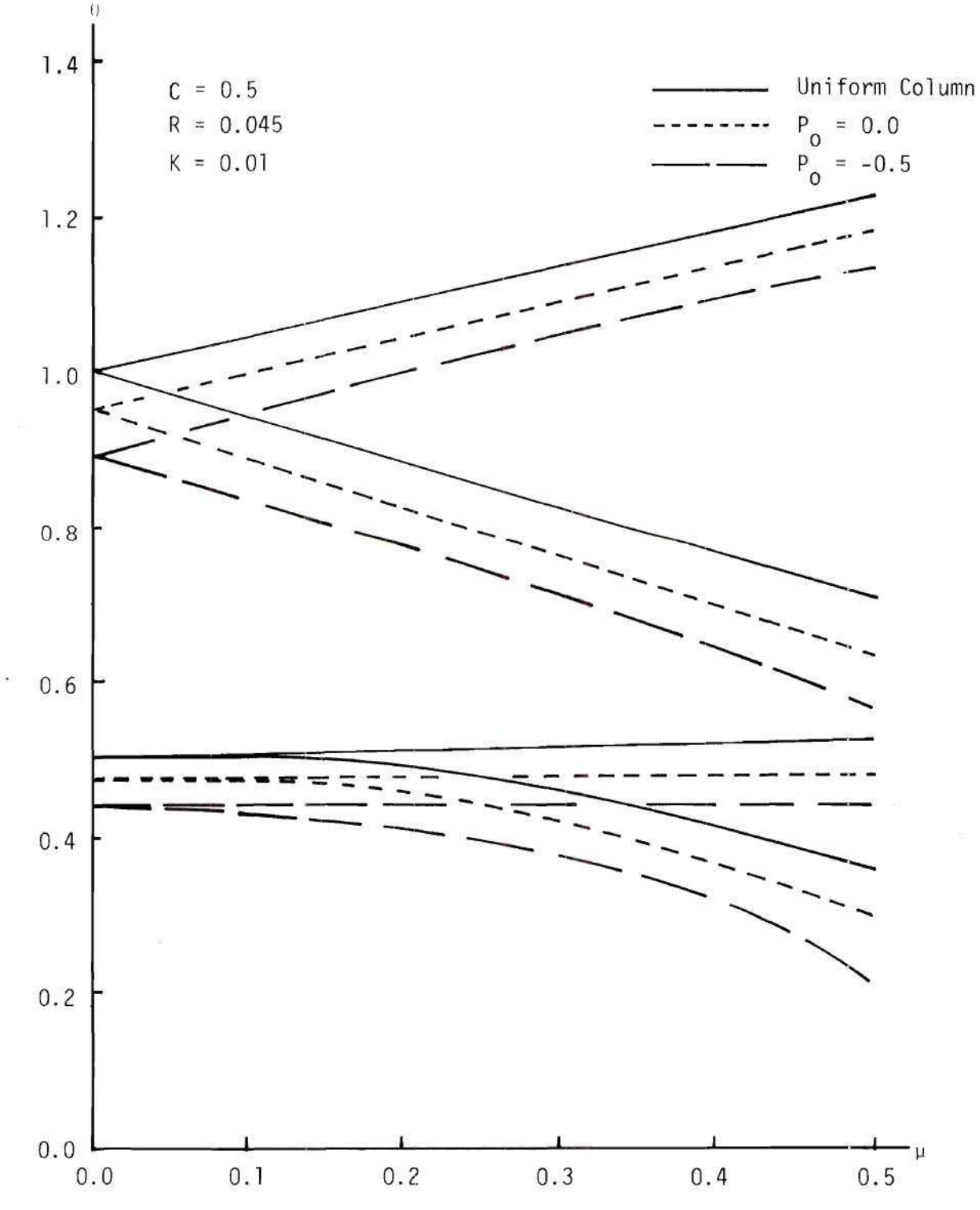

Figure 27. Effect of P_o on the Dynamic Stability with C = 0.5, R = 0.045 and K = 0.01, Case III.

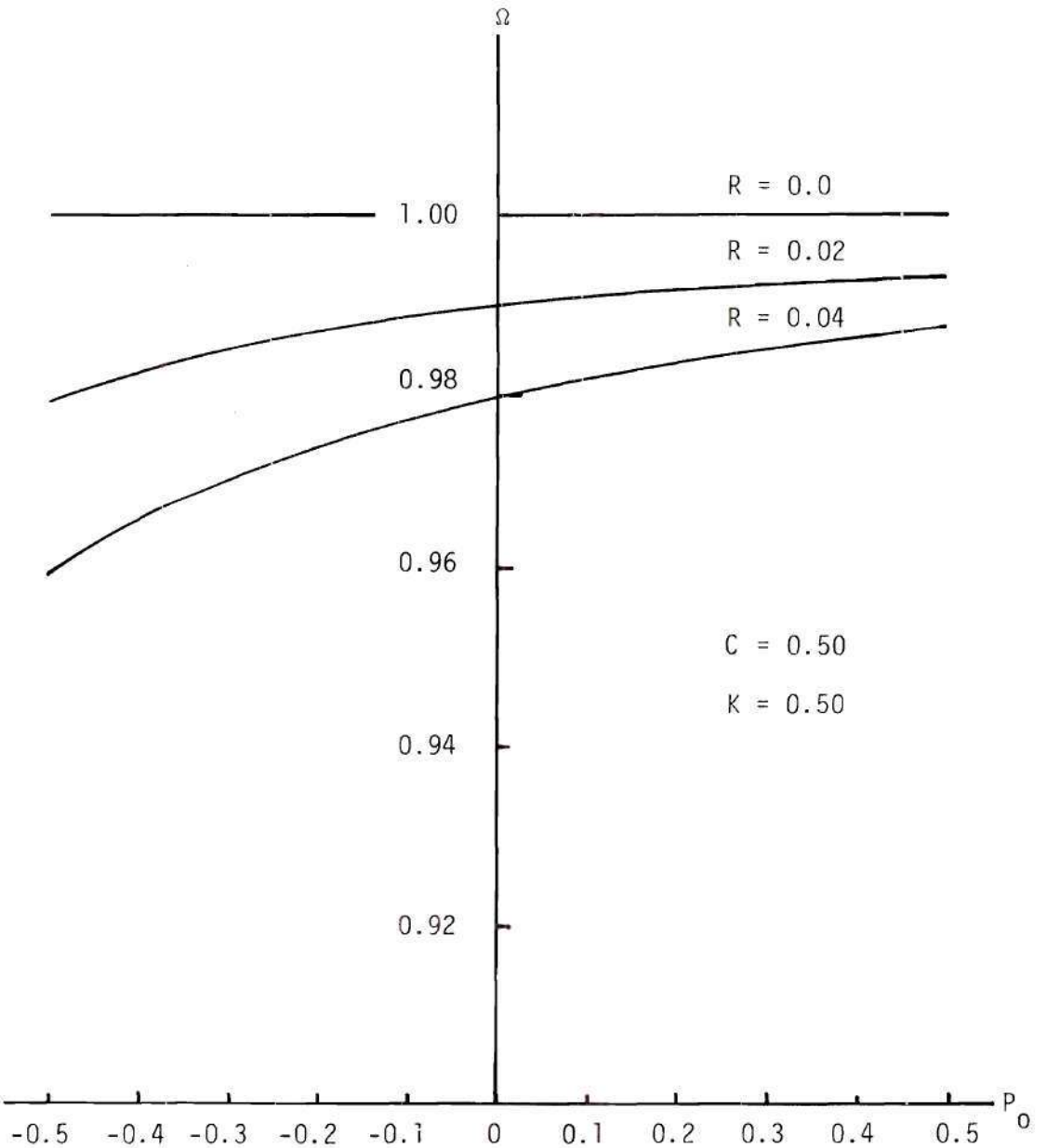

Figure 28. Effect of R on the Free-Vibration Frequency with C = 0.5 and K = 0.50, Case I and Case II.

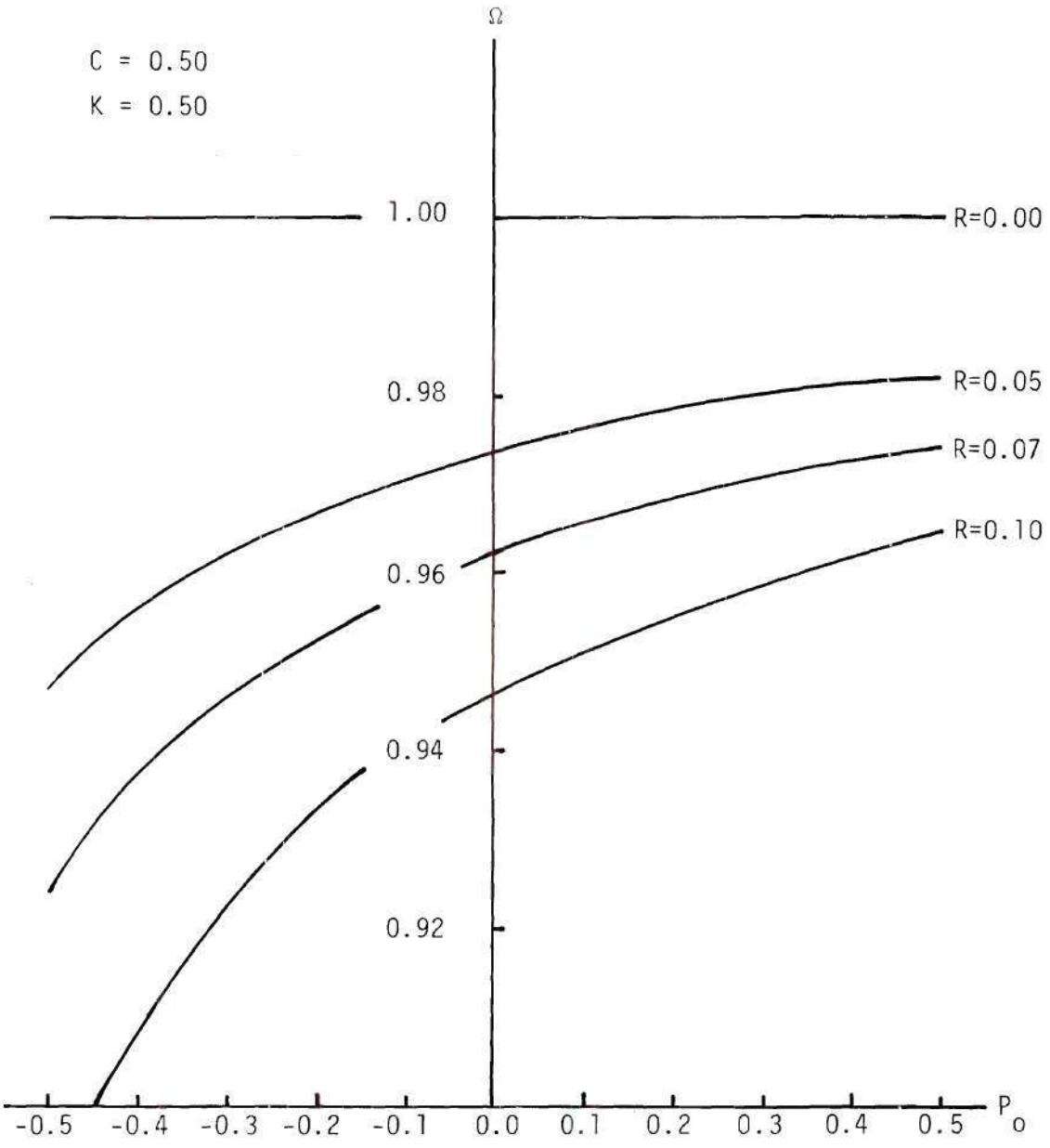

Figure 29. Effect of R on the Free-Vibration Frequency with C = 0.5 and K = 0.50, Case III.

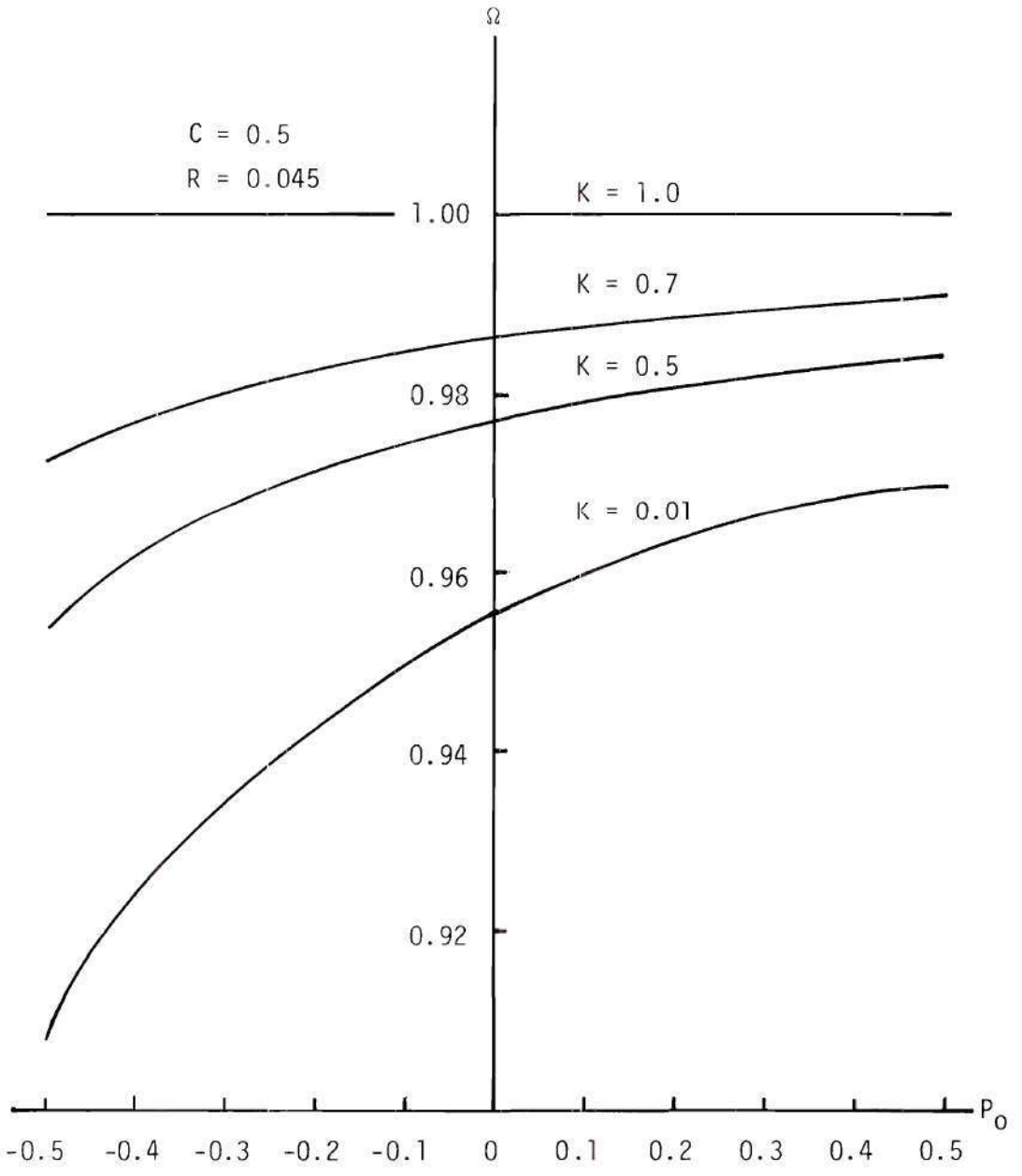

Figure 30. Effect of K on the Free-Vibration Frequency with C = 0.5 and R = 0.045, Case I and Case II.

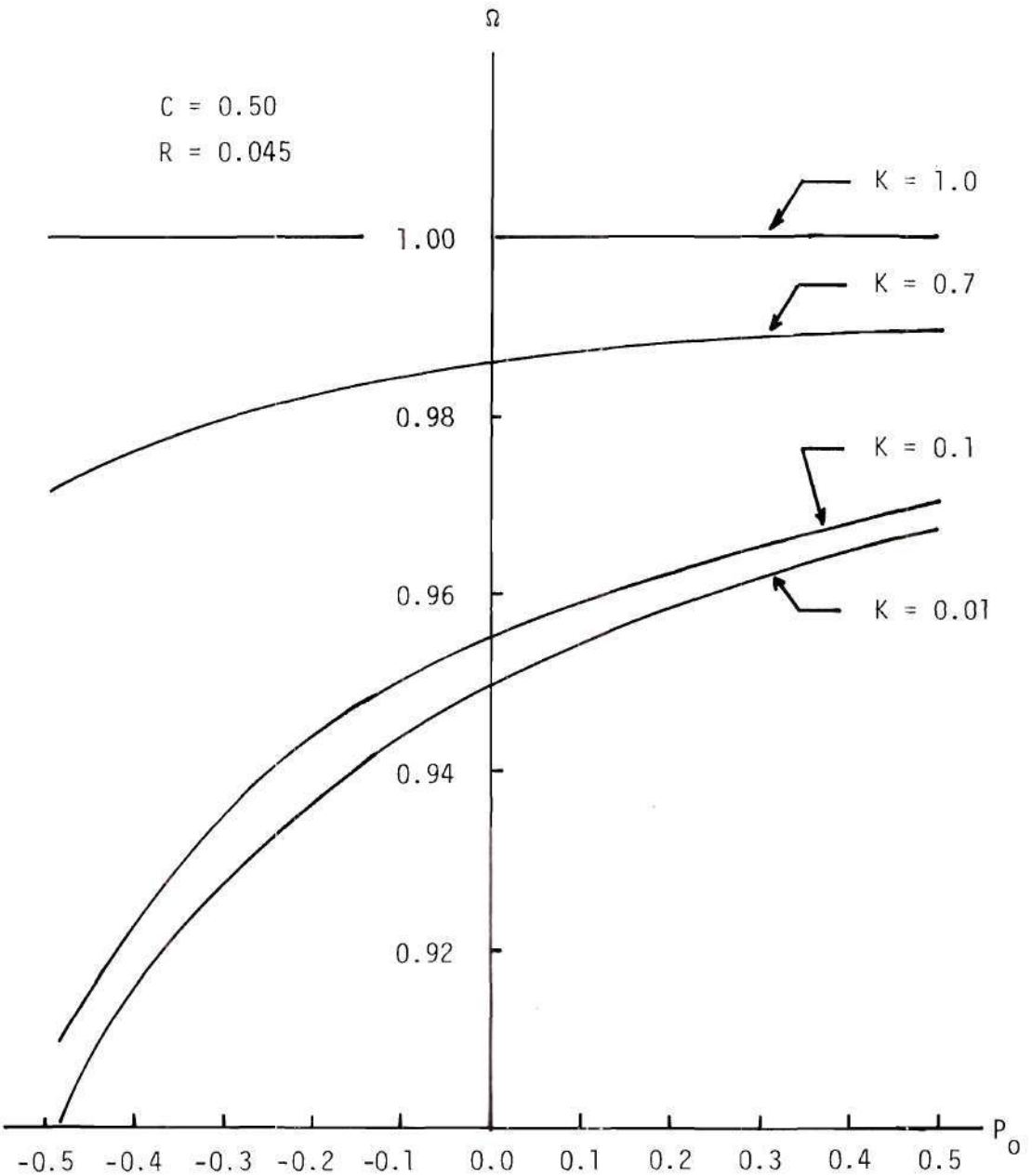

Figure 31. Effect of K on the Free-Vibration Frequency with C = 0.50 and R = 0.045, Case III.

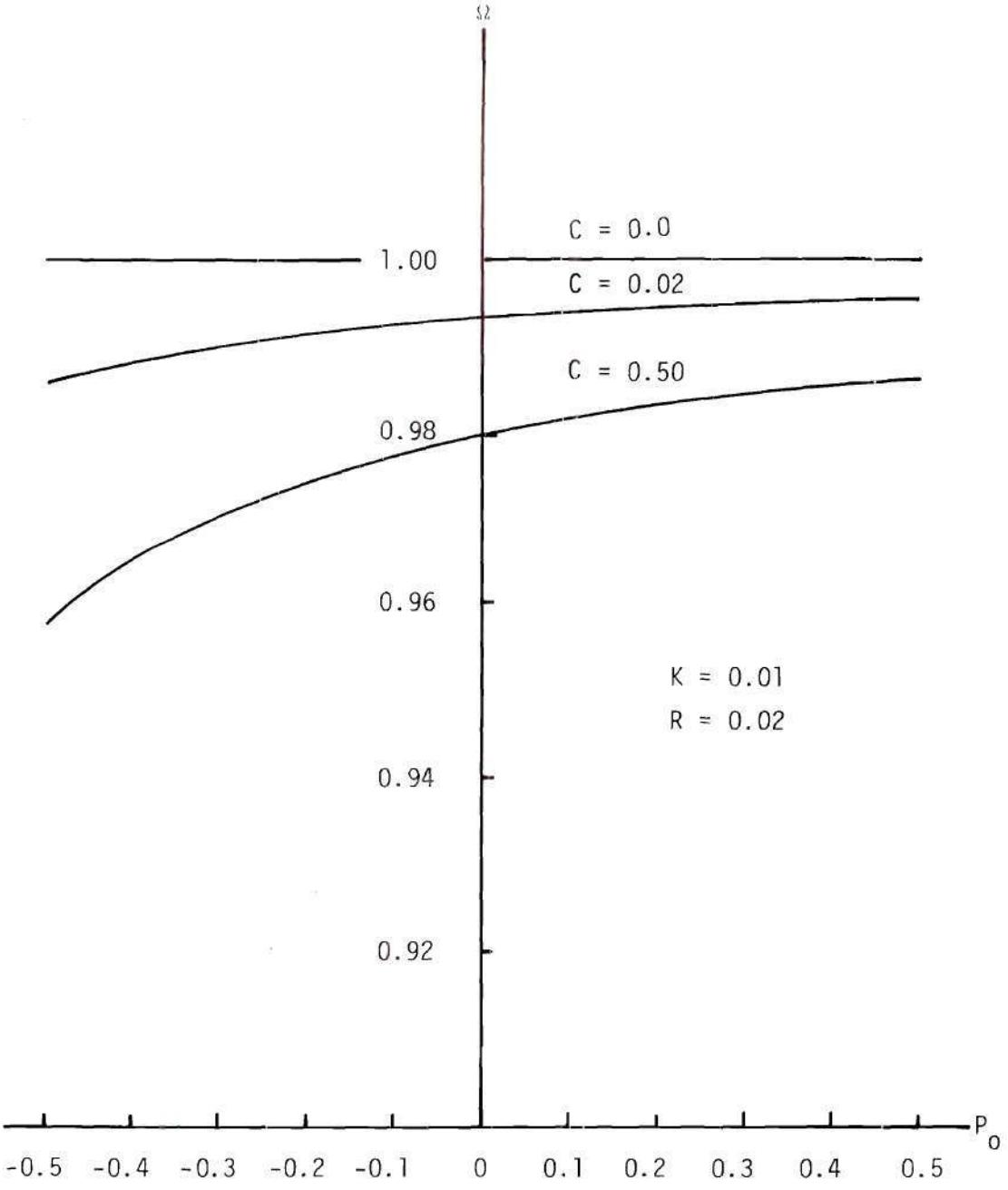

Figure 32. Effect of C on the Free-Vibration Frequency with K = 0.01 and R = 0.02, Case I.

that Ω_*, P_o, R, K, and C are the non-dimensional parameters. An examination of these figures reveals the following free-vibration behavior for a column with a region of discontinuity:

Size of Discontinuity. An examination of Figures 28 and 29 shows that for given values of C, K and P_o, the free-vibration frequency decreases as R increases. However, for given values of C, K and R the frequency increases as P_o increases from compression to tensile load, and the frequency approaches the corresponding uniform column frequency. (Note that the vibration frequency is nondimensionalized with respect to frequency of axially loaded uniform column.) It can be noted that the frequency increases more rapidly in the compression range than the tensile range as P_o increases.

Effective Stiffness. Figures 30 and 31 reveal that for given values of C, R and P_o, the free-vibration frequency decreases as K decreases. However, for given values of C, R and K the frequency increases as P_o increases from a compressive to a tensile load, and the frequency approaches the corresponding uniform column frequency. Note that the frequency increases more rapidly in the compression range than in the tensile range as P_o increases.

Location of Discontinuity. The influence of the location of a region of discontinuity on the free vibration frequency is shown in Figure 32. For given values of K, R and P_o, the free-vibration frequency decreases as C approaches 0.5 (the center) from zero. For given values C, R and K the frequency increases as P_o increases from compression to tensile load and the frequency approaches the corresponding uniform column

frequency. Note that the frequency increases more rapidly in the compressive range than in the tensile range as P_o increases. In addition to the above observations, the following points can be made:

o When the effective stiffness approaches zero and the size of discontinuity is non-zero, we obtain the free-vibration frequency of the column shown in Figure 24. However if the size of the discontinuity also, approaches zero, then the uniform column frequency is recovered.

o When effective stiffness approaches the corresponding uniform stiffness or size of the discontinuity approaches zero or center of the region discontinuity approaches either end, then again the uniform column frequency is recovered. Clearly, the center of the region of discontinuity cannot be exactly at $x = 0$ or $x = \ell$.

Static Stability

The influence of a region of discontinuity on the buckling load is shown in Figures 33 and 34. In Figures 34 the first and second successive approximations are indicated by solid and dashed lines. An examination of these figures and Equations (26), (48) and (52) of Chapter II in non-dimensional form reveals the following buckling load behavior of the column.

Size of Discontinuity. For given values of C and K the buckling load decreases as the size of discontinuity, R, increases. This behavior is linear with small values of R and when R approaches zero, $P_\star$ approaches 1, i.e., uniform column result. We recall that $0 \leq R \leq 1/2$, and Equations (25), (48) and (67) of Chapter II suggest that this range of R depends on the initial load, P_o. An examination of Equations (26),

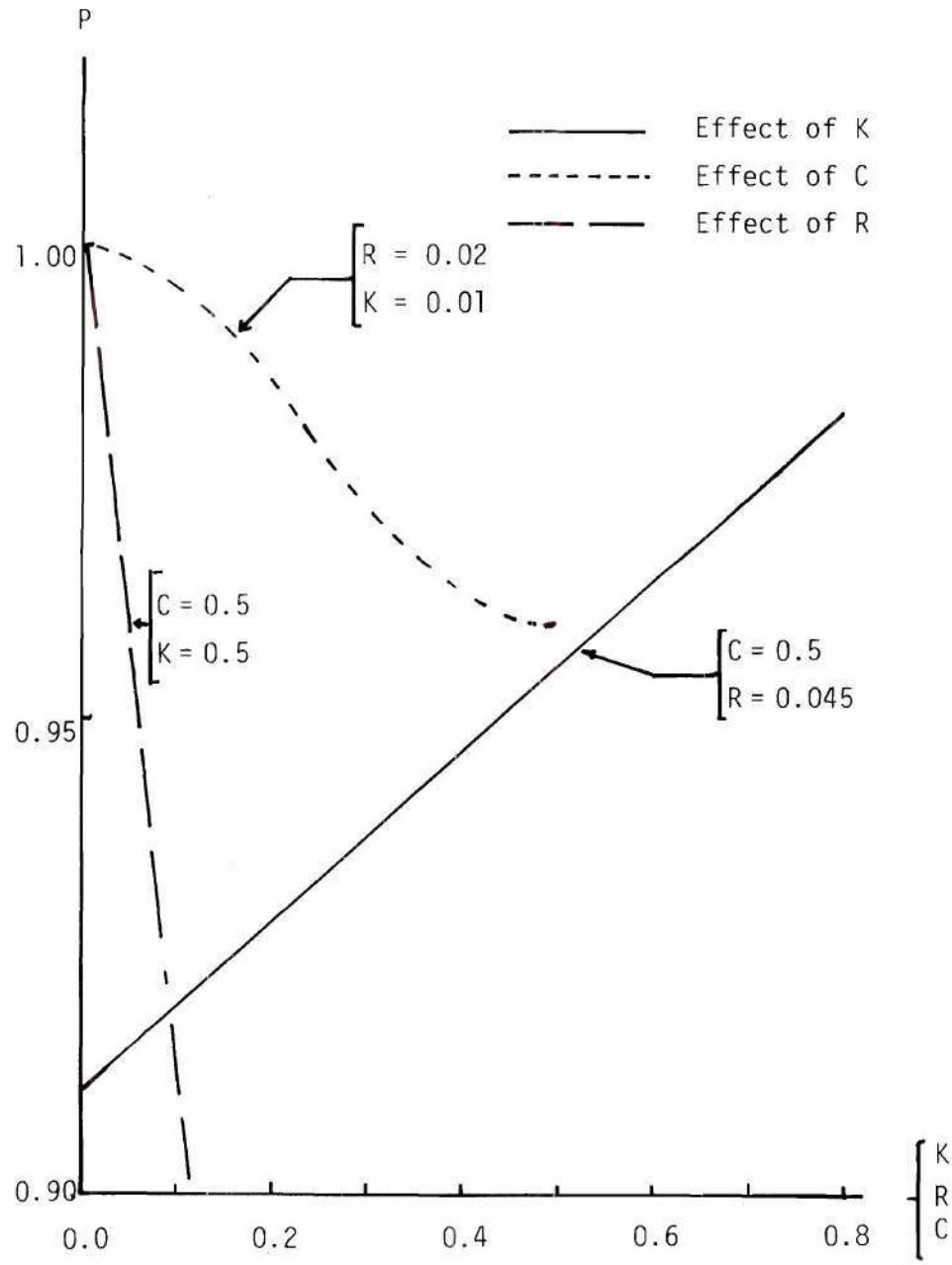

Figure 33. Effects of K, R and C on the Buckling Load, Case I.

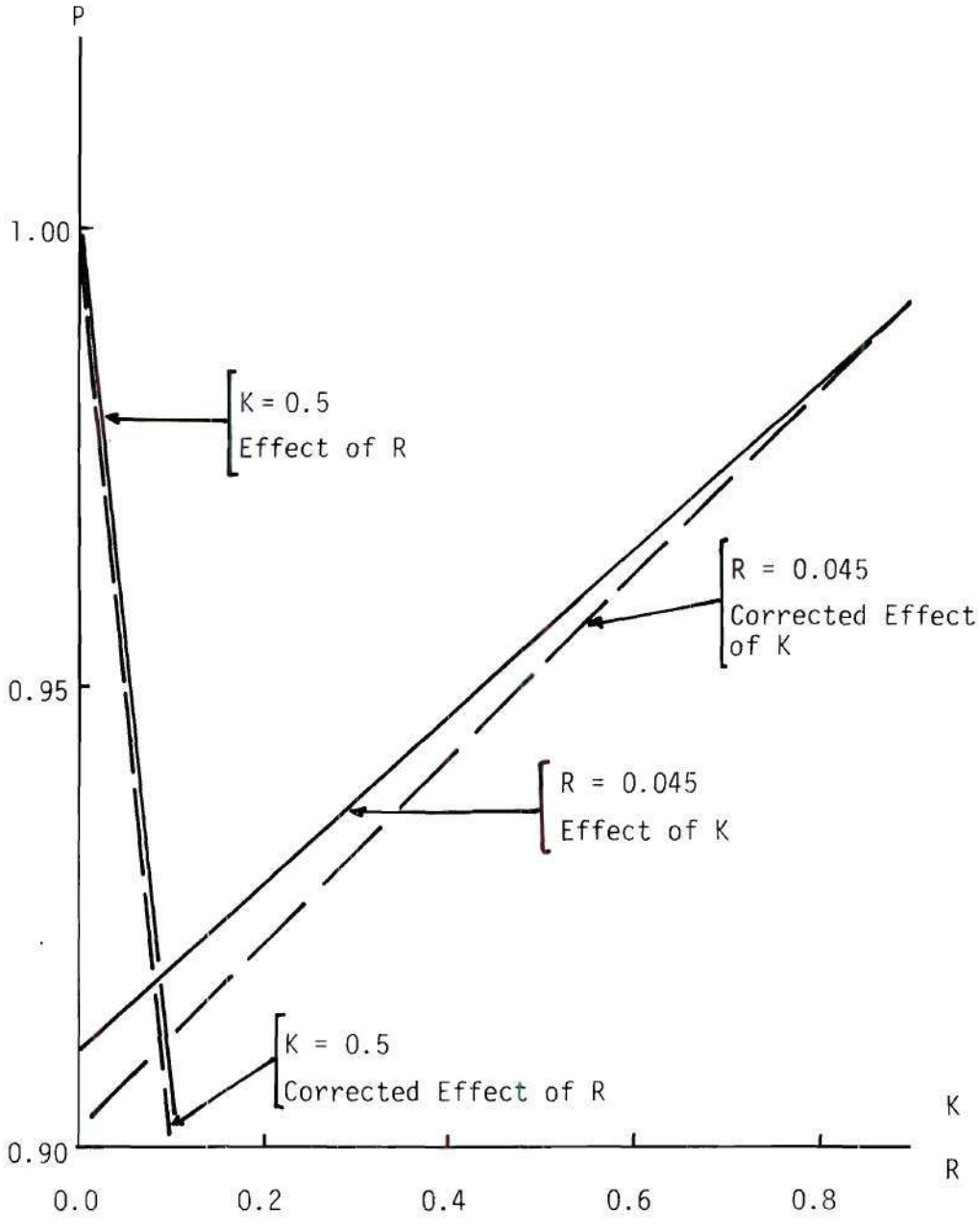

Figure 34. Effect of K and R on the Buckling Load, Case III.

(52) and (68) of Chapter II reveals that when R = 1/2 the buckling load reduces to $P_I = 1 + \frac{1}{2}(K - 1)$ for any value of C. When values of R are sufficiently large the P_* and R relations become non-linear.

Effective Stiffness. For given values of C and R the buckling load increases linearly with K. It can be noted that the buckling load approaches the corresponding uniform column buckling load as K approaches 1, i.e. effective stiffness approaches the uniform stiffness.

Location of Discontinuity. For given values R and K P_* versus C is symmetric with respect to the line C = 1/2, and the slopes are

$$\left.\frac{\partial P_*}{\partial C}\right|_{C=0,C=1/2} = 0 .$$

The buckling load decreases as the discontinuity moves toward the center of the column. If the discontinuity is at either end of the column, the uniform column buckling load is recovered. It can be noted, however, that the center of the discontinuity cannot be at C = 0 or C = 1.0. Note that the results presented in Figure 27 are for Case III where C = 0.5.

Correlation of Experimental and Analytical Results

In the last two sections, an examination of analytical stability models was presented. Three parameters: size of discontinuity, effective stiffness; and, location of discontinuity were considered in the evaluation of effects of discontinuity on the stability of a column. Substituting the four-point-load bending results of $\frac{dP}{dv}$ versus slot length, S_ℓ into Equation (9) of Chapter II, the effective stiffness parameter, K for each specimen is obtained. The non-dimensional effective stiffness

versus slot length S_ℓ is graphically presented in Figure 35. Examination of this figure reveals that the effective stiffness decreases rapidly as the length of slot increases. Using these values of K with the corresponding values of R given in Figure 36 in the parametric stability formula of Equation (63) of Chapter II, the boundaries of instability for the column are obtained. These boundaries of instability with the corresponding experimental* results are presented in Figures 37 to 46. It can be noted that Figure 37 represents the uniform column result and Figures 38 to 46 represent the parametric instability results for the columns with slot lengths, S_ℓ = 0.2, 0.3 and 0.4 inches at the center i.e. C = 0.5. An examination of Figures 37 to 46 reveals that the parametric stability behavior obtained by the experiments and the analytical stability model are in reasonable agreement. The presence of a slot in the column lowers the principal and secondary instability zones slightly. The non-dimensional load parameters μ and P_o were computed using the uniform buckling load, 195.0 pounds. The effective length of the column was 33.85 inches and the column was simply supported at both ends. The frequencies were non-dimensionalized by

---

*Note that for a uniform column with a given value of P_o and $\mu = \frac{P_1}{2(P_o + P_{*1})}$, experiments were conducted to obtain the lower and upper boundary frequencies of the secondary instability zone. It was found that the values of these frequencies differed by a fraction of a Hz. Taking into account the possibility of statistical scatter in the experimental data, the procedure for data recording presented in Chapter III was adopted. Thus, only a single point is shown for the secondary zone for each value of P_1 as noted in Chapter III this represents the average value of θ^s_{max} from above and from below.

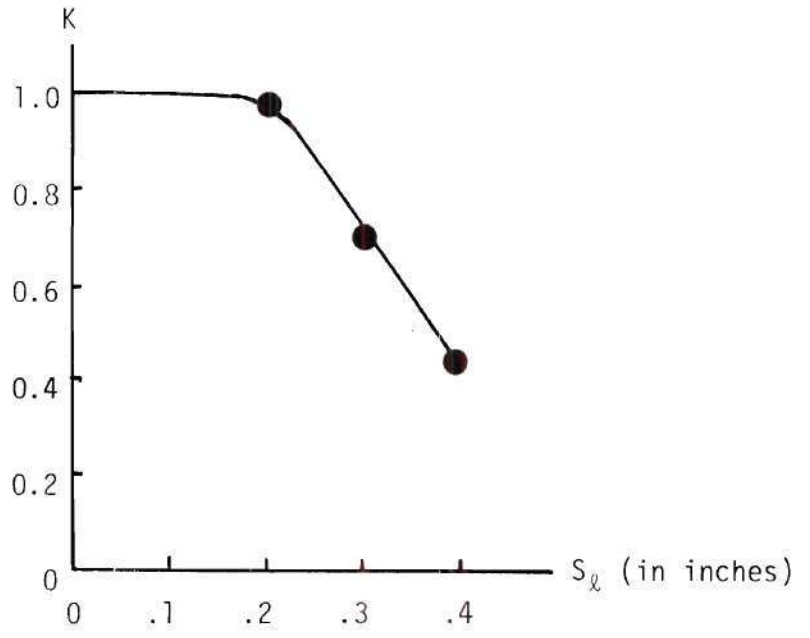

Figure 35. Slot Length Versus Non-dimensional Effective Stiffness.

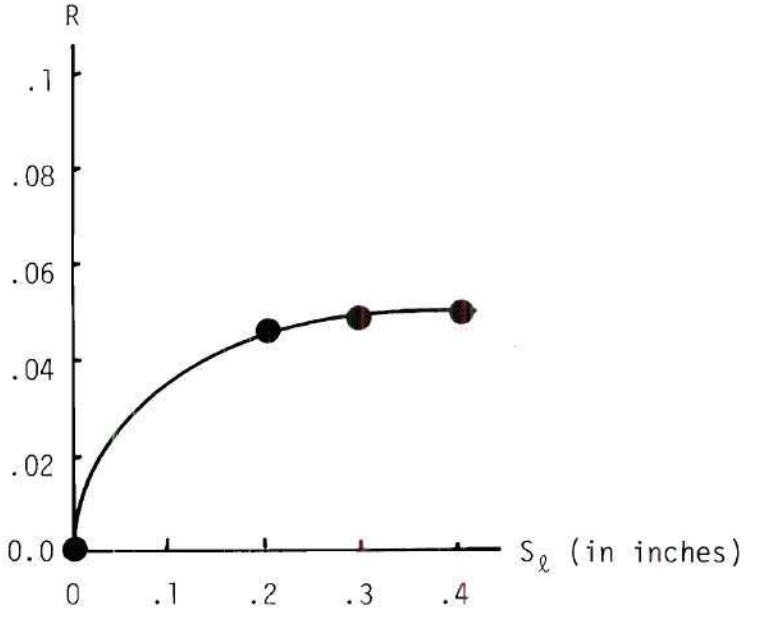

Figure 36. Slot Length Versus Non-dimensional Size of Discontinuities.

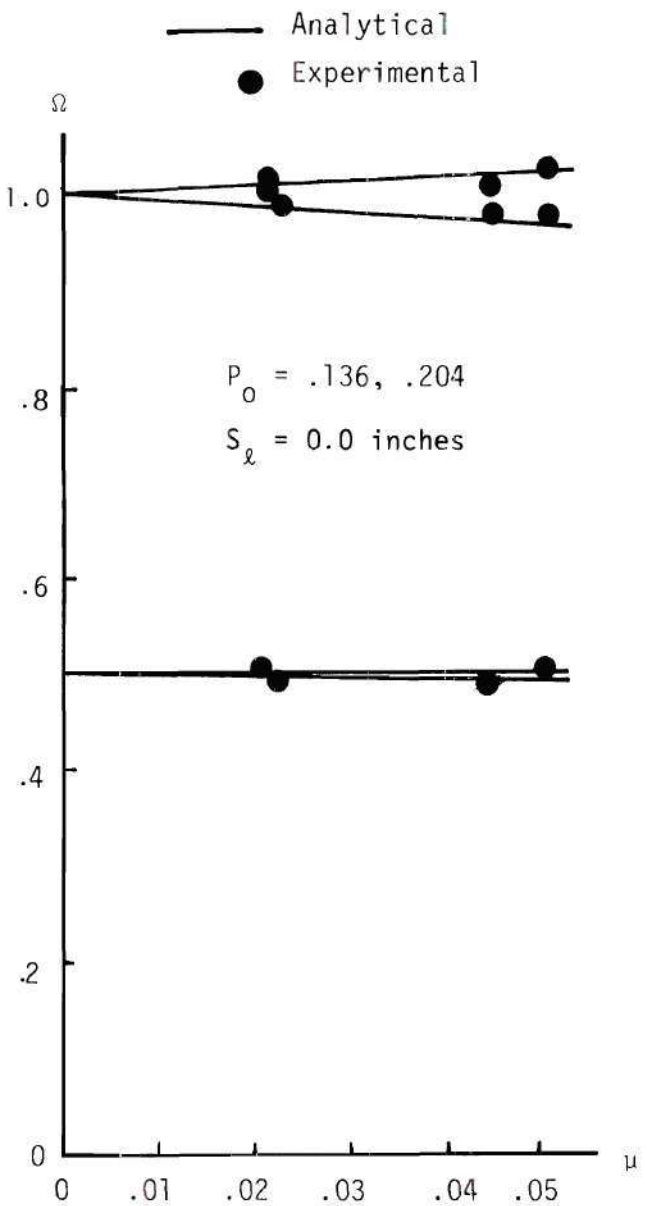

Figure 37. Dynamic Stability with $S_\ell = 0.0$, $P_o = .136$ and .204.

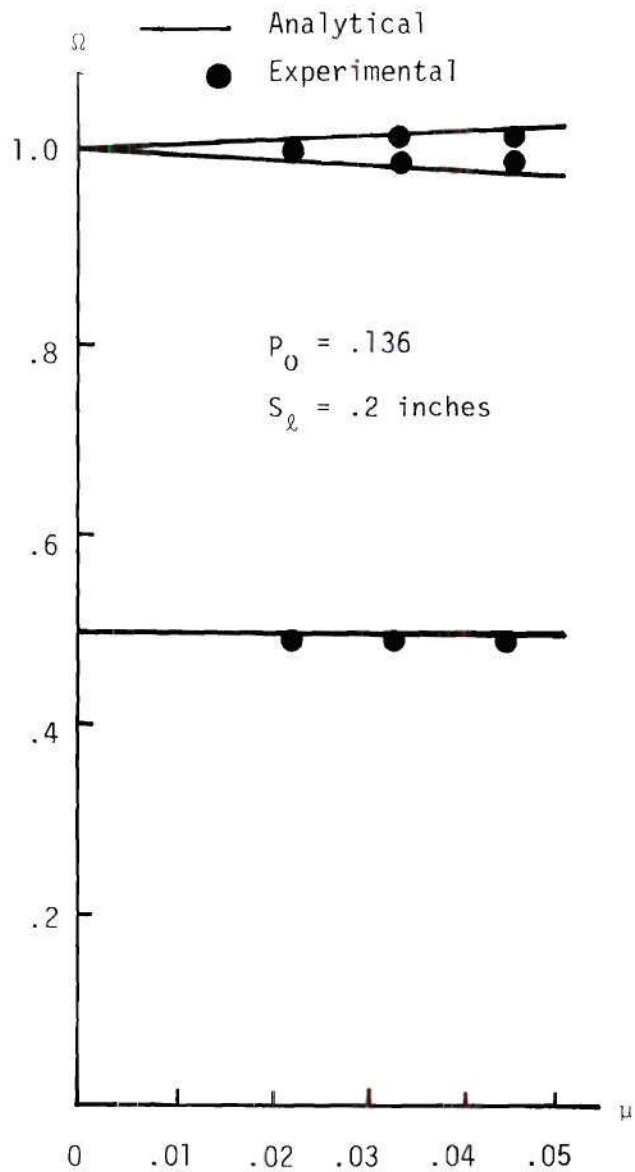

Figure 38. Dynamic Stability with S_ℓ = .2 and P_o = .136.

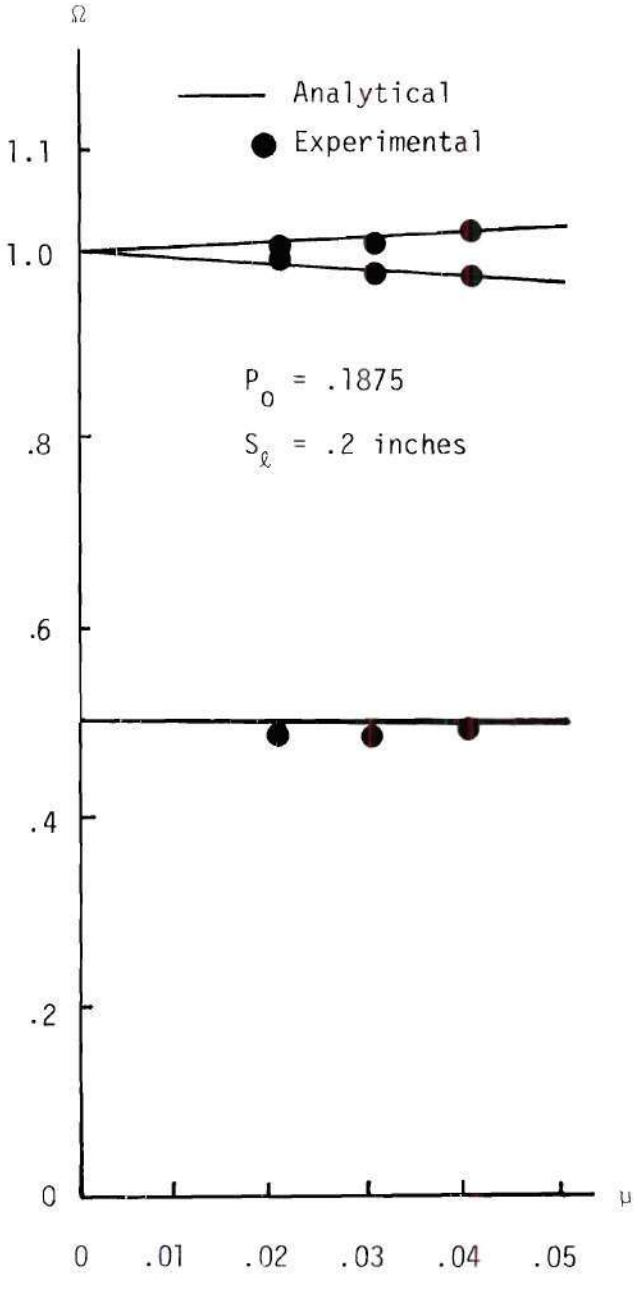

Figure 39. Dynamic Stability with S_ℓ = .2 and P_o = .1875.

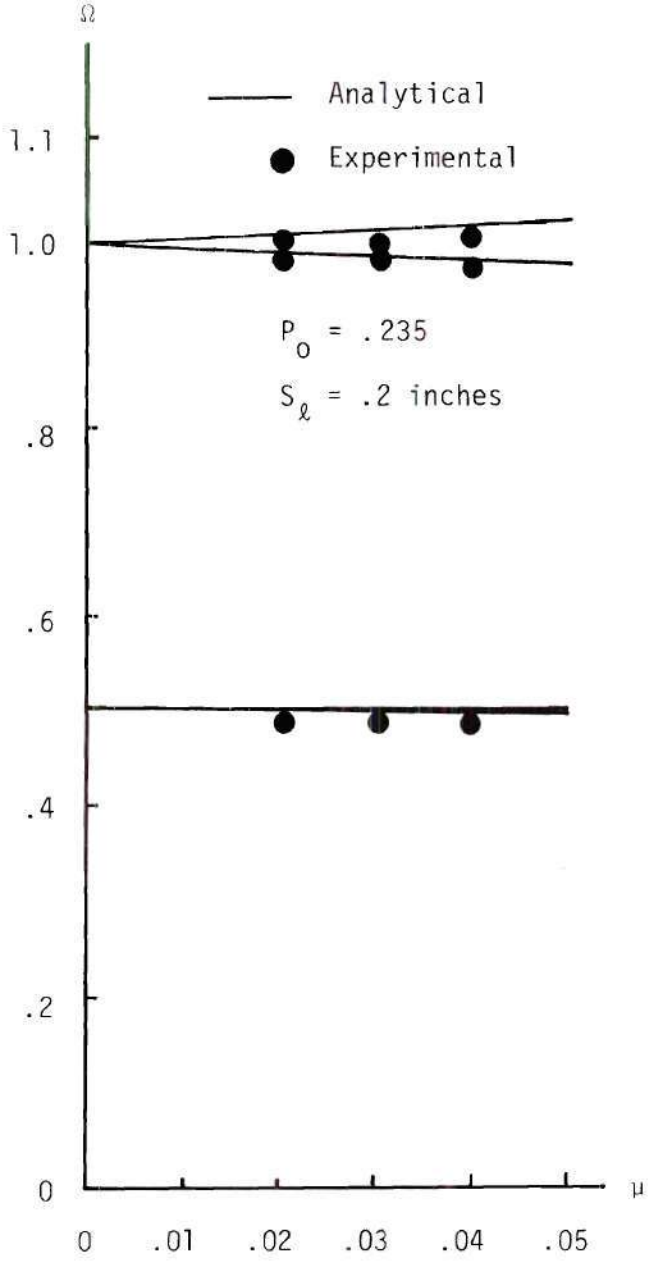

Figure 40. Dynamic Stability with S_ℓ = .2 and P_o = .235.

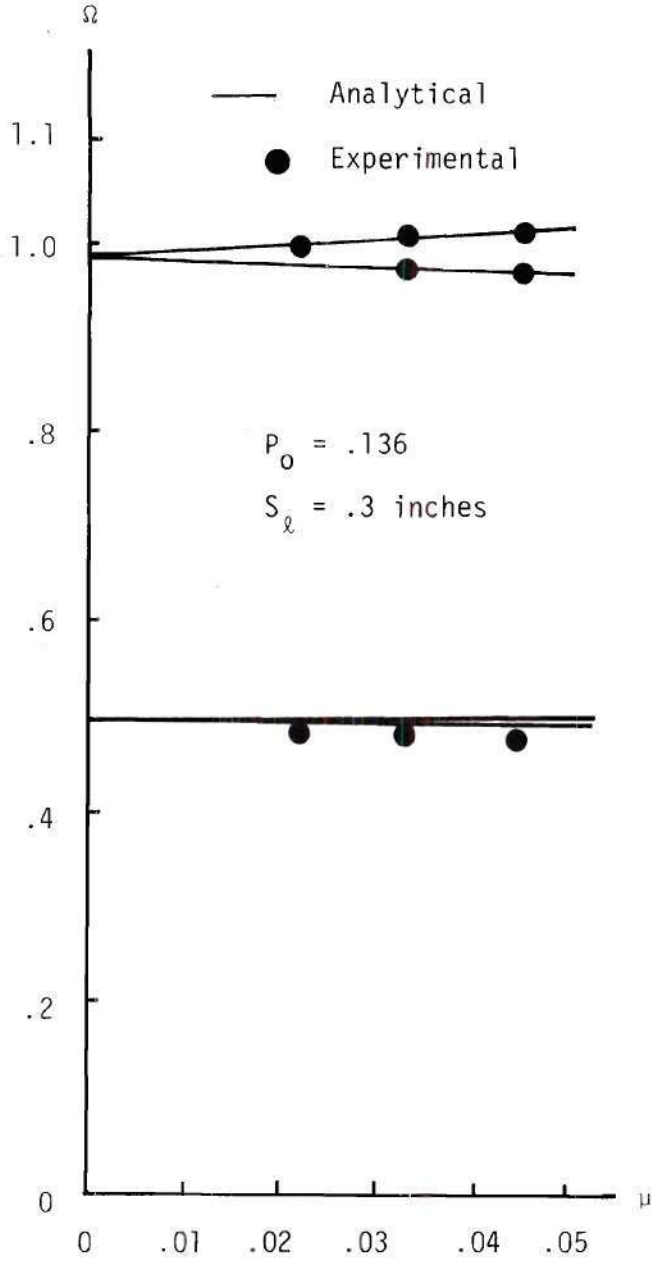

Figure 41. Dynamic Stability with S_ℓ = .3 and P_o = .136.

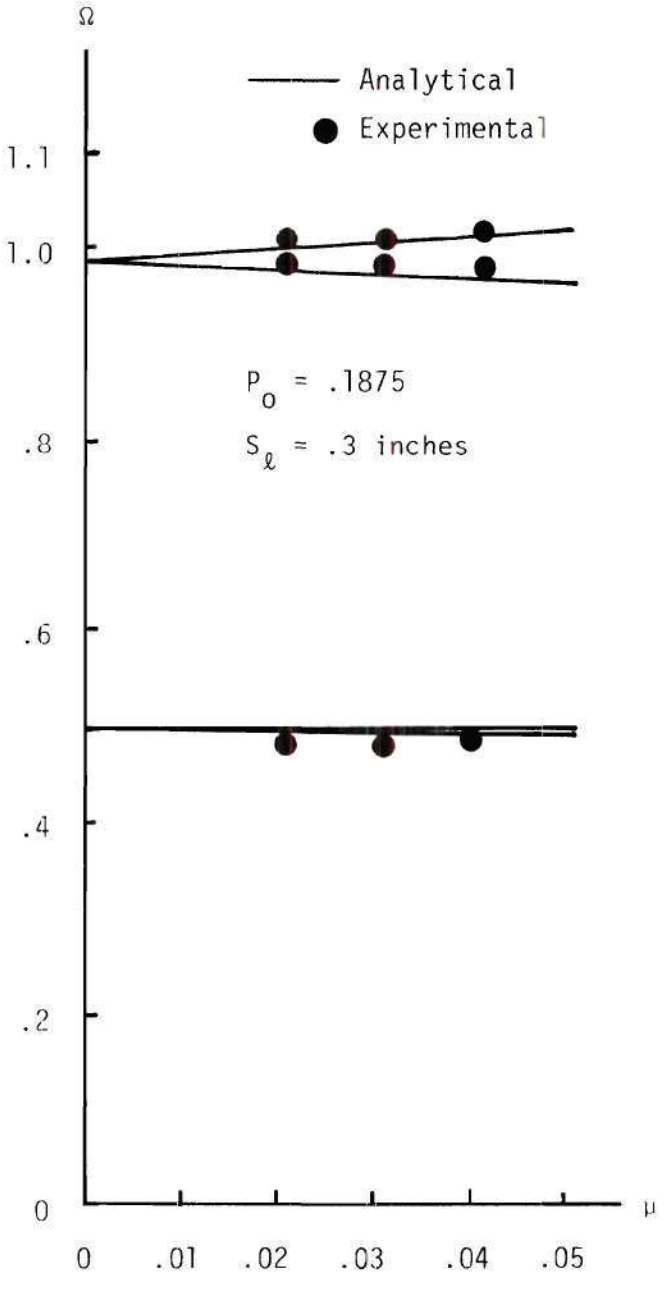

Figure 42. Dynamic Stability with S_ℓ = .3 and P_o = .1875.

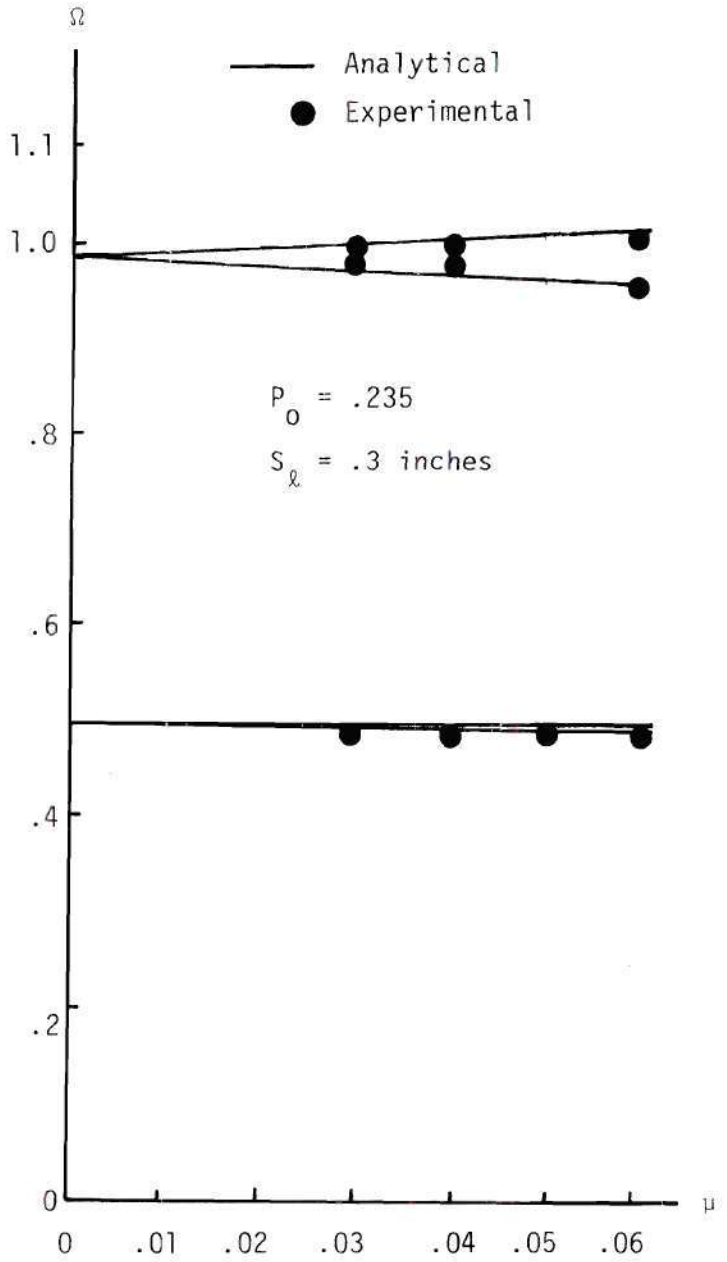

Figure 43. Dynamic Stability with S_ℓ = .3 and P_o = .235.

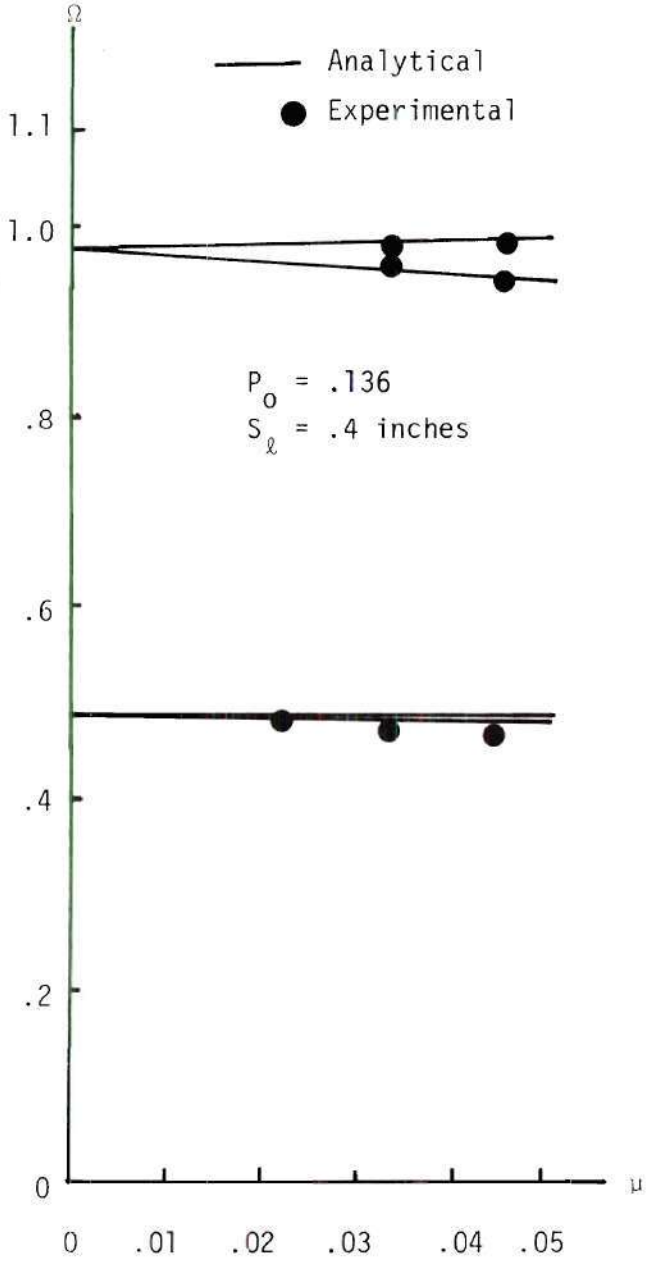

Figure 44. Dynamic Stability with S_ℓ = .4 and P_o = .136.

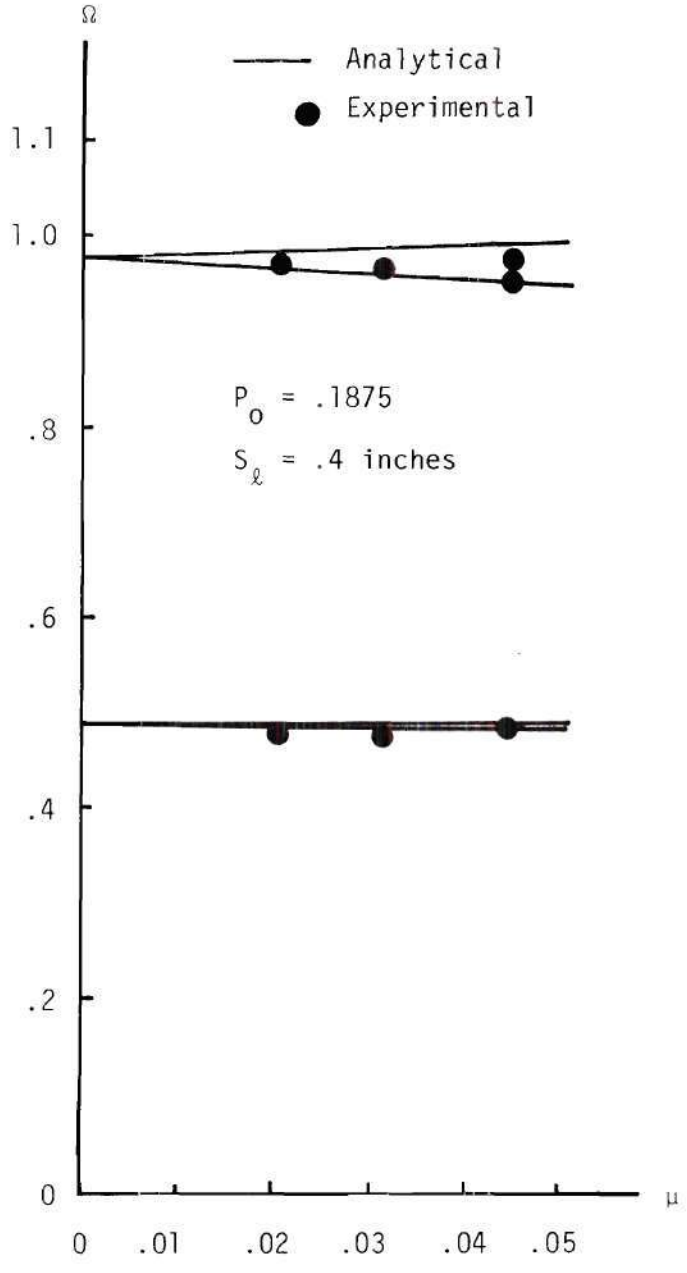

Figure 45. Dynamic Stability with S_ℓ = .4 and P_o = .1875.

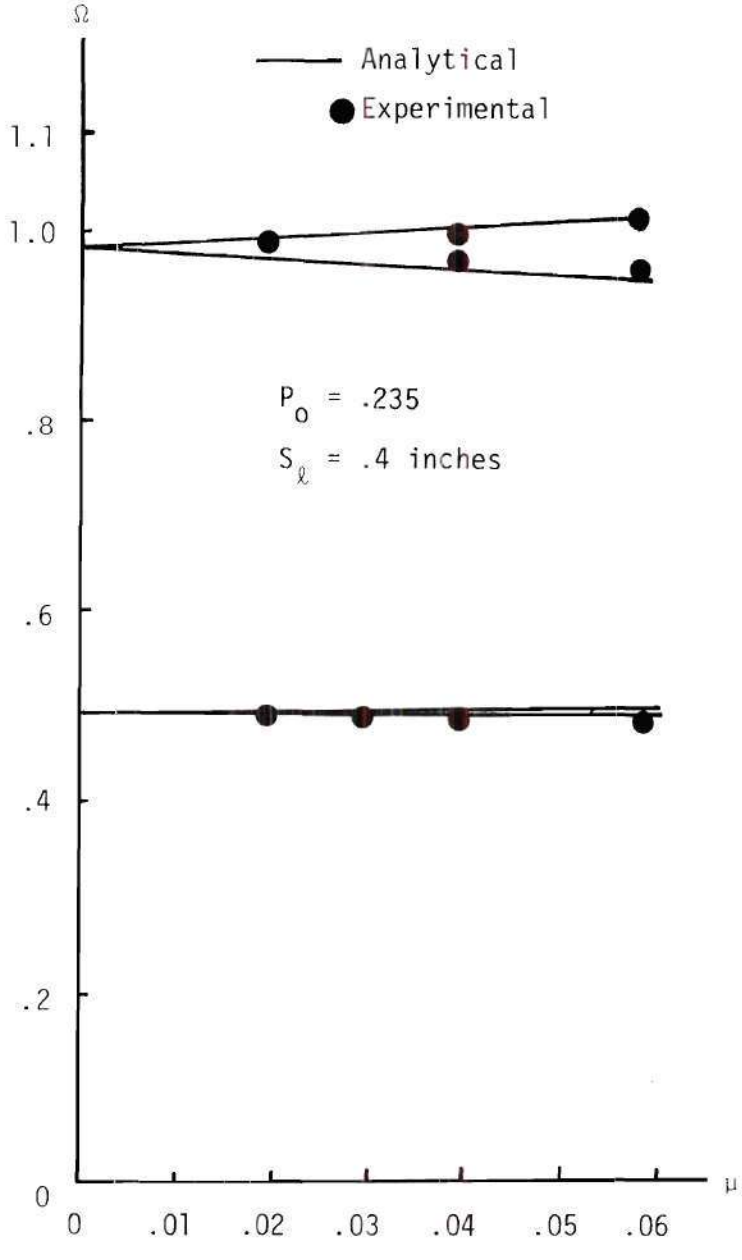

Figure 46. Dynamic Stability with S_ℓ = .4 and P_o = .235.

twice the corresponding uniform column frequency. These non-dimensionalizing parameters were computed using Equation (1) of Chapter III.

The results for the free vibration frequencies with initial load and the buckling loads were obtained using Equation (67) and (69) of Chapter II respectively. These results are presented in non-dimensional form in Figures 47 and 48. An examination of these figures reveals that there is a reduction in vibration frequency and buckling load due to the presence of a slot in the column. The reduction on the vibration frequency and buckling load increases with an increase in the slot length. The frequency of vibration decreases more rapidly in the compressive load range than the tensile load range. Note that the buckling load decrease more rapidly with the increase of the slot length. The vibration frequency and the buckling load results presented in Figures 47 and 48 are deduced using the analytical stability model. Similarly, the parametric instability zones for compressive mean loads can be obtained analytically corresponding to Figures 37 through 46. Note that these results can be deduced using Equation (63) of Chapter II in conjunction with the effective stiffness and the corresponding size of discontinuity, i.e., R presented in Figures 35 and 36.

Recall that the global properties can be correctly deduced from analyses which do not include a detailed representation of localized effects. The stability model developed in this dissertation is concerned with determining the global properties of the column; i.e. frequencies and buckling load. Therefore, the static and dynamic stability results are valid for the column with any type of discontinuity with the

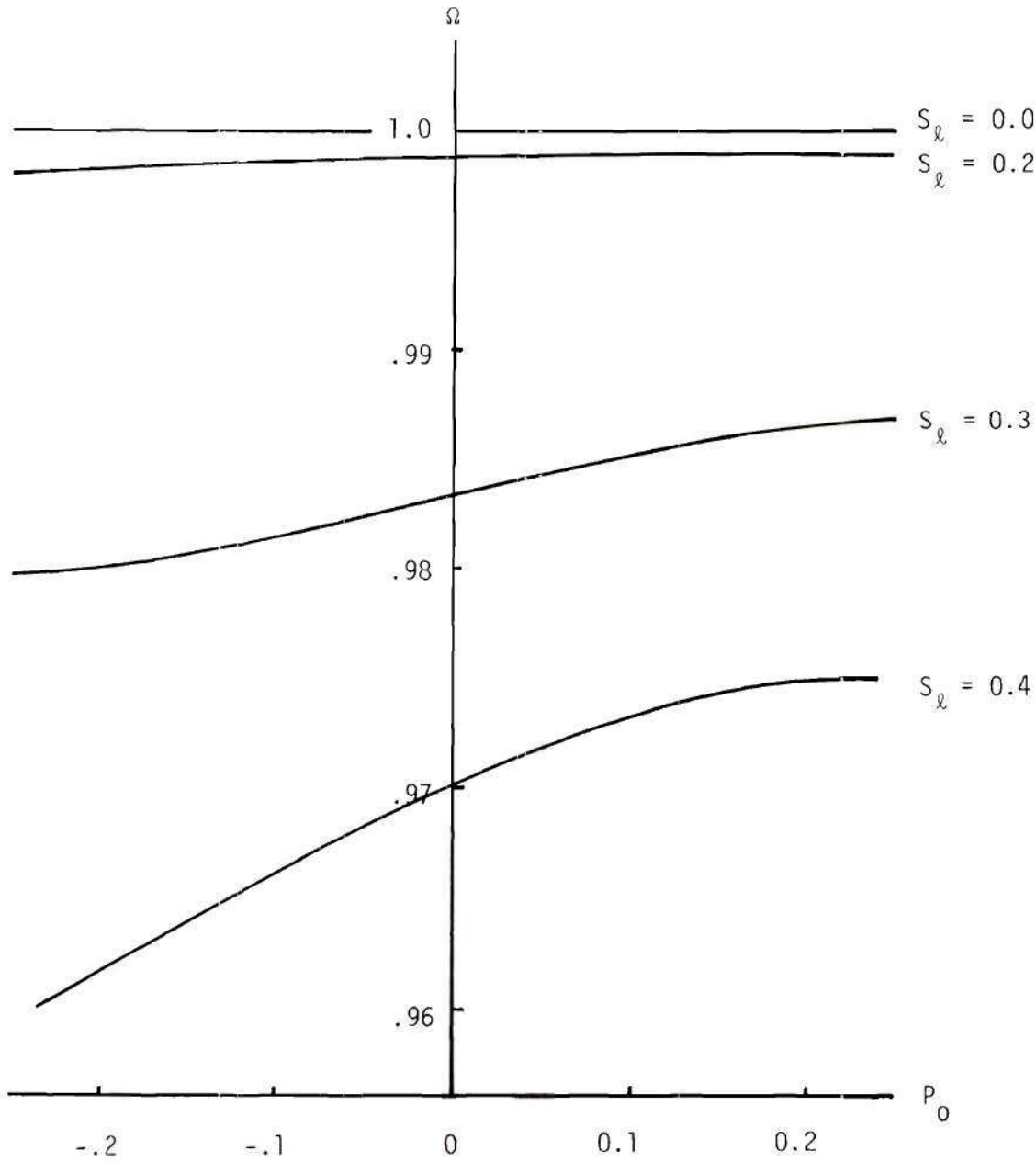

Figure 47. Free Vibration Results for the Test Specimens Using Analytical Model.

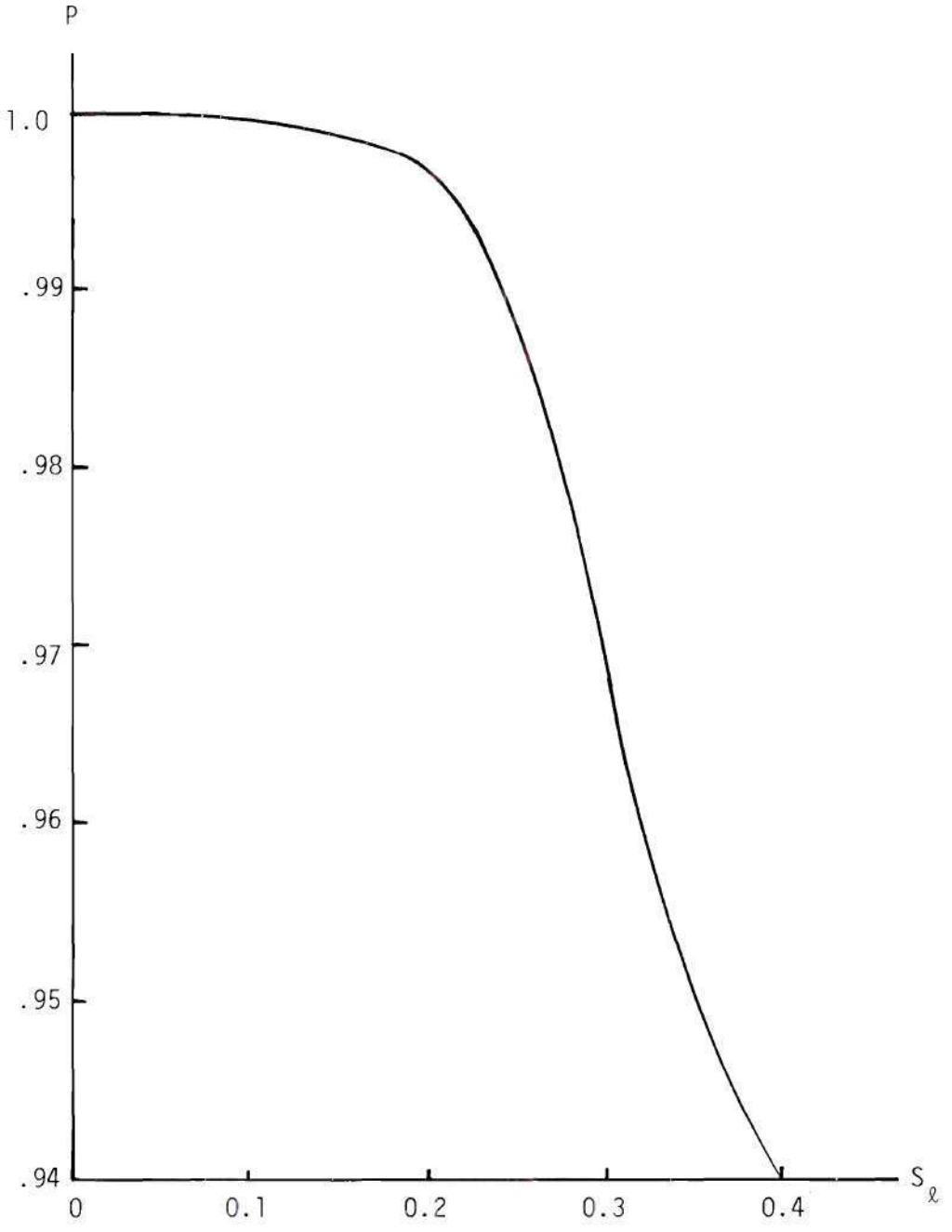

Figure 48. Analytical Buckling Loads for the Tests Specimens.

given values of effective stiffness and location and size of the discontinuity considered in this investigation. If the results presented in Figures 35 and 36 are cross plotted as shown in Figure 49, then the dynamic stability results for any column are obtained. Note that the column should have K, R and C values given in Figure 49; and simply supported end conditions.

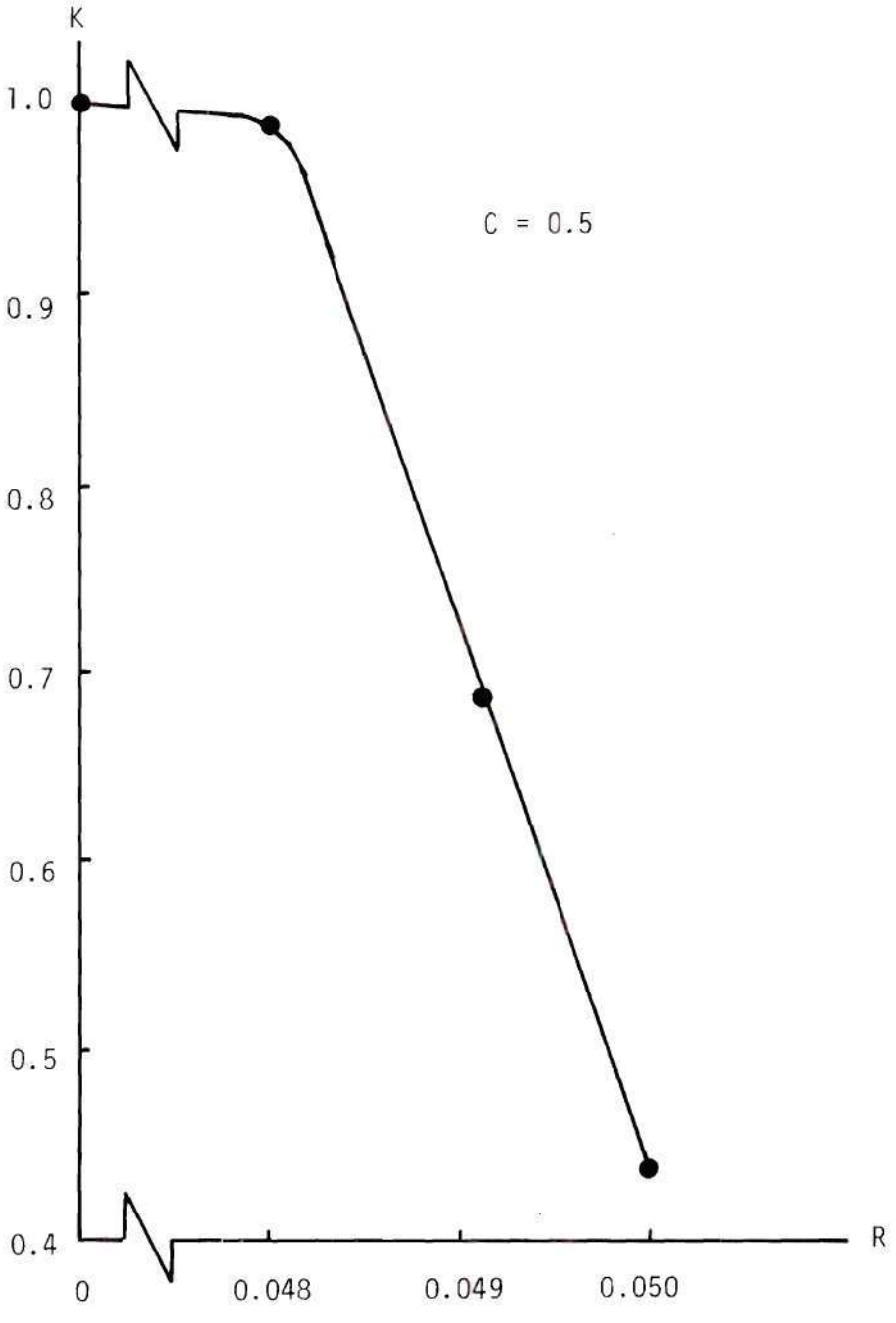

Figure 49. Effective Stiffness vs. Size of Discontinuity.

CHAPTER V

CONCLUSIONS AND RECOMMENDATIONS

An analytical stability model was developed to determine the boundaries of instability for a bar within which a region of discontinuities is present. The governing equations of motion were derived using Lagrange's equations. Using a series solution in these equations a set of approximate stability formulae were obtained. The effects of a region of discontinuity were evaluated in terms of the size of discontinuity, the effective stiffness and location of discontinuity i.e. R, K and C.

A two-part experimental program was conducted. The first part of the program was conducted to obtain the effective stiffness of the bar element with a region of discontinuity using a four-point-load bending test technique. The second part of the program was conducted to determine the boundaries of instability for a column with a region of discontinuity. In this part only the parametric dynamic loading of main interest in the present investigation was considered to obtain the dynamic stability results. These results indicated a slight effect of a region of discontinuity on the dynamic stability behavior of the bars tested.

The values of effective stiffness obtained by four-point-load bending tests were used in the analytical stability formulae to deduce the parametric stability, the free vibration and the buckling load results. The parametric stability results were in good agreement with experimental results.

Note that the analytical model can be used to deduce the stability results when the K and R relation is known. However, if this relation is not known then a relatively simple four-point-load bending test will provide the K and R relation. It should also be possible to provide the K and R relation using a finite element analysis to deduce the desired stability results by the analytical stability model presented in this report.

To realize a wider scope of application and to gain reliability in the results deduced by use of the analytical stability model, a variety of regions of discontinuities may be considered in a future investigation. For example, a test program involving columns with a region of discontinuities consisting of various distributions of small internal or surface cracks should be of a practical interest.

APPENDIX A

JUSTIFICATION FOR PERIODIC SOLUTIONS OF EQUATION (6) OF CHAPTER II

In this appendix some of the theorems related to the theory of linear homogeneous differential equations with periodic coefficients are presented. It can be noted that these theorems can be extended by mathematical induction to a system of equations involving more than two equations. A study of the structure and character of a system of coupled Mathieu equations using theorems is also presented. Finally, the forms of the solutions to obtain frequency boundaries of instability are discussed.

Theorems From the Theory of Linear Homogeneous Differential Equations with Periodic Coefficients

To study the behavior of solutions of Equations (6) in Chapter II the following theorems were found to be very useful. A general development of these theorems can be found in references [2, 32-36].

Theorem I

Let
$$\frac{d^2f_1}{dt^2} + a_{11}f_1 + a_{12}f_2 = 0 ,$$

$$\frac{d^2f_2}{dt^2} + a_{21}f_1 + a_{22}f_2 = 0 \qquad (1)$$

$$a_{ij}(t) = a_{ij}(t + T);\ i,j = 1,2,\ \text{i.e.}$$

$a_{ij}(t)$; i, j = 1,2 are periodic functions of the independent variable t with period T. If $f_1 = f_1(t)$ and $f_2 = f_2(t)$, are solutions of Equation (1), then $f_1(t + T)$ and $f_2(t + T)$ are also solutions of the system of Equation (1).

Proof.

Let z = t + T, then the system of Equations (1) transform into

$$\frac{d^2f_1(z)}{dz^2} + a_{11}(z)f_1(z) + a_{12}(z)f_2(z) = 0,$$

$$\frac{d^2f_2(z)}{dz^2} + a_{21}(z)f_1(z) + a_{22}(z)f_2(z) = 0.$$

or

$$\frac{d^2f_1(t+T)}{dt^2} + a_{11}(t+T)f_1(t+T) + a_{12}(t+T)f_2(t+T) = 0 ,$$

$$\frac{d^2f_2(t+T)}{dt^2} + a_{21}(t+T)f_1(t+T) + a_{22}(t+T)f_2(t+T) = 0 .$$

Since $a_{ij}(t) = a_{ij}(t+T)$, i,j = 1,2 we get

$$\begin{aligned} &\frac{d^2f_1(t+T)}{dt^2} + a_{11}(t)f_1(t+T) + a_{12}(t)f_2(t+T) = 0 , \\ &\frac{d^2f_2(t+T)}{dt^2} + a_{21}(t)f_1(t+T) + a_{22}(t)f_2(t+T) = 0 ; \end{aligned} \tag{2}$$

thus $f_1(t+T)$ and $f_2(t+T)$ are also solutions of Equation (1). Hence the proof is complete.

Theorem II

The system of Equations (1) can be transformed into a system of four first order linear homogeneous differential equations with periodic coefficients.

Proof.

Let $f_1 = x_1$

$f_2 = x_2$

$\frac{df_1}{dt} = x_3 = \frac{dx_1}{dt}$

$\frac{df_2}{dt} = x_4 = \frac{dx_2}{dt}$, and system of Equations (1)

can be written as

$$\frac{dx_1}{dt} - x_3 = 0$$

$$\frac{dx_2}{dt} - x_4 = 0$$

$$\frac{dx_3}{dt} + a_{11}x_1 + a_{21}x_2 = 0$$

$$\frac{dx_4}{dt} + a_{21}x_1 + a_{22}x_2 = 0$$

or in matrix notation:

$$\frac{d}{dt}\begin{bmatrix} x_1 \\ x_2 \\ x_3 \\ x_4 \end{bmatrix} + \begin{bmatrix} 0 & 0 & -1 & 0 \\ 0 & 0 & 0 & -1 \\ a_{11} & a_{12} & 0 & 0 \\ a_{21} & a_{22} & 0 & 0 \end{bmatrix} \begin{bmatrix} x_1 \\ x_2 \\ x_3 \\ x_4 \end{bmatrix} = \begin{bmatrix} 0 \\ 0 \\ 0 \\ 0 \end{bmatrix}$$

$$\underset{\sim}{X} \qquad \underline{A} \qquad \underset{\sim}{X} \qquad \underset{\sim}{0}$$

or
$$\frac{d\underset{\sim}{X}}{dt} + \underline{A}\,\underset{\sim}{X} = \underset{\sim}{0} \tag{3}$$

Note that above equations are a system of four first order linear differential equations and $\underline{A}$ is a periodic matrix with period T. Hence the proof is complete.

Applying the fundamental existence theorem [34] to the system of Equations (3), there exists a set of four linearly independent solutions

$\phi_{ij}(t)$, $\phi_{2j}(t)$, $\phi_{3j}(t)$, $\phi_{4j}(t)$; $j = 1,2,3,4$, subject to a set of initial conditions $\phi_{ij}(0) = c_{ij}$; $i = 1,2,3,4$ as constants. This system of solutions, called the fundamental system, forms a matrix

$$\underline{\phi}(t) = \begin{bmatrix} \phi_{11}(t) & \phi_{12}(t) & \phi_{13}(t) & \phi_{14}(t) \\ \phi_{21}(t) & \phi_{22}(t) & \phi_{23}(t) & \phi_{24}(t) \\ \phi_{31}(t) & \phi_{32}(t) & \phi_{33}(t) & \phi_{34}(t) \\ \phi_{41}(t) & \phi_{42}(t) & \phi_{43}(t) & \phi_{44}(t) \end{bmatrix}$$

where the first subscript denotes the number of function and the second

subscript the number of solution. In the following a theorem involving $\underline{\phi}(t)$ with initial condition

$$\underline{\phi}(0) = \begin{bmatrix} 1 & & & 0 \\ & 1 & & \\ & & 1 & \\ 0 & & & 1 \end{bmatrix} = \underline{I} \text{ is stated and proved.}$$

Theorem III

If $\underline{\phi}(t)$ is a matrix solution of the system of equation (3) with initial conditions $\underline{\phi}(0)$, then $\underline{\phi}(t + T)$ is also a matrix solution with initial condition $\underline{\phi}(T)$.

Proof.

Since $\underline{\phi}(t)$ is a matrix solution of equation (3), we get

$$\frac{d}{dt}\,[\underline{\phi}(t)] + \underline{A}(t)\underline{\phi}(t) = \underline{0}\,.$$

Let $z = t + T$, then above equation transforms into the following

$$\frac{d}{dt}\,[\underline{\phi}(t+T)] + \underline{A}(t+T)\underline{\phi}(t+T) = \underline{0}\,.$$

Since $\underline{A}(t+T) = \underline{A}(t)$, then $\underline{\phi}(t+T)$ is also a solution of equation (3) and the initial condition $\underline{\phi}(t+T)\Big|_{t=0} = \underline{\phi}(T)$.

Theorem IV

Let $\underline{\phi}(t)$ be a matrix solution of the system of Equations (3) with initial condition $\underline{\phi}(0) = \underline{I}$ then $\underline{\phi}(t+T) = \underline{\phi}(t)\underline{\phi}(T)$.

Proof.

It follows that $\underline{\phi}(t+T)$ is also a matrix solution of Equations (3) with initial conditions $\underline{\phi}(T)$ (by Theorem III). From theory of linear homogeneous differential equations the solutions $\underline{\phi}(t+T)$ can be represented in a linear combination of the functions $\underline{\phi}(t)$.

Thus

$$\underline{\phi}(t+T) = \underline{\phi}(t)\underline{B} \ , \tag{4}$$

where $\underline{B}$ is a matrix of order 4×4 with constant elements. Substitution of $t = 0$ in Equation (4) yields, $\underline{\phi}(T) = \underline{\phi}(0)\underline{B}$. Since $\underline{\phi}(0) = \underline{I}$ then $\underline{B} = \underline{\phi}(T)$. Using this result in Equation (4) gives the desired result:

$$\underline{\phi}(t+T) = \underline{\phi}(t)\underline{\phi}(T) \tag{5}$$

Example:

Given a second order linear homogeneous differential equation,

$$\frac{d^2y}{dt^2} + y = 0 \ , \tag{5a}$$

show that Equation (5a) can be transformed into a system of two first order linear homogeneous differential equations and a matrix solution of this system, $\underline{\phi}(t)$ with initial condition $\underline{\phi}(0) = \underline{I}$ satisfies Equation (5).

Using the transformation,

$$x_1 = y$$

$$x_2 = \frac{dy}{dt} = \frac{dx_1}{dt}$$

into Equation (5a), the following system of two first order linear homogeneous differential equations can be obtained.

$$\frac{d\underset{\sim}{X}}{dt} = \underline{A}\,\underset{\sim}{X}\ , \tag{5b}$$

where, $\underline{A} = \begin{bmatrix} 0 & 1 \\ -1 & 0 \end{bmatrix}$ and $\underset{\sim}{X} = \begin{bmatrix} x_1 \\ x_2 \end{bmatrix}$.

Let

$$\underline{\phi}(t) = \begin{bmatrix} \cos t & \sin t \\ -\sin t & \cos t \end{bmatrix}, \tag{5c}$$

then

$$\frac{d}{dt}\,[\underline{\phi}(t)] = \begin{bmatrix} -\sin t & \cos t \\ -\cos t & -\sin t \end{bmatrix}, \quad \text{and}$$

$$\underline{A}\,\underline{\phi} = \begin{bmatrix} 0 & 1 \\ -1 & 0 \end{bmatrix}\begin{bmatrix} \cos t & \sin t \\ -\sin t & \cos t \end{bmatrix} = \begin{bmatrix} -\sin t & \cos t \\ -\cos t & -\sin t \end{bmatrix}$$

Thus the matrix, $\underline{\phi}(t)$ defined in Equation (5c) is a solution of Equation (5b) with the initial condition,

$$\underline{\phi}(0) = \begin{bmatrix} 1 & 0 \\ 0 & 1 \end{bmatrix} = \underline{I}\ .$$

Since $\underline{A}(t+T) = \underline{A}(t)$, then using Theorem III

$$\underline{\phi}(t+T) = \begin{bmatrix} \cos(t+T) & \sin(t+T) \\ -\sin(t+T) & \cos(t+T) \end{bmatrix} \tag{5d}$$

is also a solution of Equation (5b). Evaluation of the product of the matrices $\underline{\phi}(t)$ and $\underline{\phi}(T)$ gives

$$\underline{\phi}(t)\underline{\phi}(T) = \begin{bmatrix} \cos t & \sin t \\ -\sin t & \cos t \end{bmatrix} \begin{bmatrix} \cos T & \sin T \\ -\sin T & \cos T \end{bmatrix},$$

or

$$\underline{\phi}(t)\underline{\phi}(T) = \begin{bmatrix} \cos t \cos T - \sin t \sin T & \cos t \sin T + \sin t \cos T \\ -\sin t \cos T - \cos t \sin T & -\sin t \sin T + \cos t \cos T \end{bmatrix}. \tag{5e}$$

Using the trigonometric identities,

$$\cos t \cos T - \sin t \sin T = \cos(t+T) \quad \text{and}$$

$$\cos t \sin T + \sin t \cos T = \sin(t+T) ,$$

into Equation (5e) gives

$$\underline{\phi}(t)\underline{\phi}(T) = \begin{bmatrix} \cos(t+T) & \sin(t+T) \\ -\sin(t+T) & \cos(t+T) \end{bmatrix} .$$

An observation of the above equation and Equation (5d) reveals the following result:

$$\underline{\phi}(t+T) = \underline{\phi}(t)\underline{\phi}(T) .$$

Thus the Theorem IV can be verified for the Example.

Theorem V.

If $|\underline{\phi}(T) - \mu \underline{I}| = 0$ has distinct roots μ_1, μ_2, μ_3 and μ_4 then

$$\underset{\sim}{X}_i(t) = e^{\frac{t}{T}\ln(\mu_i)} \underset{\sim}{P}_i(t) \tag{6}$$

is a solution vector of the system differential Equation (3) where $\underset{\sim}{X}_i$ is an i^{th} vector solution and $\underset{\sim}{P}_i(t)$ is the i^{th} corresponding periodic vector with period T.

Proof.

Since $|\underline{\phi}(T) - \mu \underline{I}| = 0$ has distinct roots μ_1, μ_2, μ_3 and μ_4, then there exists a nonsingular matrix $\underline{S}$ such that

$$\underline{S}^{-1}\underline{\phi}(T)\underline{S} = \underline{D} \tag{7}$$

where $\underline{D}$ is the diagonal matrix with the eigenvalues of $\underline{\phi}(T)$ as diagonal elements.

Define a matrix $\underline{\psi}(t) \equiv \underline{\phi}(t)\underline{S}$.

Since $\underline{\phi}(t)$ is a matrix solution of Equation (3), then

$$\frac{d\underline{\phi}(t)}{dt} + \underline{A}(t)\underline{\phi}(t) = \underline{0} .$$

Therefore

$$\frac{d\underline{\phi}(t)}{dt}\underline{S} + \underline{A}(t)\underline{\phi}(t)\underline{S} = \underline{0}$$

and since $\underline{S}$ is a matrix with constant elements $\underline{\psi}(t)$ is a matrix solution of Equation (3). By using Theorem II $\underline{\psi}(t+T)$ is also a solution of

Equation (3). Further,

$$\underline{\psi}(t+T) = \underline{\phi}(t+T)\underline{S} \quad \text{and}$$

using the result, $\underline{\phi}(t+T) = \underline{\phi}(t)\underline{\phi}(T)$ of Theorem IV gives

$$\underline{\psi}(t+T) = \underline{\phi}(t)\underline{\phi}(T)\underline{S} \ .$$

From Equation (7) $\underline{\phi}(t)\underline{S} = \underline{S}\ \underline{D}$ and substituting this result in above equation yields

$$\underline{\psi}(t+T) = \underline{\phi}(t)\underline{S}\ \underline{D} \ .$$

Recall that $\underline{\phi}(t)\underline{S} \equiv \underline{\psi}(t)$, then above equation becomes

$$\underline{\psi}(t+T) = \underline{\psi}(t)\underline{D} \ . \tag{8}$$

If $\underset{\sim}{X}_1$, $\underset{\sim}{X}_2$, $\underset{\sim}{X}_3$ and $\underset{\sim}{X}_4$ denote the vector solutions of Equation (3) and if these are also the vector columns of $\underline{\psi}(t)$ then from Equation (8) it follows that

$$\underset{\sim}{X}_i(t+T) = \mu_i \underset{\sim}{X}_i(t) \tag{9}$$

$$i = 1,2,3,4.$$

Let

$$\underline{R}(t) \equiv \begin{bmatrix} e^{\frac{t}{T}\ln \mu_1} & & & \\ & e^{\frac{t}{T}\ln \mu_2} & & \\ & & e^{\frac{t}{T}\ln \mu_3} & \\ & & & e^{\frac{t}{T}\ln \mu_4} \end{bmatrix} \quad \text{and} \tag{10}$$

$$\underline{P}(t) \equiv \underline{\psi}(t)\underline{R}^{-1}(t) \ . \tag{11}$$

Then

$$\underline{P}(t+T) = \underline{\psi}(t+T)\underline{R}^{-1}(t+T),$$

and using Equation (8) yields

$$\underline{P}(t+T) = \underline{\psi}(t)\underline{D}\ \underline{R}^{-1}(t+T) \ .$$

It can be verified using Equation (10) that $\underline{R}^{-1}(t+T) = \underline{R}^{-1}(T)\underline{R}^{-1}(t)$ and

$$\underline{R}^{-1}(T) = \begin{bmatrix} \frac{1}{\mu_1} & & & \\ & \frac{1}{\mu_2} & & \\ & & \frac{1}{\mu_3} & \\ & & & \frac{1}{\mu_4} \end{bmatrix} .$$

Therefore

$$\underline{P}(t+T) = \underline{\psi}(t)\underline{D}\ \underline{R}^{-1}(T)\underline{R}^{-1}(t)$$

Recall that

$$\underline{D} = \begin{bmatrix} \mu_1 & & & \\ & \mu_2 & & \\ & & \mu_3 & \\ & & & \mu_4 \end{bmatrix} .$$

Thus $\underline{D}\,\underline{R}^{-1}(T) = \underline{I}$ and

$$\underline{P}(t+T) = \underline{\psi}(t)\underline{R}^{-1}(t) \ .$$

It follows by use of Equation (11) into the above equation that

$$\underline{P}(t+T) = \underline{P}(t)$$

It follows that whenever $\underline{\phi}(T)$ can be diagonalized, one obtains four linearly independent solutions, which satisfy Equation (9) and these have form $\underset{\sim}{X}_i(t) = e^{\frac{t}{T}\ln \mu_i}\underset{\sim}{P}_i(t)$ where $\underset{\sim}{P}_1(t)$ are vectors with period T. When characteristic roots are multiple roots, the structure of the solutions of Equation (6) is similar. A discussion of these solutions can be found in reference [2].

Theorem VI

Let the matrix $\underline{A}$ in Equation (3) satisfy

$$\underline{A}(-t) = \underline{A}(t) \tag{12}$$

i.e. it is even function t. If a root of $|\underline{\phi}(T) - \rho\underline{I}| = 0$ is ρ_1, then $\frac{1}{\rho_1}$ is also a root of $|\underline{\phi}(T) - \rho\underline{I}| = 0$.

Proof.

By Theorem V a solution of differential Equation (3) has the form

$$\underset{\sim}{X}_1(t) = e^{\frac{t}{T}\ln \rho_1}\ \underset{\sim}{P}_1(t) \ .$$

Since $\underline{A}(-t) = \underline{A}$, the differential Equation (3) does not change its form when t is replaced by -t. Consequently, if

$$\underset{\sim}{X}_1 = e^{\frac{t}{T}\ln \rho_1}\, \underset{\sim}{P}_1(t) \tag{13}$$

is one of the solutions of Equation (3), then

$$\underset{\sim}{X}_1(-t) = e^{-\frac{t}{T}\ln \rho_1}\, \underset{\sim}{P}_1(-t) = e^{\frac{t}{T}\ln (\frac{1}{\rho_1})}\, \underset{\sim}{P}_1(t) \tag{14}$$

is also one of its solutions, i.e. $1/\rho_1$ is one of the characteristic roots.

A more general theorem (Liapunov Theorem [2]) corresponding to this theorem does not require $\underline{A}(-t) = \underline{A}(t)$, to obtain the results. However, in the present investigation this condition is satisfied (Equation (6) in Chapter II).

It may be noted that the two solutions (Equations (13) and (14) are often called a pair of solutions which correspond to a pair of reciprocal characteristic roots i.e. ρ_1 and $\frac{1}{\rho_1}$.

Characteristic Exponent and Stability Behavior

The system of differential Equations (1) has an identically vanishing solution

$$f_1(t) = 0, \quad f_2(t) = 0.$$

Besides this trivial solution, which represents the initial equilibrium state in the mechanical problem under consideration, the system also admits nontrivial solutions, whose form has been examined in previous sections.

The characteristic exponent is defined by the equation $h = \frac{1}{T} \ln \mu$, where h may be complex. From the form of the solution (Equation (6)) it follows that if all characteristic exponents have negative real parts, then the general solution of Equation (1) will damp out with time. In other words, the initial equilibrium state is stable. But if among the characteristic exponents there appears even one which has positive real part, then the system will have particular solutions increasing unboundedly with time; consequently, the initial state is unstable.

Taking into account that

$$\ln \mu = \ln|\mu| + i \arg \mu$$

gives the following conclusion. If all the roots of the characteristic equation have absolute values smaller than unity, then the initial equilibrium state is stable. If among the characteristic roots there appears even one with an absolute value greater than unity, then the initial equilibrium is unstable.

To the characteristic roots with absolute values equal to one there correspond purely imaginary characteristic exponents. In this case either stability or instability can take place. If the characteristic numbers are non-repeated, then the corresponding solution will be bounded for all time. In the case of multiple roots, the character of the solution will depend on the structure of elementary divisors, i.e. type of multiplicity of roots. If the elementary divisors are repeated, then secular instability, specified by the appearance in the general integral of secular terms of the types $t^m \underset{\sim}{P}(t)$ will take place [2].

Determination of Conditions for Periodic Solutions On the Frequency Boundary and Dirichlet's Conditions

Consider a pair of particular solutions of Equation (1) corresponding to a pair of reciprocal characteristic roots, ρ_1 and $\frac{1}{\rho_1}$:

$$f_1(t) = P_1(t)e^{\frac{t}{T}\ln(\rho_1)}$$

$$f_3(t) = P_3(t)e^{-\frac{t}{T}\ln(\rho_1)} \qquad (15)$$

Let ρ_1 be real and different from ± 1; then one of the particular solutions will unboundedly increase with time. Therefore, the region of real ρ will be the region of unboundedly increasing solutions (region of instability).

By varying the coefficients (a_{ij}, i,j = 1,2,...,4 in Equation (1)) of the system, one can obtain the condition that the characteristic number will remain $\rho_1 = 1$ or $\rho_1 = -1$ and will be multiple. In the first case the solution will be periodic with period T (substitution of $\mu_1 = \rho_1 = 1$ in Equation (9) gives $\underset{\sim}{X}(t+T) = \underset{\sim}{X}(t)$); in the second case it will be periodic with period 2T (substitution of $\mu_1 = \rho_1 = -1$ in Equation (9) gives $\underset{\sim}{X}(t+T) = -\underset{\sim}{X}(t)$, it follows then $\underset{\sim}{X}(t+2T) = \underset{\sim}{X}(t)$). Upon further variation of coefficients (a_{ij}, i, j = 1,2,...,4 in Equation (1)), the considered pair of characteristic roots will become complex conjugates $\rho_1 = a + ib$ and $\rho_2 = a - ib$ and by virtue of the relation $\rho_1\rho_2 = 1$, will have absolute value equal to one. The region of complex roots is thus a region of bounded solutions. It can be noted that when imaginary roots

are repeated linearized equations of present investigation are not adequate. However when more than two real roots are repeated, it should be noted that linearized equations indicates secular instability.

Hence it follows that on the boundaries of the regions of instability the differential equation system has periodic solutions with period T or 2T. More precisely, two solutions with same period bound the region of instability, and two solutions with different periods bound the region of stability.

On this basis the series solutions used in Chapter II can be justified to obtain the frequency boundaries. It can be noted that the 2T and T type solutions are an odd-harmonic and even-harmonic Fourier series representing $\underset{\sim}{f}(t)$, $0 < t < T$; satisfying Dirichlet's conditions in the manner of the following theorem.

Dirichlet's Theorem

For $-\pi \leq x \leq \pi$ suppose $f(x)$ is well defined, is bounded, has only a finite number of maxima and minima, and has only a finite number of discontinuities. Let $f(x)$ be defined for other values of x by the periodicity condition $f(\pi + 2\pi) = f(x)$. Then Fourier series for $f(x)$ converges to

$$\frac{1}{2}\,[f(+x) + f(x-)]$$

at every value of x and hence it converges to $f(x)$ at points where $f(x)$ is continuous.

The conditions imposed on $f(x)$ are called Dirichlet conditions [34].

APPENDIX B

ADDITIONAL RESULTS AND DISCUSSIONS

An analysis with k = 3, k = 4 and typical results are presented in this appendix. Also, features and procedure of the method of successive approximation are discussed. Additionally, notes on some points of interest are presented.

An Analysis with k = 3, k = 4 and Typical Numerical Results

It should be recalled that the harmonic approximations Equations (18a) and (20a) of Chapter II are periodic functions of t with period 2T and T respectively. These approximations correspond to series solutions

$$\underset{\sim}{f}(t) = \sum_{k=1,3,5}^{\infty} \underset{\sim}{a}_k \sin\frac{k\theta t}{2} + \underset{\sim}{b}_k \cos\frac{k\theta t}{2}, \qquad (1)$$

and

$$\underset{\sim}{f}(t) = \frac{1}{2}\underset{\sim}{b}_o + \sum_{k=2,4,6}^{\infty} \underset{\sim}{a}_k \sin\frac{k\theta t}{2} + \underset{\sim}{b}_k \cos\frac{k\theta t}{2} \qquad (2)$$

truncated at k = 1 and k = 2 respectively.

If above series are truncated at k = 3 and k = 4, then

$$\underset{\sim}{f}(t) = \underset{\sim}{a}_1 \sin\frac{\theta t}{2} + \underset{\sim}{b}_1 \cos\frac{\theta t}{2} + \underset{\sim}{a}_3 \sin\frac{3\theta t}{2} + \underset{\sim}{b}_3 \cos\frac{3\theta t}{2} \quad \text{and}$$

$$\underset{\sim}{f}(t) = \frac{1}{2}\underset{\sim}{b}_o + \underset{\sim}{a}_2 \sin\theta t + \underset{\sim}{b}_2 \cos\theta t + \underset{\sim}{a}_4 \sin 2\theta t + \underset{\sim}{b}_4 \cos 2\theta t$$

are the approximations with periods 2T and T respectively.

The conditions of existence of periodic solutions can be identified from equations (8), (9) and (10) of Chapter II

$$\begin{vmatrix} \underline{E} - \alpha\underline{A} \pm \frac{1}{2}\beta\underline{B} - \frac{1}{4}\theta^2\underline{C} & -\frac{1}{2}\beta\underline{B} \\ -\frac{1}{2}\beta\underline{B} & \underline{E} - \alpha\underline{A} - \frac{9}{4}\theta^2\underline{C} \end{vmatrix} = 0 ,$$

$$\begin{vmatrix} \underline{E} - \alpha\underline{A} - \theta^2\underline{C} & -\frac{1}{2}\beta\underline{B} \\ -\frac{1}{2}\beta\underline{B} & \underline{E} - \alpha\underline{A} - 4\theta^2\underline{C} \end{vmatrix} = 0 \quad \text{and} \qquad (3)$$

$$\begin{vmatrix} \underline{E} - \alpha\underline{A} & -\beta\underline{B} & 0 \\ -\frac{1}{2}\beta\underline{B} & \underline{E} - \alpha\underline{A} - \theta^2\underline{C} & -\frac{1}{2}\beta\underline{B} \\ \underline{0} & -\frac{1}{2}\beta\underline{B} & \underline{E} - \alpha\underline{A} - 4\theta^2\underline{C} \end{vmatrix} = 0 .$$

It can be noted that the order of matrix elements $\underline{E}$, $\underline{A}$ and $\underline{C}$ is N×N, when the series (2) of Chapter II is truncated at n = N. An observation of equations (3) reveals that it should involve a polynomial equation greater than two for $N \geq 1$ and $k \geq 3$. Therefore, using the method of successive approximation on Equation (3) boundary frequencies were computed for primary and secondary zones. It was found that these values were improved by less than 1% when compared to the results of Case I, Case II and Case III. A comparison of these results is presented in Table 6. The physical parameters are in non-dimensional form as defined by Equation (1) in Chapter IV.

It was pointed out in Chapter II that in a vibration problem

Table 6. Typical Numerical Results for Primary Upper Frequency Boundary with $P_o = -.5$, $K = .5$, $C = .5$ and $R = .045$

μ	$k = 1$ $n = 1$ θ^*	$k = 1$ $n = 2$ θ^*	$k = 1$ $n = 3$ θ^*	$k = 2$ $n = 1$ θ^*	$k = 3$ $n = 2$ θ^*	$k = 3$ $n = 3$ θ^*	Method
0	.95425	.9542532	.9520357	.95425	-	-	Exact: Using Quadratic Formula
	-	.9542532	.9520354	-	.954232	.9520354	Successive Approximation
.3	1.1027	1.1002723	1.0983802	1.10433	-	-	Exact
	-	1.1002723	1.0983807	-	1.1043282	1.1024582	Successive Approximation
.475	1.17711	1.1771148	1.1753626	1.18525	-	-	Exact
	-	1.1771148	1.1753634	-	1.1852549	1.1835405	Successive Approximation

stiffness must be represented better than the approximation for the time functions to describe the motion. Therefore a reasonable balance between the space functions $\sin \frac{n\pi x}{\ell}$ and time functions $\underset{\sim}{f}_n(t)$ is one time function and more than one space functions (Table 6).

A Discussion On the Method of Successive Approximation

An observation of Equation (3) suggest that these equations involve a polynomial in θ with degree greater than four for $k > 1$ and $N > 1$. Therefore, it is appropriate to extract roots of such equations by a numerical method. There are several numerical methods that can be used to obtain the roots of a polynomial equation. Among these a few are listed below [37].

- Method of Successive Approximation
- Newton-Raphson Method
- Half-interval Method
- Searching Method

These numerical methods can be classified as "iterative" methods. The iterative methods require an initial approximate value of the roots and the value of roots is refined by substitution of the initial approximate value into a rearrangement of the polynomial equation. When a good initial value is not known an approximate value may be obtained by searching for a sign change of the polynomial expression.

In the present investigation the method of successive approximation was chosen, with initial values taken from the result of Case I or from uniform column results of Equation (1) in Chapter III. To illustrate the

method consider Equation (28) of Chapter II

$$\begin{vmatrix} d_1 - \frac{\theta^2}{4} & d_3 \\ d_3 & d_2 - \frac{\theta^2}{4} \end{vmatrix} = 0, \text{ where} \qquad (4)$$

d_1, d_2 and d_3 are defined by Equation (30) in Chapter II. Expanding the determinant in Equation (4) gives

$$(d_1 - \frac{\theta^2}{4})(d_2 - \frac{\theta^2}{4}) - d_3^2 = 0 . \qquad (5)$$

Equation (5) can be rewritten as

$$\frac{\theta^2}{4} = d_1 - \frac{d_3^2}{(d_2 - \frac{\theta^2}{4})} \quad \text{or} \qquad (6)$$

$$\frac{\theta^2}{4} = d_2 - \frac{d_3^2}{(d_1 - \frac{\theta^2}{4})} \qquad (7)$$

If $d_3^2 < (d_2 - \frac{\theta^2}{4})$ and then

$$\begin{aligned} \frac{\theta_o^2}{4} &= d_1 \\ \frac{\theta_1^2}{4} &= d_1 - \frac{d_3^2}{(d_2 - \frac{\theta_o^2}{4})} \\ &\vdots \\ \frac{\theta_i^2}{4} &= d_1 - \frac{d_3^2}{(d_2 - \frac{\theta_{i-1}^2}{4})} \end{aligned} \qquad (8)$$

will give the i^{th} successive approximate value of the root near $\theta^2 = 4\ d_1$ and the error due to this is $\frac{1}{4}|\theta_i^2 - \theta_{i-1}^2|$. The error can be made as small as desired by evaluating required i^{th} successive approximation for θ using algorithm given in Equation (8). Similarly, the root near $\theta = 2(d_2)^{1/2}$ can be evaluated using Equation (7) and corresponding algorithm.

It can be noted that the initial value of the root of Equation (4) is obtained by $d_1 - \frac{\theta^2}{4} = 0$ i.e. first element on the principal diagonal is made zero. Solving this equation for $\frac{\theta^2}{4}$ and substituting in the second element of the principal diagonal of the determinant in Equation (4) and solving the equation for $\frac{\theta^2}{4}$, gives the second equation in Equations (8). Thus, the method of successive approximations used in Chapter II is identical to the algorithm (8).

Discussion on Equations (45) and (40) of Chapter II

It can be noted that these equations are the formulae for the upper and lower boundary of secondary zones. In evaluating the numerical values of these boundaries, an algorithm corresponding to Equations (8) was developed to get the i^{th} successive approximation. It was found that the first successive approximation gave the results within the error of one percent of the next approximation.

Experimental Instability Zone Response

In the experiments it was very difficult to record the values for upper and lower secondary instability boundary frequency because the zone thickness was very small. However, there was evidence of existence of

this zone. Therefore it was reasonable to record θ^{s}_{max}, i.e. frequency when the bending strain amplitude was maximum near that zone. In the experimental investigation of Bolotin [2] these zones were not found. The possible reason he gave was the presence of structural damping and small thickness of the zone.

Similarly, for small values of P_1 there is a possibility of not observing the instability for even primary zones.

A Schematic Representation of the Principal and the Secondary Regions

An observation of Equation (1) of Chapter III reveals that the principal and secondary regions for the uniform column can be represented schematically as shown in Figures (50) and (51) respectively. Note that the parameters θ, P_o and P_1 are represented in the dimensional form. The dimensional quantities $P_\star$ and ω are the first buckling load and fundamental natural frequency of vibration for the uniform column.

A Comparison of the Widths of the Instability Zones

A typical set of non-dimensional values for the widths of the instability zones of a column with a region of discontinuities and the corresponding uniform column are presented in Table 7. Note that the stability model (Case III of Chapter II) with $\mu = 0.4$, $R = 0.045$, $C = 0.5$

Table 7. A Typical Comparison of the Widths of the Instability Zones

Instability	Width for a Column with a Region of Discontinuities	Width for the Corresponding Uniform Column
Principal	0.46162	0.40862
Secondary	0.1296061	0.10085

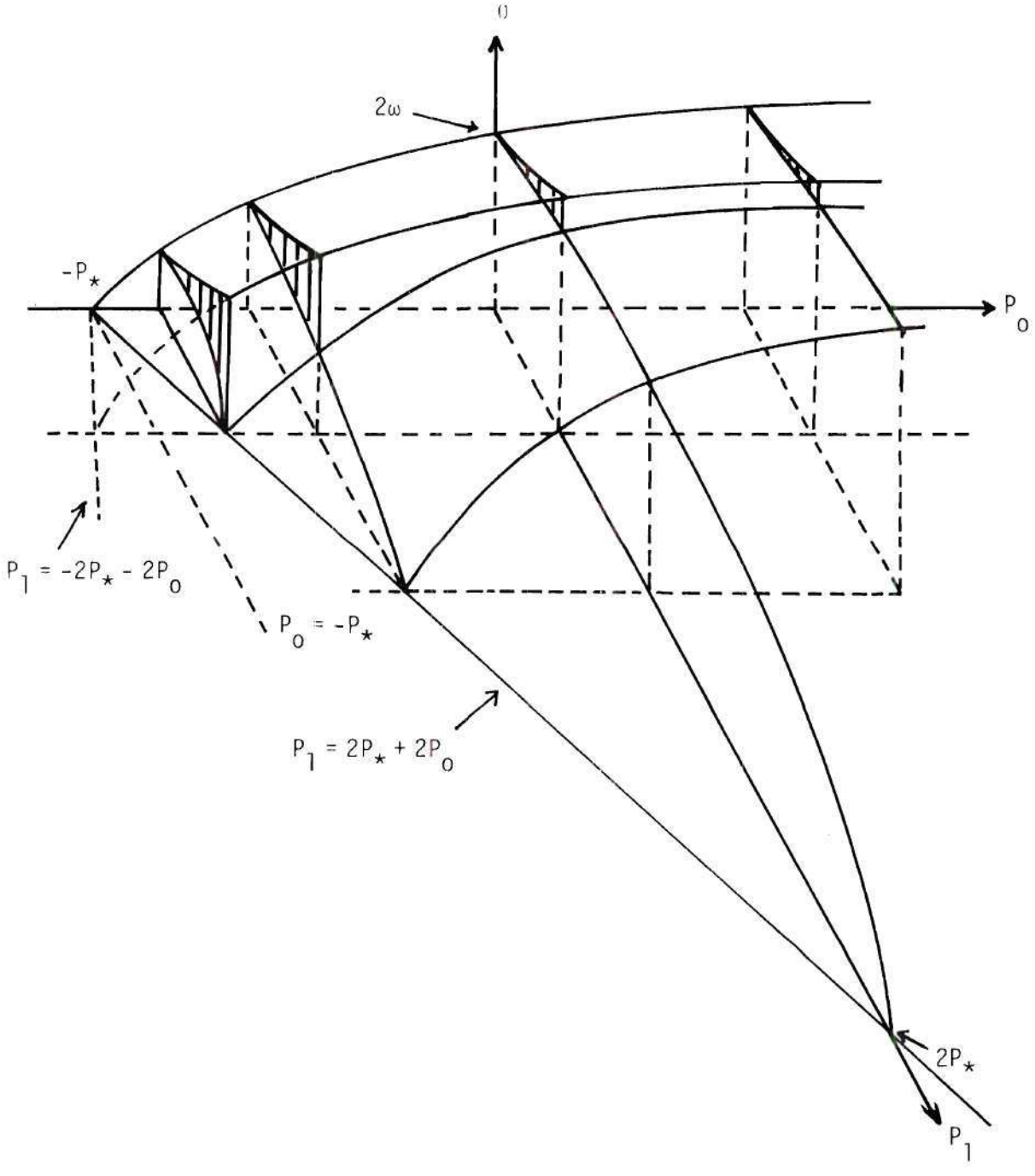

Figure 50. The Principal Region

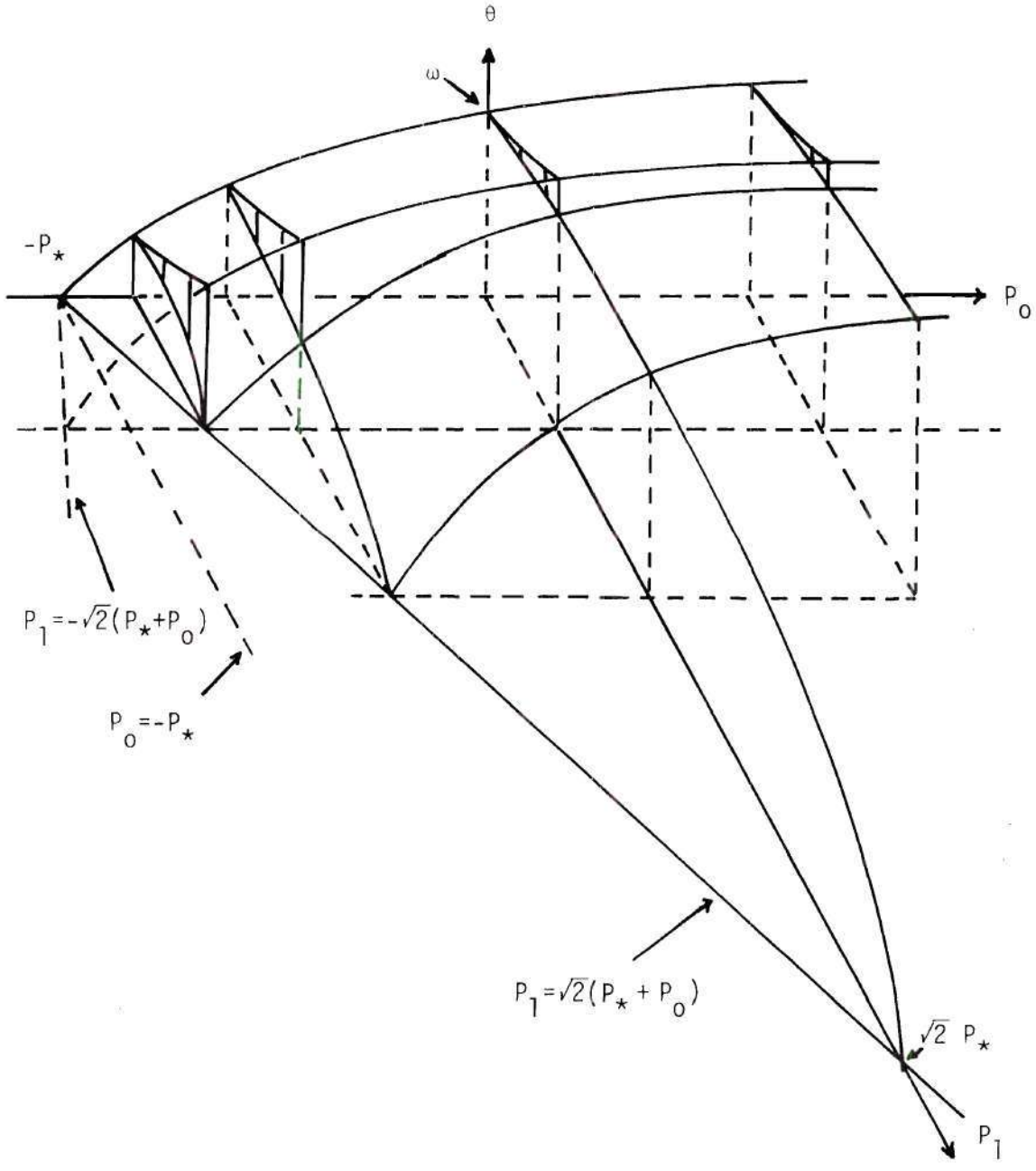

Figure 51. The Secondary Region.

$K = 0.01$ and $P_o = -0.5$ was used to compute the widths of the instability zones for the column with a region of discontinuities. However, Equations (1) were used to evaluate the widths of the instability zones for the corresponding uniform column. An examination of Table 7 reveals that the widths for the column with a region of discontinuities are slightly larger than the widths for the corresponding uniform column.

REFERENCES

1. Evan-Iwanowski, R. M. "On the Parametric (dynamic Stability) of Elastic Systems, Proc. First South Eastern Conf. on Theoretical and Applied Mechanics, Gatlinburg, Tenn., Proceedings, 1962.

2. Bolotin, V. V., The Dynamic Stability of Elastic Systems, Holden-Day, San Francisco, 1964.

3. Barr, A. D. S., and Done, T. S., "Parametric Oscillation in Aircraft Structures," Aero J. of the Royal Aero. Soc., Vol. 75, September, 1971, pp. 654-658.

4. Evan-Iwanowski, R. M., "On the Parametric Response of Structures," Applied Mechanics Reviews, Sept. 1965, pp. 699-703.

5. Evansen, H. A., and Evan-Iwanowski, R. M., "Effect of Longitudinal Inertial Upon the Parametric Response of Elastic Columns." J. Appl. Mech., Vol. 33 (1966), pp. 141-148.

6. Somerset, J. M., and Evan-Iwanowski, R. M., "Experiments on Parametric Instability of Columns," Proc. Second Southeastern Conf. on Theoretical and Applied Mech., Atlanta, Ga., March 1964, pp. 503-515.

7. Evan-Iwanowski, R. M., "Nonstationary Vibrations of Mechanical Systems," Applied Mechanics Reviews, March 1969, pp. 213-217.

8. Evan-Iwanowski, R. M., Stanford, W. F., and Kehagioglou, T., "Nonstationary Parametric Response of a Nonlinear Column." Proc. of the 5th Southeastern Conf. on Theoretical and Applied Mechanics, April, 1970.

9. Haight, E. C., and King, W. W., "Stability of Parametrically Excited Vibrations of an Elastic Rod," Proceedings of the 5th Southeastern Conf. on Theoretical and Applied Mechanics, April, 1970.

10. Stevens, K. K., "The Use of Fourier Transforms in Parametric Excitation Problems," Journal of Applied Mechanics, December 1972, pp. 1161-1162.

11. Dzygadlo, Z., and Solarz, L., "On Nonautonomous Vibrations of a Self-Excited System with Tangential Force," Proc. of Vibration Problems, Warsaw, 1972, pp. 157-177.

12. Deygadlo, Z., "Forced Parametrically-Excited Vibration of a Plate of Finite Length in Plane Supersonic Flow," Proc. of Vibration Problems, Warsaw, 1969, pp. 232-244.

13. Cauhey, T. K., and Dickerson, J. R., "Stability of Linear Dynamic Systems with Narrow-Band Parametric Excitation," J. of Applied Mechanics, Sept., 1967, pp. 709-713.

14. Tso, W. K., "Parametric Torsonal Stability of a Bar Under Axial Excitation, Journal of Applied Mechanics, March 1968, pp. 13-19.

15. Masaaki Sano, "Dynamic Stability of a Connected Rod Under Periodic Longitudinal Force," National Aerospace Lab., Tokyo, 1972 (English summary STAR 1972).

16. Ghobarah, A. A., "Dynamic Stability of Monosymmetrical Thin-Walled Structures," J. of Appl. Mech., December, 1972, pp. 1055-59.

17. Iwatsubu, T., Ishihara, K., and Sugiyama, Y., "Instability Problems of Columns under Periodic Loads," Proceedings of the 20th Japan National Congress for Applied Mechanics, 1970, pp. 211-18.

18. Inove, J., Araki, Y., and Urushizaki, Y., "On the Dynamic Stability of Coil Spring," Proceedings of the 15th Japan National Congress for Applied Mechanics, 1965, pp. 228-32.

19. Tso, W. K., and Fung, D. P. K., "Dynamic Instability Under the Combined Actions of Nonconservative Loading and Base Motion," Journal of Applied Mech., Dec., 1971, pp. 1074-1078.

20. Tsalik, A. M., "Free Vibration of Reinforced Concrete Bars with Cracks in Flexure," Soviet Appl. Mech., 1967, pp. 71-73.

21. Carlson, R. L., Zielsdorff, G. and Harrison, J., "Buckling in Cracked Thin Sheets," Proc. on the Air Force Conf. on Fatigue and Fracture of Aircraft Structures and Materials, AFFDL-TR-70-144, 1970.

22. Datta, P. K., and Carlson, R. L., "Buckling and Vibration of a Thin Tensioned Sheet with an Elliptical Hole," Exp. Mech., Vol. 13, No. 9, 1973, pp. 280-285.

23. Carlson, R. L., "An Experimental Study of the Parametric Excitation of a Tensioned Sheet with a Cracklike Opening," Accepted publication in ASTM, 1973.

24. Lubahn, J. D., "Experimental Determination of Energy Release Rate for Notched Bending and Notch Tension," ASTM, 1959, pp. 1-29.

25. Gross, B., Srawley, J. E., and Brown, W. F., Jr., "Stress-Intensity Factors for a Single-Edge-Notch Tension Specimen By Boundary Callocation of a Stress Function," NASA TN D-2396, 1964.

26. Gross, B., and Srawley, J. E., "Stress-Intensity Factors by Boundary Callocation for Single-Edge-Notch Specimens Subject to Splitting Forces," NASA TN D-3295, 1966.

27. Vanderveldt, H., and Liebowitz, H., "Theoretical and Experimental Studies of Notched Columns Having One End Fixed and Other End Pinned," Engr., Frac., Mech., 1970, pp. 675-689.

28. Berkovits, A. and Golod, A., "Buckling of an Elastic Column Containing a Fatigue Crack," Experimental Mechanics, Aug., 1972, pp. 358-371.

29. Lubkin, S. and Stoker, J. J., "Stability of Columns and Strings Under Periodically Varying Forces," Quarterly of Applied Mathematics, Vol. I, No. 3, 1943, pp. 215-236.

30. Stahl, B., and Keer, L. M., "Vibration and Stability of Cracked Rectangular Plates," Inst. J. Solids Structures, 1972, Vol. 8, pp. 69-91.

31. Lynn, P. P., and Kumbasar, "Free Vibrations of Rectangular Plates Having Narrow Cracks and Simply Supported Edges," Developments in Mechanics, Vol. 4, Proc. 10th Midwestern Mechanics Conf., Colorado State University, Fort Collins, Colorado, Aug. 1967, pp. 911-928.

32. Hsu, C. S., "On the Restricted Class of Coupled Hill's Equations and Some Applications," Journal of Applied Mechanics, Vol. 28, Trans. ASME, Vol. 83, Series E, 1961, pp. 551-556.

33. Hsu, C. S., and Lee, T. H., "A Stability Study of Continuous Systems under Parametric Excitation Via Liapunov's Direct Method," Instability of Continuous Systems, Symp., Herrenalb, Sept., 1961.

34. Ince, E. L., Ordinary Differential Equations, Dover Publications, Inc., 920 Broadway, New York 10, N. Y., 1956.

35. Forsyth, A. R., Theory of Differential Equations, Vol. IV: Ordinary Linear Equations, Dover Publications, Inc., New York, New York, 1959.

36. Hochstadt, H., Differential Equations: A Modern Approach, Holt, Rinehart and Winston, New York, New York, 1964.

37. Southworth, R. W., and Deleeuw, S. L., Digital Computation and Numerical Methods, McGraw-Hill Book Company, New York, New York, 1965.

VITA

Vijaykumar Navnitlel Parekh was born on October 10, 1940 in Dharangaon, India.

He received a Bachelor of Science (with a major in Physics and a minor in Mathematics) from the University of Bombay in 1961. In 1967 he received a Bachelor of Science in Aerospace Engineering from the University of Alabama. He obtained an M.S. in Aerospace Engineering from the Georgia Institute of Technology in 1971.

Mr. Parekh is employed by the Lockheed-Georgia Company. He is married to the former Asha P. Shah and has one son, Rajeev.